New methods in stray light correction and multi-imaging spectroradiometry

Der Fakultät für Mathematik und Physik
der Gottfried Wilhelm Leibniz Universität Hannover

zur Erlangung des akademischen Grades
Doktor der Naturwissenschaften
Dr. rer. nat.

genehmigte Dissertation von

M. Sc. (hons) Ralf Zuber

2020

Referent: Prof. Dr. Gunther Seckmeyer (Universität Hannover)
Korreferent: Prof. Dr. Manfred Wendisch (Universität Leipzig)
Korreferent: Prof. Dr. Detlef Ristau (Universität Hannover)

Tag der Promotion: 28.04.2020

Kurzfassung

Insbesondere bei Messungen im UV-Spektralbereich mit Array Spektralradiometern trägt das interne Streulicht häufig erheblich zur Messunsicherheit bei. In der vorliegenden Arbeit wurde für den genannten Anwendungsfall ein technischer Ansatz zur signifikanten Streulichtreduzierung entwickelt. Mit einem auf dieser Technologie basierenden Messgerät konnten in Messkampagnen Abweichungen des UV-Index kleiner 1% oder bei der vertikalen Ozondickebestimmung kleiner 2% im Vergleich zu etablierten Doppelmonochromator Referenzsystemen erzielt werden. Die Nachweisgrenze der solaren spektralen Bestrahlungsstärke wurde dabei um etwa zwei Größenordnungen auf $5 \cdot 10^{-5}$ $Wm^{-2}nm^{-1}$ im Vergleich zu $2 \cdot 10^{-3}$ $Wm^{-2}nm^{-1}$, dem Level von typischen Array Spektralradiometern, reduziert. Infolgedessen rückt die Nachweisgrenze dem empfohlenen Level eines Doppelmonochromators (S-2 Instrument der WMO) von $1 \cdot 10^{-6}$ $Wm^{-2}nm^{-1}$ signifikant näher. Die erreichte Gesamtmesszeit einer typischen solaren spektralen Bestrahlungsstärkemessung liegt dabei bei etwa 8 Sekunden. Sie ist damit entscheidend kürzer als die von Doppelmonochromatoren, welche bei ähnlichem Spektralbereich und -auflösung bei typischerweise 16 Minuten liegt. Es ist zu erwähnen, dass Änderungen der spektralen Bestrahlungsstärke innerhalb der genannten 8 Sekunden zu erhöhten Messunsicherheiten bei Messvergleichen führen können. Die zeitliche Synchronisierung einzelner Wellenlängenmesspunkte, wie etwa bei Doppelmonochromatoren (eigener Zeitstempel pro Wellenlängenschritt), ist in dieser Zeit nicht möglich.

Dieser technische Ansatz wurde entwickelt um eine deutliche Verbesserung der Streulichtkorrektur von Array Spektralradiometern zu erreichen, um dadurch deren Vorteile sowohl hinsichtlich der Gesamtmesszeit als auch weitere Vorteile wie beispielsweise die kleinere Bauform im Vergleich zu den bisher etablierten Doppelmonochromatoren nutzen zu können.

Erreicht wurde dies durch die spektrale Vorfilterung der zu messenden Strahlung mittels verschiedener optischer Bandpass- und Kantenfilter, welche mit einem Filterrad in den optischen Strahlengang eingefahren werden. Durch die optische Vorfilterung kann die eingekoppelte Strahlung spektral auf den zu messenden Spektralbereich, Teile des Spektralbereichs oder den nicht zu messenden Spektralbereich eingeschränkt werden. Folglich ist die potenzielle Strahlung, welche im Gerät Streulicht erzeugen kann, bedeutend reduziert oder sie dient zur Charakterisierung des Streulichts. Auf diese Weise können verschiedene Filtermessungen miteinander zu einer streulichtreduzierten Messung des gesamten Spektralbereichs des Messgeräts kombiniert werden. Die Dauer der Einzelmessungen ist ausschlaggebend für die erreichte Gesamtmesszeit.

Für die zeitlich simultane Vermessung von Strahldichteverteilungen, auch „spectral snapshot imaging“ genannt, wurde im Rahmen dieser Arbeit ein weiterer Ansatz ergänzend zu den bereits existierenden optischen Verfahren entwickelt. Der dabei entstandene Prototyp erlaubt bei voller Nutzung seines Sichtfeldes die simultane Vermessung von 196 Messkanälen (14 x 14).

Für den Machbarkeitsnachweis wurde eine Labormessung dieser 196 Messkanäle von einem 10 mm x 10 mm großen Messfelds im Spektralbereich von 380 nm bis 800 nm mit 10 nm optischer Bandbreite (FHWM) durchgeführt. Hierbei wurde ein Messkanalübersprechen von 4% erreicht. Zudem wurde eine räumlich aufgelöste Messung der Zenitstrahldichte bei einem FOV von 0,5° und gleicher Messkanalanzahl, im Spektralbereich 280 nm bis 470 nm bei 3 nm optischer Bandbreite (FWHM) umgesetzt. Die ermittelte Abweichung von -30% zu UVSPEC modellierten Daten ist nicht optimal, aber gemäß anderer Veröffentlichungen im Rahmen der zu erwartenden Abweichungen zwischen unabhängig kalibrierten Messsystemen und Modelldaten. Dies liegt insbesondere daran, dass der Prototyp nicht temperaturgeregelt und hinsichtlich mechanischer Umsetzung und Licht-Dichtheit wesentlich zu optimieren ist. Anzumerken ist, dass die erreichten 3 nm optische Bandbreite zu einer

erhöhten Messunsicherheit bei der Vermessung der solaren spektralen Strahldichte vor allem im UVB Spektralbereich führen. Ergänzend wurde die Machbarkeit eines teilhemisphärischen Sichtfeldes mit Zenitwinkeln von 17° bis 74° mittels einer von einem Kollegen speziell hierfür entwickelten Eingangsoptik gezeigt. Die Anzahl der nutzbaren Messkanäle reduzierte sich durch diese Eingangsoptik bedingt durch mechanische Abschattungen und einer nicht vollen Nutzung des Sichtfelds auf 120. Bei allen genannten Messungen lag die Gesamtmesszeit im Bereich weniger Sekunden. Wichtig zu erwähnen ist, dass die im Rahmen dieser Arbeit erzielten Ergebnisse des Prototyps als Machbarkeits- und Potenzialstudie des Verfahrens einzuschätzen sind.

Die Motivation für die Entwicklung dieses neuartigen Messsystems liegt darin, die Anzahl an optischen Komponenten gegenüber bestehenden Systemen signifikant zu reduzieren sowie weitere Vorteile wie beispielweise die mögliche Adaption verschiedener FOV bei gleicher oder höherer Anzahl an Messkanälen zu nutzen. Für die Analyse von sich zeitlich schnell ändernden Strahldichteverteilungen ist es vorteilhaft eine zeitlich simultan und örtlich hochauflösende (Anzahl der Messkanäle) spektrale Strahldichtemessung durchführen zu können. Denn alle abtastenden Technologien, sei es spektrale oder räumliche Abtastung, haben den gemeinsamen Nachteil, dass zeitaufgelöste Effekte nur analysiert werden können, wenn diese deutlich langsamer sind als die Abtastung selbst. Eine komplexe und sich schnell ändernde spektrale Strahldichteverteilung tritt beispielsweise häufig bei durchbrochener Bewölkung auf. In den letzten Jahren wurden bereits hierfür ausgelegte Messkonzepte vorgestellt, beispielsweise das MUDIS Messsystem, mit 113 nutzbaren Messkanälen im Spektralbereich 250 nm bis 600 nm, sowie dessen Weiterentwicklung AMUDIS, welches sich zum Veröffentlichungszeitpunkt dieser Arbeit mit 150 Messkanälen im Spektralbereich von etwa 300 nm bis 1700 nm, in der Testphase befindet.

Das Verfahren basiert auf einem speziellen optischen Aufbau, welcher an ein linienscannendes Spektrometer angekoppelt wird. Dieser optische Aufbau erzeugt Mehrfachabbildungen des Messobjektes, d.h. der Strahldichteverteilung, mittels einer Facettenspiegeloptik. Von jeder dieser Abbildungen kann anschließend ein anderer Teil der zu vermessenden Strahldichteverteilung über Blenden selektiert und in ein Spektrometer für die weitere spektrale Analyse eingekoppelt werden. Dabei zeichnet sich das neue Verfahren durch die Nutzung von nur wenigen optischen Elementen aus.

Schlüsselwörter: Array Spektralradiometer, UV Spektralradiometrie, Streulichtkorrektur, bildgebende multispektrale Messung

Abstract

Especially for measurements in the UV spectral range the internal stray light is often a crucial contribution to the measurement uncertainty for array spectroradiometers. In this work a technical procedure for significant stray light correction for the application mentioned has been developed. With a measurement device based on this procedure deviations in the UV index of less than 1% and vertical ozone thickness of less than 2%, compared to established double monochromator reference systems, have been achieved. The detection limit of the spectral irradiance of solar radiation was reduced by about two orders of magnitude, $5 \cdot 10^{-5}$ $Wm^{-2}nm^{-1}$ compared to $2 \cdot 10^{-3}$ $Wm^{-2}nm^{-1}$, the level of a typical array spectroradiometer. As a result, the achieved detection limit is significantly closer to the recommended level of a double monochromator (S-2 instrument according to WMO UV instrumentation specifications) with $1 \cdot 10^{-6}$ $Wm^{-2}nm^{-1}$. The total measurement time of a typical solar spectral irradiance measurement is about 8 seconds. This is significantly shorter than that of double monochromators, which typically require 16 minutes for a measurement in comparable spectral range and resolution. It should be mentioned that changes in the spectral irradiance within the stated 8 seconds can lead to increased measurement uncertainties in measurement intercomparisons. A comparatively precise time synchronization of individual wavelength measuring points, such as with a double monochromator (own time stamp per wavelength step), is not possible.

This approach was developed to achieve a significant improvement in the stray light correction of array spectroradiometers in order to be able to use their temporal advantages in terms of total measurement time as well as other advantages such as the smaller size compared to established double monochromators.

This was achieved by a spectral pre-filtering of the optical radiation to be measured by means of various optical bandpass and edge filters, which are moved in the optical path with a filter wheel. Due to the optical pre-filtering, the in-coupled optical radiation can be spectrally limited to the spectral range to be measured, parts of the spectral range or the spectral range not to be measured. Consequently the potential optical radiation, which is able to generate stray light in the device, is significantly reduced or serves to characterize the stray light. In this way different filter measurements can be combined with each other in order to obain a stray light corrected measurement of the entire spectral range. The duration of the several individual measurements is decisive for the total measurement time achieved.

For the simultaneous measurement of radiance distributions, also called "spectral snapshot imaging", a further optical approach was developed as part of this work. The resulting prototype allows by use of the complete field of view the simultaneous measurement of 196 measurement channels (14 x 14).

For the proof of feasibility, a laboratory measurement of a 10 mm x 10 mm measuring field with these 196 measurement channels in the spectral range from 380 nm to 800 nm with 10 nm optical bandwidth (FHWM) was performed. A channel crosstalk of 4% was achieved. In addition, a spatially resolved measurement with the same amount of measurement channels of the zenith radiance of the atmosphere at a FOV of 0.5 °, in the spectral range 280 nm to 470 nm at 3 nm optical bandwidth (FWHM) was accomplished. Here a suboptimal deviation of -30% to UVSPEC modeled data was determined. However, according to other publications, this deviation is within the expected deviations between independently calibrated measuring systems and model data. Especially for a prototype that is not temperature stabilized and has to be optimized substantial with regard to mechanical implementation and light-tightness. It has to be mentioned that the achieved 3 nm optical bandwidth leads to an increased measurement uncertainty especially in the UVB spectral region for solar spectral radiance measurements. Supplementary, the feasibility of a partial hemispherical field of view with solar zenith angles from 17 ° to 74 ° was demonstrated by means of a specially designed additional entrance optics developed by a colleague. The number of usable measurement channels was reduced by this entrance

optic due to mechanical shading and incomplete use of the field of view to 120. For all measurements, the total measurement time was in the range of a few seconds. It is important to note, that the results achieved by the prototype in this work are to be assessed as a feasibility and potential study of the new procedure.

The motivation for developing this novel measurement system was to reduce the number of optical components significantly compared to existing systems and to use benefits such as possible adaption of different FOVs, ideally with the same or higher number of measurement channels. For the analysis of rapidly changing radiance distributions, it is advantageous to be able to carry out a spectral radiance measurement simultaneously and with a high spatial resolution (number of measurement channels). All scanning technologies (spectral or spatial scanning) have the common disadvantage that time-resolved effects can only be analyzed if they are significantly slower than the scan itself. A complex and rapidly changing spectral radiance distribution for instance often occurs in the presence of broken clouds. In recent years some measurement concepts have already been presented. For example, the MUDIS measurement system with 113 measurement channels in the spectral range 250 nm to 600 nm and its further developed system AMUDIS, which is at the time of publication of this work in the test phase with 150 measuring channels in the spectral range of about 300 nm to 1700 nm.

The approach is based on a special designed input optics, which is adapted to a line scanning spectrometer. This input optics produces multiple images of the radiance distribution to be measured, by using a facet mirror based optics. A different part of the radiance distribution to be measured can then be selected from each of these images by apertures and coupled into a spectrometer for further spectral analysis.

Keywords: Array spectroradiometer, UV spectroradiometry, stray light correction, spectral snapshot imaging

Table of Contents

List of Figures

List of Tables

List of Symbols and Abbreviations

Abbreviations:

ADC	Analog Digital Converter
AMUDIS	Advanced Multidirectional Spectroradiometer system
BTS	BiTec Sensor
CCD	Charged-Coupled Device
CET	Central European Time
CMOS	Complementary Metal-Oxide-Semiconductor
CTIS	Computed Tomography Imaging Spectrometry
cts	Counts
DU	Dobson Units
DUT	Device Under Test
FOV	field of view
FWHM	Full Width at Half Maximum
IFS-F	Integral Field Spectrometry – Fiber Arrays
IFS-M	Integral Field Spectrometry – with Facet Mirror
IMuK	Institut für Meteorologie und Klimatologie
IR	Infrared
ISS	Image Slicing Spectrometer
LED	Light Emitting Diode
LSF	Line Spread Function
MUDIS	Multidirectional Spectroradiometer system
NDACC	Network for the Detection of Atmospheric Composition Change
NMI	National Metrology Institute
OLED	Organic Light Emitting Diode
OoR	Out of Range
OPO	Optical Parameter Oscillator
PTB	Physikalisch-Technische Bundesanstalt
QASUME	Quality Assurance of Spectral UV Measurements portable system
RGB	Red Green Blue
SNR	Signal Noise Ratio
SZA	Solar Zenith Angle
TOC	Total Ozone Column
UTC	Coordinated Universal Time
UV	Ultraviolet
VIS	Visible

Symbols:

E_e	irradiance
E_v	illuminance
L_e	radiance
L_v	luminance
Φ_e	radiant power
Φ_v	luminous flux
I_e	radiant intensity
I_v	luminous intensity
A	area
Ω	solid angle
θ	angle of projected area $dA\cos(\theta)$
λ	wavelength
V(λ)	photometric weighting function
$r(\lambda)$	spectral responsivity
$Cal(\lambda)$	calibration source
$S(\lambda)$	signal measured

1. Introduction

Spectroradiometric measurements and derived quantities are one of the fundamental methods in radiometry and photometry (ISO/CIE, 1984). These measurements are for instance widely used for the qualification or characterization of artificial light sources like classical halogen lamps or modern solid state lighting devices as light emitting diodes (LED) (ISO/CIE, 1984, 2017). In addition, spectroradiometric measurements are used to investigate solar radiation and its effects in many different perspectives. For instance, solar irradiance or solar radiance measurements are used to investigate the effect to biological organism in terms of erythema hazard (Seckmeyer *et al.*, 2012; McKenzie *et al.*, 2009), photosynthetic active radiation (Meek *et al.*, 1984; Gueymard, 2008), circadian and melanopic effects (Webb, 2006) or vitamin D production (Engelsen *et al.*, 2005; Webb and Engelsen, 2006; Seckmeyer *et al.*, 2013; Mithal *et al.*, 2009). In addition, solar radiation is a significant parameter in climate models (He *et al.*, 2014; Brovkin *et al.*, 2013) and can be used to determine the atmospheric ozone column (Vaskuri *et al.*, 2018; Dobson, 1931). The trace gas ozone hit the headlines for instance in the 1980's regarding the ozone hole driven by Chlorofluorocarbons (CFCs) and the resulting Montreal protocol in 1987 (UN, 1987). Studies show that ozone-depleting substances are successfully declining due to the Montreal protocol (McKenzie *et al.*, 2011; Bais *et al.*, 2015), however an ozone column statistically significant increase could not been observed (Bais *et al.*, 2019). As a consequence it is argued that ozone monitoring is still needed in order to monitor the recovery process or its failure (Newman and McKenzie, 2011; Chipperfield *et al.*, 2015). The skepticism was supported by a recent study showing CFC-11 increased unexpended due to emissions in China (Montzka *et al.*, 2018). The erythema weighted irradiance, is considered in research topics for instance as a contribution for melanoma skin cancer or eye and immune system disease (Armstrong and Kricker, 2001; WHO, 2002; Godar, 2005; Seckmeyer *et al.*, 2010). The dimensionless standardized UV index (WHO, 2002), which is generally understood the maximum of the erythema weighted global solar irradiance divided by 25 mW/m^2, is displayed in weather forecast to inform the population about the maximum expected daily UV exposure and corresponding erythema risk (Blumthaler, 2018; WHO, 2002; Allinson *et al.*, 2012). Furthermore solar irradiance measurements are used as input parameters of models for photovoltaic systems (Hofmann and Seckmeyer, 2017; Hofmann *et al.*, 2014; Ineichen, 2011; Loutzenhiser *et al.*, 2007; Demain *et al.*, 2013).

However, changes of aerosols, atmospheric gases, clouds and albedo are expected due to the climate change (Bais *et al.*, 2018; Bais *et al.*, 2015; McKenzie *et al.*, 2011; WMO, 2018; Bais *et al.*, 2019). Since these parameters affect the solar radiation, ozone in particular the UV radiation, changes can be expected for the solar spectral radiance and irradiance (Seckmeyer *et al.*, 2018; Bais *et al.*, 2018; Bais *et al.*, 2015; McKenzie *et al.*, 2011; WMO, 2018; Bais *et al.*, 2019). Due to the mentioned biological effects of solar radiation on humans, these changes are an important scientific question (McKenzie *et al.*, 2009) and further research based on spectroradiometric measurements might be needed. The expected changes due to the climate change are for instance presented in much detail in McKenzie *et al.* (2011); Bais *et al.* (2015); Bais *et al.* (2018) and Bais *et al.* (2019), an overview of the biological effects of solar radiation is given for instance in Seckmeyer *et al.* (2018) and Seckmeyer *et al.* (2012).

When considering further investigations by means of spectroradiometric measurements, two restrictions could result:

〉 A limiting factor for spectroradiometric measurements with array spectroradiometers in the ultraviolet (UV) region are internal stray light effects. Egli *et al.* (2016) showed and stated that none of 14 tested array spectroradiometers, some of them are elaborate characterized and stray light corrected devices according to Nevas *et al.* (2014), is able to perform comparable measurements to double monochromators below 310 nm. Furthermore Egli *et al.* (2016) at smaller solar zenith angles (SZAs) the ratios between the reference double monochromator and the best stray light corrected instruments were between 0.95 and 1.05. This shows why double monochromator based systems, which are scientifically accepted (Seckmeyer *et al.*, 2001), validated in many measurement campaigns (Wuttke *et al.*, 2006; Lantz *et al.*, 2008; Bais, 1998; Webb *et al.*, 1998; Seckmeyer *et al.*, 1997; Seckmeyer, 1989; Hülsen *et al.*, 2016; Gröbner *et al.*, 2005) and analyzed in detail in terms of measurement uncertainty (Cordero *et al.*, 2013; Bernhard and Seckmeyer, 1999) are still used today.

  In order to overcome the limitations imposed by the internal stray light of array spectroradiometers and use their temporal advantages, some new methods were developed in the past (see section 2.3.1). However, none of these methods have been evolved in a way to overcome the mentioned limitations in the UV and reach for instance the specifications (S-2 instrument of the WMO) given in Seckmeyer *et al.* (2001). This was the motivation to develop an array spectroradiometer, which is able to achieve an internal stray light reduction, which can compete with scanning double monochromator systems, but still allows shorter measurement times.

〉 When thinking about the spectral radiance measurement of complex rapidly changing radiance distributions, which for instance often occur during hemispherical measurements by the presence of broken clouds, the angular, spectral and temporal resolution might play a key role for possible investigations. E.g., cloud movement or the exposure of a human in a 3D model (Riechelmann *et al.*, 2013; Seckmeyer *et al.*, 2018; Seckmeyer *et al.*, 2013). By scanning e.g. in high spatial resolution a long measurement time will be the result and the temporal resolution will be limited (Sigernes *et al.*, 2012; Hardeberg *et al.*, 2002; Gupta and Voloshinov, 2004; Mathews, 2008). In the last years, advances have been made with so-called spectral snapshot imaging equipment (Hagen and Kudenov, 2013; Riechelmann *et al.*, 2013; Seckmeyer *et al.*, 2018), which perform multi-channel spectral radiance measurements without scanning (see section 0). In the field of radiometry the IFS-F (Integral Field Spectrometry - Fiber arrays) approach, which was for instance selected by Riechelmann *et al.* (2013) for the MUDIS system and by Seckmeyer *et al.* (2018) for the AMUDIS system, seems to be an appropriate choice for hemispherical measurements. This approach uses multiple optical fibers, which are coupled into a line scanning spectrometer (see Section 2.2) as separate measurement channels. For MUDIS for instance 113 optical fibers for the same amount of measurement channels in the spectral range of 250 nm to 600 nm and for AMUDIS 495 optical fibers for 150 measurement channels in the spectral range 300 nm to 1700 nm are used (Riechelmann *et al.*, 2013; Seckmeyer *et al.*, 2018). However, the large number of optical fibers comes with mechanical challenges and possibly

limitations. This was the motivation to develop a new only on optical imaging based IFS-M (Integral Field Spectrometry – with facet Mirror) approach, which reduces the number of optical components significantly by ideally the same or higher number of measurement channels, and to enable the adaptation of different FOVs.

Chapter 2 introduces the state of the art. The scope of this thesis is given in Chapter 3. Chapter 4 describes the methods, which are the basis for the research articles of this thesis. The articles itself are presented in Chapter 5. A discussion and conclusions is given in Chapter 6, followed by an outlook in Chapter 7.

2. State of the art

In Section 2.1 fundamental radiometric and photometric quantities for this thesis are introduced. In Section 2.2 different types of well-known spectrometer optical designs are presented. In Section 2.3, two open issues in spectroradiometry are introduced and a motivation for the research in this thesis is given.

2.1 Spectroradiometric measurements

For the quantitative measurement of optical radiation several physical quantities are used that differ by their measurement geometries. In this thesis two so-called radiometric quantities are of main interest, the *irradiance* and *radiance*. In the visible spectral region, weighted with the V(λ) function, the photometric equivalents to these two quantities are *illuminance* and *luminance* (CIE, 2011b). In the following Table 1 these frequently used radiometric and photometric quantities are listed. The definitions of this Section are based on literature as the cited CIE documents (ISO/CIE, 1984; CIE, 2011b) and literature as Wendisch and Yang (2012).

Table 1 Illustration of the most frequently used radiometric and photometric quantities and its unit and symbol.

Radiometry			**Photometry**		
Quantity	**Unit**	**Symbol**	**Quantity**	**Unit**	**Symbol**
irradiance	W/m²	E_e	Illuminance	lx	E_v
radiance	W/(m²sr)	L_e	Luminance	cd/m²	L_v
radiant power	W	Φ_e	luminous flux	lm	Φ_v
radiant intensity	W/sr	I_e	luminous intensity	cd	I_v

The definition of the irradiance is the ratio of the radiant power $d\Phi_e$ per unit area dA (CIE, 2011b):

$$E_e = \frac{d\Phi_e}{dA}. \tag{1}$$

The radiance is defined as the radiant power $d\Phi_e$ of a surface per unit solid angle $d\Omega$ and unit projected area $\cos(\theta)\, dA$ (CIE, 2011b):

$$L_e = \frac{d^2\Phi_e}{dA\cos(\theta)d\Omega}. \tag{2}$$

The photometric quantities are defined analogously:

$$E_v = \frac{d\Phi_v}{dA}, \tag{3}$$

$$L_v = \frac{d^2\Phi_v}{dA\cos(\theta)d\Omega}. \tag{4}$$

For the measurement of these introduced quantities different devices exist. The radiometric quantities can be measured, for instance, with radiometric filtered photodiodes and the photometric equivalents with V(λ) matched photodiodes. These so-called integrating devices (CIE, 2011b) are not capable to provide spectral information about the measured light source.

The spectral quantities are noted by an additional λ. Hence the spectral irradiance is the irradiance in a given wavelength range $d\lambda$:

$$E_{e,\lambda} = \frac{d^2\Phi_e}{dA\, d\lambda}. \tag{5}$$

Equivalent the spectral radiance can be defined as:

$$L_{e,\lambda} = \frac{d^3\Phi_e}{dA\cos(\theta)d\Omega d\lambda}. \tag{6}$$

For the measurement of the spectral radiometric quantities (often called spectroradiometric quantities), so-called spectroradiometers are used. These are spectrometers (device which measures the spectral distribution of a light source) which are absolute radiometric calibrated (ISO/CIE, 1984).

Beside this physical quantities as well some geometrical terms need to be introduced for this work. The FOV of a camera is defined by the CIE as “solid angle as "seen" by the detector (acceptance angle), e.g. of a radiometer or spectroradiometer, out of which the detector receives radiation” (CIE, 2011b definition 17-429). In the case of radiance imaging measurements by a radiance camera several detector pixels exist (spatial resolution), resulting it can be distinguished between the FOV of the camera or the FOV of single detector pixels (DIN, 2019). For spectral snapshot imaging devices (see section 2.3.2), the use of the term “detector pixels” in respect with the FOV can be unclear since the wavelength is as well resolved by detector pixels. Thus, in this work such a spatial resolved FOV which is additionally spectrally measured is called measurement channel (see figure 1).

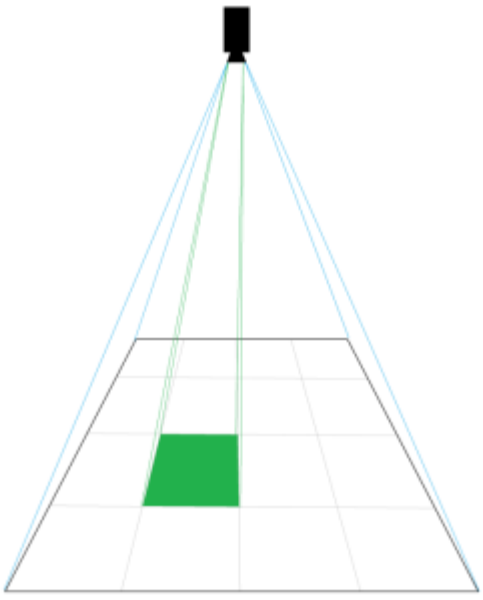

Figure 1 Illustration of the field of view (FOV). The green area is the FOV of a single measurement channel; the completely black bordered area is the FOV of the measurement device (all channels).

2.2 Type of spectrometers

In this Section a brief overview of a few well-known and widely used spectrometer designs is given. Most information of this section is based on the pertinent literature of Neumann (2014), Hagen and Kudenov (2013) and ISO/CIE (1984). The use of this section is to better describe the development of the relatively new spectral snapshot imaging technologies and the new approach presented in research article C of this thesis (see section 5.3). In Table 2 for each spectrometer design typical main features and the type of measurement result are stated for classification purposes.

Table 2 Overview of the introduced type of spectrometers with its main features and type of measurement result. Otherwise specified differently this information is taken from Neumann (2014), Hagen and Kudenov (2013) and ISO/CIE (1984)

	Main features	**Type of measurement result**
Scanning monochromator	Scanning device, limited internal stray light reduction	Single measurement channel by wavelength scanning
Scanning double monochromator	Scanning device, excellent internal stray light reduction	Single measurement channel by wavelength scanning
Array spectrometer	Limited internal stray light reduction, fast measurement	Single measurement channel, no scanning needed
Filter spectrometer	Scanning device, limited number of optical filters available	Single measurement channel by wavelength scanning
Line scanning (also called push-broom scanning) array spectrometer	Limited internal stray light reduction, fast measurement of multiple measurement channels	Multiple measurement channels arranged on a line, no scanning needed

Scanning monochromator:

The most common design of a scanning monochromator is based on the following setup. Optical radiation passes an entrance slit after which it is collimated by a mirror, followed by a diffraction grating which spectrally separates the collimated radiation (angle of diffracted beams is wavelength dependent). A focusing mirror images the collimated optical radiation to the exit slit where only the optical radiation of a small wavelength range will pass. At this exit slit/port of the monochromator system a detector, e.g. a photodiode or photomultiplier is placed. The detected energy of the given small wavelength interval can be controlled by the mechanical angle of the optical grating. This setup, which is illustrated in Figure 2, is called Czerny-Turner setup. With crossed optical path, it is called crossed Czerny-Turner setup (Shafer *et al.*, 1964; Czerny and Turner, 1930; Neumann, 2014; ISO/CIE, 1984).

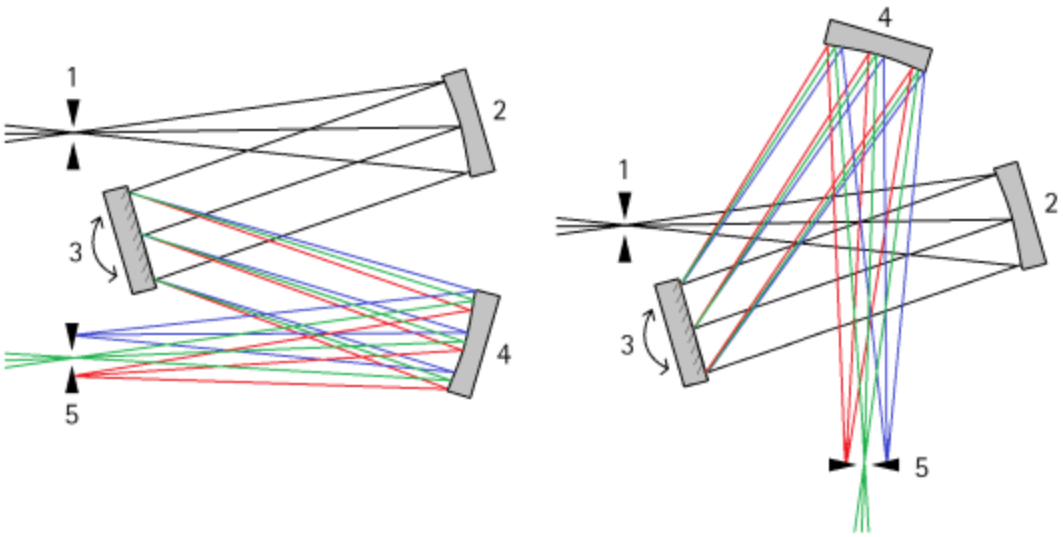

Figure 2 Schematic setup of a scanning monochromator (left: Czerny-Turner, right: crossed Czerny-Turner) based on an entrance slit (1), collimating mirror (2), rotating diffraction grating (3), focusing mirror (4) and exit slit to detector (5).

Note: If the two single mirrors are replaced by one large mirror, then the design is called Ebert-Fastie setup (Ebert, 1889).

Scanning double monochromator:

Based on two scanning monochromator setups, which are arranged in series, the internal stray light reduction capability can be significantly improved compared to a single monochromator (Walsh, 1952; Neumann, 2014; ISO/CIE, 1984). The input signal of the second scanning monochromator consists of monochromatic light and its corresponding stray light delivered from the first scanning monochromator. The second monochromator further reduces the remaining stray light and no significant additional stray light can be generated in the second monochromator which could be imaged on the detector (Neumann, 2014; Walsh, 1952).

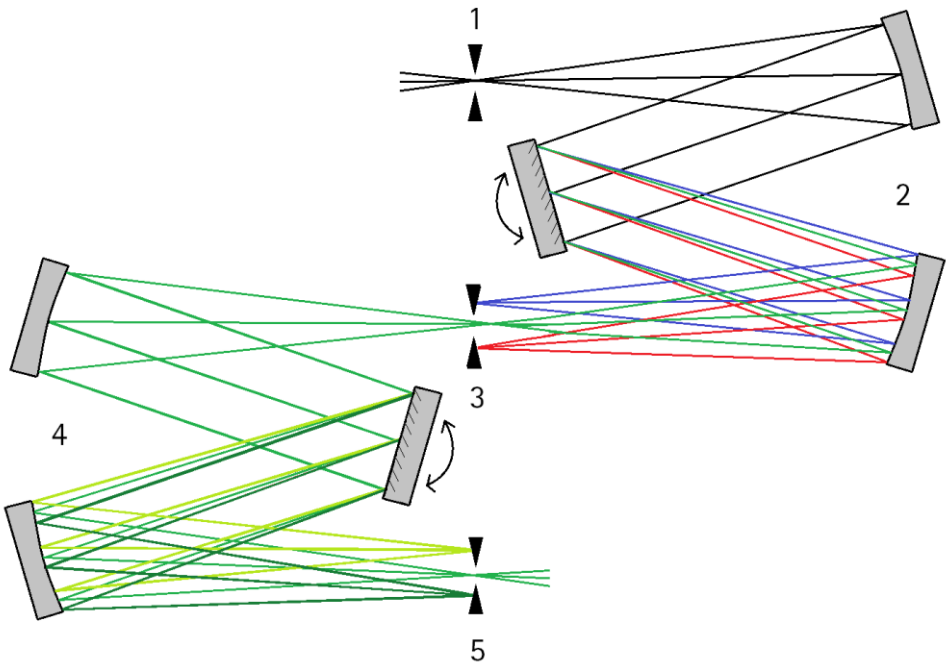

Figure 3 Schematic setup of a scanning double monochromator based on an entrance slit (1), scanning monochromator for first spectrally cleaning (2), separating slit (3), second scanning monochromator for spectrally precise selection (4) and exit slit to detector (5).

Array spectrometer:

Array spectrometers are very often based on similar optical setups as scanning monochromators. However, instead of a single photodiode an array of diodes, a so called charged-coupled device (CCD) or complementary metal–oxide–semiconductor (CMOS) array is used (Neumann, 2014). With these detectors, multiple wavelengths can be measured simultaneously.

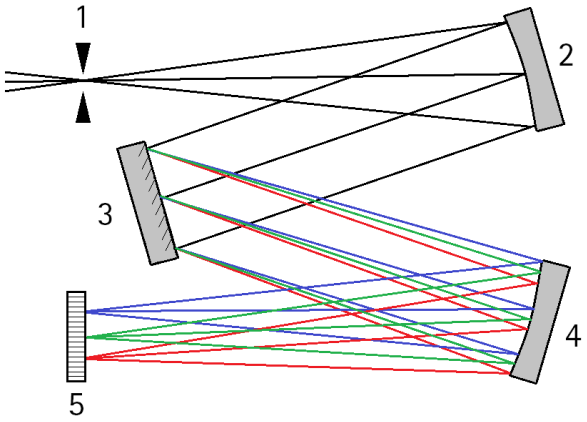

Figure 4 Schematic setup of an array spectrometer based on an entrance slit (1), collimating mirror (2), fixed diffraction grating (3), focusing mirror (4) and one-dimensional detector (5).

Filter spectrometer:

A filter spectrometer (also called filter-based spectrometer or tunable filter camera) is a scanning device that performs the spectral scan with the help of several optical bandpass (e.g. interference) filters, which are usually positioned with a filter wheel (Saptari, 2003; Hardeberg *et al.*, 2002; Hagen and Kudenov, 2013).

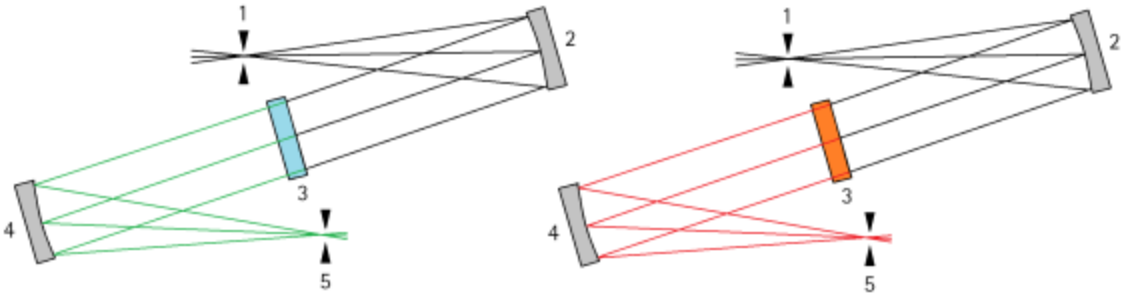

Figure 5 Schematic setup of a filter spectrometer based on an entrance slit (1), collimating mirror (2), optical bandpass filter wheel (3), focusing mirror (4) and detector (5). Difference between left and right illustration is a different transmission wavelength of the optical bandpass filter.

Note: In this thesis, no Fourier-spectrometers are considered which perform the spectral scan with an interferometer. Such a device is for instance introduced in Bianco et al. (2010).

Line scanning (also called push-broom scanning) array spectrometer:

The optical ray path of a line scanning array spectrometer is basically similar to array spectrometer. In principle, only the one-dimensional detector is replaced with a two-dimensional detector and the size of the entrance slit is adapted to the detector. Accordingly a full measurement line (multiple measurement channels) and not only one measurement channel at the entrance slit can be spectrally resolved (Davis *et al.*, 2002; Brown *et al.*, 2008; Neumann, 2014; Hagen and Kudenov, 2013).

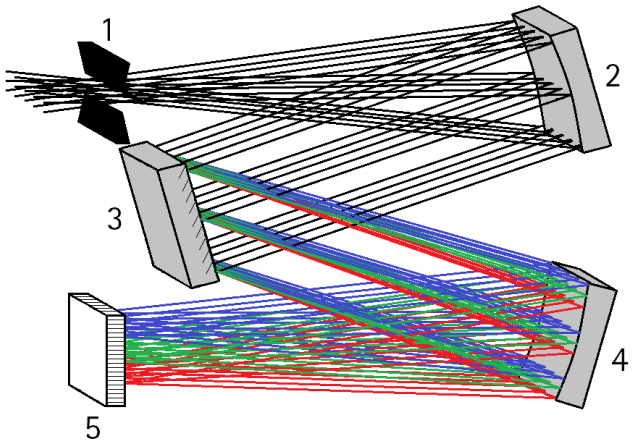

Figure 6 Schematic setup of a line scanning array spectrometer based on an entrance slit (1), collimating mirror (2), fixed diffraction grating (3), focusing mirror (4) and two-dimensional detector (5).

2.3 Current state of research

2.3.1 Stray light correction methods for array spectroradiometers

As already introduced in Chapter 1 (Introduction) many applications in the ultraviolet spectral range, cannot be addressed with array spectroradiometers since they are often limited by internal stray light effects (Egli *et al.*, 2016; Nevas *et al.*, 2014). Egli *et al.* (2016) stated and showed that a comparable accurate measurement of solar spectral irradiance below 310 nm to a double monochromator was not possible for all 14 tested array spectroradiometers. This results in larger uncertainties for derived quantities like the UV Index (Cordero *et al.*, 2007; Egli *et al.*, 2016). Only the best tested devices in Egli *et al.* (2016) achieved an deviation of 5% for SZA smaller 50° to the reference spectroradiometer. The radiation of visible and infrared generates stray light within the spectrometer, which is often higher than the lower UV signal (Seckmeyer *et al.*, 2010; Nevas *et al.*, 2014). This may be demonstrated by a measurement with cut-off filters, see for instance in Seckmeyer *et al.* (2010), Nevas (2015) or Shaw and Goodman (2008)). Resulting, scanning double monochromators are often used instead of array spectroradiometers in the UV spectral range (Gröbner *et al.*, 2005; Hülsen *et al.*, 2016; Seckmeyer *et al.*, 2001; Wuttke *et al.*, 2006)

Driven by the advantages of array spectroradiometers compared to scanning double monochromators (see Section 2.2 Type of spectrometers) in the last years new methodologies of internal stray light correction have been developed. A widely used methodology is the mathematical stray light correction which was developed by Zong *et al.* (2006) and has been extended by Nevas *et al.* (2012b). These methods are based on a full characterization of the internal stray light properties of the spectroradiometer with the help of a wavelength tunable laser source, also called optical parametric oscillator (OPO) (Byer, 1976). In principle the response of the spectroradiometer is measured separately for each wavelength of the spectroradiometers spectral range (Zong *et al.*, 2006). Resulting a correction matrix is determined, which is the basis for the later mathematical correction of the measurement data (Zong *et al.*, 2006; Nevas *et al.*, 2012b). Zong *et al.* (2006) showed that this approach can correct the so-called internal stray light by about two orders of magnitude. However, this correction method is not able to correct for so-called out-of-range (OoR) stray light that is generated in spectral bands outside the spectroradiometer measurement spectral range where the detector is still sensitive (Nevas *et al.*, 2014). If, for instance, a Si detector-based UV spectroradiometer is designed for the spectral range from 200 nm to 400 nm, with the method of Zong *et al.* (2006) only stray light originating between 200 nm to 400 nm can be corrected. However, the Si detector itself is sensitive to radiation up to about 1100 nm and stray light originating from this out-of-range spectral region (in this case 400 nm to 1100 nm) cannot be characterized with LSF's and thus cannot be corrected by this method (Nevas *et al.*, 2014). This limitation for pure UV spectroradiometers might be overcome by characterizing the stray light using an additional parallel-measuring spectroradiometer with an extended wavelength range (Nevas *et al.,* 2014). However, such a correction method requires knowledge about the OoR spectrum not only during the instrument characterization and calibration but also during the measurement of the unknown radiation source, which might be not possible due to limitations of the input optics. By analyzing the measurement results of such a sophisticated system, with additional mathematical OoR correction, of Nevas *et al.* (2014) it can be stated that for instance the

specifications for stray light S2 instruments specified by WMO (Seckmeyer *et al.* (2001) cannot be achieved.

This short introduction of the mathematical correction approaches shows that these approaches can be quite effective. However, its practical capability is limited especially for spectroradiometric measurements in the UV spectral range.

2.3.2 Spectral snapshot imaging technologies

In recent years, new technologies for detecting multiple spatial channels (measurement channels) simultaneously for multiple wavelengths have been developed (Hagen and Kudenov, 2013; Content, 1997; Henault *et al.*, 2004; Matsuoka *et al.*, 2002; Gehm *et al.*, 2007; Wagadarikar *et al.*, 2008; Gao *et al.*, 2010; Riechelmann *et al.*, 2013). These are so-called spectral snapshot imaging technologies. With the help of such a measurement devices, for instance temporal effects of spectral radiance distributions can be analyzed in higher temporal resolution since no angular or spectral scanning is needed (Riechelmann *et al.*, 2013).

In the publication of Hagen and Kudenov (2013) an overview of 13 known approaches/technologies is published. In research article C of this thesis, on page 58 and 59 of this work, a selection of these approaches is presented.

In most cases, the application with its requirements (spatial and spectral resolution, wavelength range, size of the measurement object/FOV, optical stray light performance, etc.) or boundary conditions (possible size of the measurement device, costs, etc.) restricts the approaches to be considered. The IFS-F approach, which was selected by Riechelmann *et al.* (2013) and Seckmeyer *et al.* (2018), seems to be an appropriate choice for the application of hemispherical spectral snapshot imaging measurements as long as the large number of optical fibers and possible resulting mechanical challenges do not limit the application. One challenge, is the transport of such a measuring system from the laboratory to the location of the outdoor measurement, as the fiber bundle may need to be removed (Riechelmann, 2014). In Riechelmann (2014) this fiber bundle removing and attaching introduced a wavelength shift of about 1.2 nm, which was corrected by an additional wavelength calibration at the location of the outdoor measurement.

3. Scope of this thesis

Section 2.3.1 (Stray light correction methods for array spectroradiometers) briefly exemplified that internal stray light effects are a limiting factor for many applications of array spectroradiometers in the UV spectral region. In the **research articles A and B** the following major research objective has been treated:

〉 Development of a stray light correction procedure for array spectroradiometers in order to achieve comparable stray light performance as double monochromators in the UV spectral range

Research article A focused on the following objectives:

〉 Adaption of a measurement device based on the developed procedure for direct solar irradiance measurements in the UV
〉 Quality assessment at an international measurement campaign for total ozone column (TOC) and spectral direct solar irradiance with reference devices like Dobson, Brewer and QASUME (double Monochromator based traveling reference spectroradiometer)

In **research article B** the objectives have been:

〉 Adaption of a measurement system based on the developed procedure for global solar irradiance measurements in the UV to NIR
〉 Quality assessment by an intercomparison of the newly developed devices to a double monochromator based NDACC system

As described in Section 2.3.2 (

Spectral snapshot imaging technologies), there has been recent progress in the development of spectral snapshot imaging devices for radiometric measurements. However, the large amount of optical fibers of the IFS-F approach can lead to mechanical challenges in some applications. Therefore, the research goals of the presented **research article C** are:

〉 Development of a new technique for spectral snapshot imaging based on only a few optical components (without optical fibers)
〉 Investigation whether a higher number of measurement channels can be achieved
〉 The FOV should be adaptable for different spectral radiance measurement tasks, such as a rectangular or hemispherical FOV

In the Chapter 4, the fundamental concepts and methods, which are used in the research articles A to C, are presented. The research articles itself are shown in the Chapter 5. This is followed by a discussion and conclusions in Chapter 6. Chapter 7 will finally give some outlook for further possible research objectives and open questions.

4. Methods

Section 4 describes the methods, which are used in the research articles of section 5. In section 4.1, the most important measurement device characterization steps are introduced. Section 4.2 shows the applied wavelength and radiometric calibration. In section 4.3 interpolation and in section 4.4 peculiarities of spectral snapshot imaging technologies are given.

4.1 Characterization of array spectroradiometers

The characterization of a spectroradiometer is an important process for analyzing the expected measurement performance, e.g. by the means of a measurement uncertainty determination (Bernhard and Seckmeyer, 1999). The characterization data of the BTS2048-UV-S, which is introduced in research article A, was the basis for the uncertainty evaluation of Vaskuri *et al.* (2018). Furthermore, characterization data can very often used as the basis for correction methods (Zong *et al.*, 2006; Nevas *et al.*, 2012b; CIE, 2019)

4.1.1 Dark Signal, Linearity and Dynamic range

Pulli *et al.* (2017) stated in his discussion section "a nonlinearity correction is required in order to reach low uncertainties". He analyzed two array spectroradiometers and showed non-linearity standard deviations of 10% before and 1.4% respectively 3.5% after correction. Due to given large differences (irradiance and its spectral distribution) between the calibration lamp (typically tungsten lamps) and the solar radiation, according to Pulli *et al.* (2017) it is especially important to perform a non-linearity correction. Bernhard and Seckmeyer (1999) and Cordero *et al.* (2008) show as well that a non-linearity correction can reduce the measurement uncertainty. The main non-linearity contributions for array spectroradiometers are the array detector and the signal processing electronics (Pulli *et al.*, 2017; Nevas *et al.*, 2012a). As well, a non-linear relationship between detector signal and temperature may be present (Luke *et al.*, 2014; Starks *et al.*, 1995). For the non-linearity characterization different approaches are applicable (Nevas *et al.*, 2012a; Fu *et al.*, 2014; Schubert *et al.*, 2015; Pacheco-Labrador *et al.*, 2014; Baczynska *et al.*, 2016; Salim *et al.*, 2011; CIE, 2019) and a correction can be applied after each measurement (Salim *et al.*, 2011; William *et al.*, 2004; CIE, 2019).

Since most CCD or CMOS sensors show a certain signal level even without illumination, many spectroradiometers use a so-called dark signal measurement (sometimes also called baseline measurement), which is captured and subtracted from each measurement by shuttering the detector (Neumann, 2014; Bohn and Lohse, 2017). The dark signal itself shows a dependency on the integration time and is pixel and temperature dependent (Seckmeyer *et al.*, 2010). Accordingly, the dark signal is captured at the same integration time as the later measurement and is subtracted pixel wise. For higher stability some spectroradiometers use temperature controlled detectors by thermoelectric Peltier devices (Luke *et al.*, 2014; Baczynska and Khazova, 2015). To reduce the contribution of noise of the dark signal measurement, it is appropriate to apply averaging (Dezhi *et al.*, 2010; Neumann, 2014).

The lower end of the measurement devices usable dynamic range is reached if the measured signal does not exceed the noise level anymore by maximum integration time; hence cannot be detected with a certain confidence level (SNR = 1). This lower end of the usable

dynamic range is often called detection threshold (Seckmeyer *et al.*, 2010; Neumann, 2014). If the detector, respectively single pixels, run in saturation by exceed its full well capacity by shortest possible integration time, the maximum of the dynamic is reached (Neumann, 2014).

The measurement devices used in the research articles of this thesis possess a shutter for dark signal measurements and correction. The CCD detectors are temperature controlled and a non-linearity characterization and correction has been applied. According to Vaskuri *et al.* (2018) the uncertainty contribution of non-linearity is below 0.8% (k=2) for the measurement devices used in research article A and B, which is an improvement since it is significantly lower as the contributions stated by Pulli *et al.* (2017). The prototype of research article C represents a feasibility study, which is why a complete uncertainty analysis has not yet been carried out.

4.1.2 Optical bandwidth

The range of wavelength passed by a spectrometer or spectroradiometer with finite resolution at a given wavelength setting is determined by the line spread function (LSF), also called slit function (CIE, 2014). The LSF can be determined by the measurement with for instance a tunable laser (Zong *et al.*, 2006). Based on the LSF the optical bandpass function can be determined, which is mathematically derived in detail in the technical report CIE (2014) on page 4. Finally the CIE (2014) defines the optical bandwidth as half of the full base-width of the bandpass function. Since this definition requires the signal "to go to zero" (CIE, 2014 page 4), a procedure for practical implementation is also given in CIE (2014). However, in this thesis the widely used definition of the WMO documents Seckmeyer *et al.* (2001) and Seckmeyer *et al.* (2010) is used as a specification for the optical bandwidth. In Seckmeyer *et al.* (2001) the optical bandwidth, which is usually expressed in *nm,* is defined as the FWHM (full width at half maximum) of the spectroradiometers slit function.

Bandwidth has the effect of broadening and reducing peaks of the spectral distribution to be measured (CIE, 2014). The unbroadend spectrum is called "true spectrum" (CIE, 2014 page 6). To obtain this "true spectrum" so-called bandpass correction methods have been developed (CIE, 2014). The first method of Stearns and Stearns (1988) can be applied for triangular bandpass functions. The advanced methods of Ohno (2005) or Woolliams *et al.* (2011) can be applied for every shape of bandpass function. This is as well true for the method of Eichstädt *et al.* (2013), which uses an iterative method based on a Richardson-Lucy algorithm. It is important to mention that no correction method can provide perfect correction (CIE, 2014).

The FWHM of the different measurement devices used in this thesis were measured with a tunable light source (OPO). No bandpass correction was applied to measurements.

4.1.3 Stray light

The CIE (2011b) defines two different types of stray light. The first type is often called, according e.g. Zong *et al.* (2006), spectral or internal stray light. The CIE definition is "radiation that reaches the detector, which is at a wavelength other than that which is intended to be measured" (CIE, 2011b definition 17-1271, 3). Similar definitions can be found in Neumann (2014) or Pribram and Penchina (1968). The second type of stray light, according to CIE (1996) or CIE (2011b) called spatial or external stray light, is defined as "light that reaches the detector in a measurement system from directions other than the direct path from the light source to

the detector, e.g. radiation scattered from walls, ceilings or optical components within the measuring system" (CIE, 2011b definition 17-1271, 2).

External stray light is a part of the measurement uncertainty budget and not part of the spectroradiometer characterization itself (CIE, 2018). In the following, if not stated differently, with stray light the spectral stray light is meant.

It should be noted that spectral stray light itself is further differentiated in near-field and far-field stray light (see Figure 7). In the following Table 3 an overview of the most frequent sources is given.

Table 3 Overview of the most frequent sources of stray light. Otherwise specified differently this information is taken from Neumann (2014), Zong *et al.* (2006), Nevas *et al.* (2012b), Fest (2013) and CIE (2019).

Type of stray light	Source
Near-field stray light	Inter-reflection on the detector and its entrance window or blocking filters (2nd order filter, etc.).
Far-field stray light	Scattering on optical components
	Zero order reflection of the optical grating
	Reflections from the spectrometer inside walls
	Inter-reflections between optical parts
	Higher diffraction orders
	Grating ghosts: Ruled diffraction gratings are mostly produced by a master. If this master shows systematic errors in the grooving spacing, so-called grating ghosts can origin.

The stated effects of Table 3 can be characterized by for instance a LSF measurement (Zong *et al.*, 2006), see Figure 7.

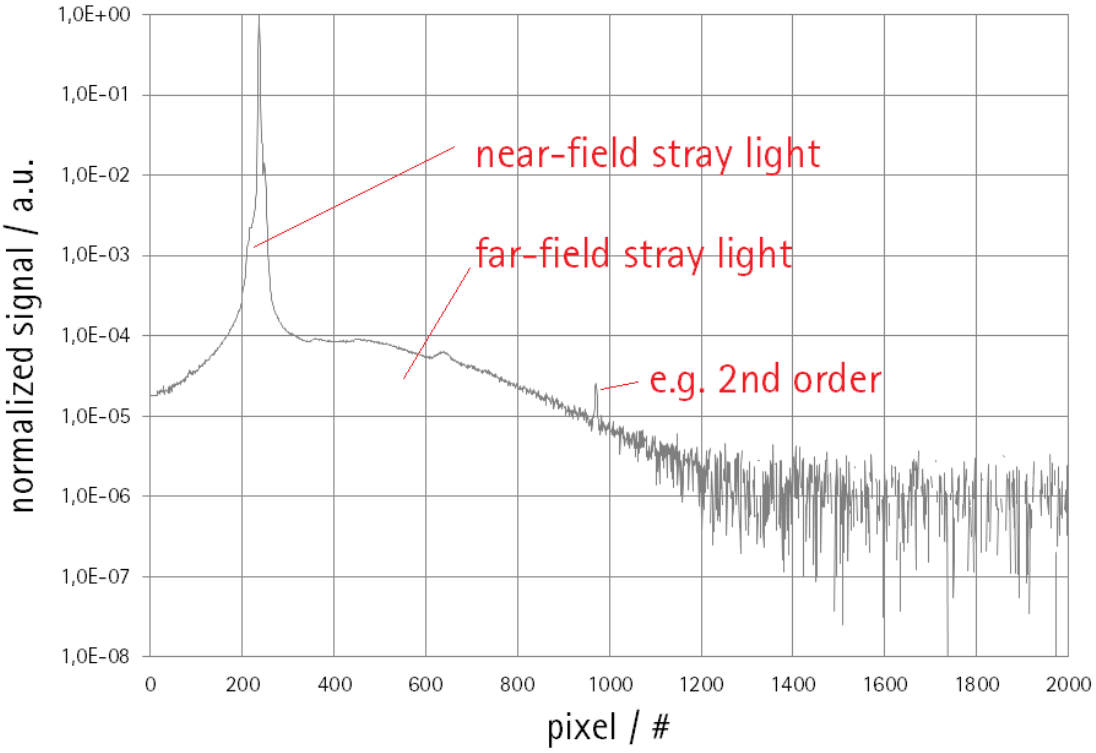

Figure 7 LSF of a BTS2048-VL-TEC array spectroradiometer measured with a tunable laser source. Near-field and far-field characteristic with different signal levels and some specific details like the 2nd order of the diffraction grating are noticeable.

For the characterization of stray light a widely used method is the measurement of a filter transmission (e.g. GG475) with a broadband source (e.g. a halogen lamp) illumination (Nevas and Sperfeld, 2015; Seckmeyer *et al.*, 2010). Within the blocking wavelength range of the filter, no transmission should be measured (if filter is blocking sufficiently and does not fluorescence). Accordingly, signal measured in the blocking region represents stray light (superimposed by noise); see Figure 8.

The atmospheric absorption by ozone at about 290 nm acts like a transmission filter (Läuchli, 1929; Meyer, 1903), hence the measurement data can be used for stray light characterizations. This method was used in research article B for stray light characterization by solar irradiance measurements.

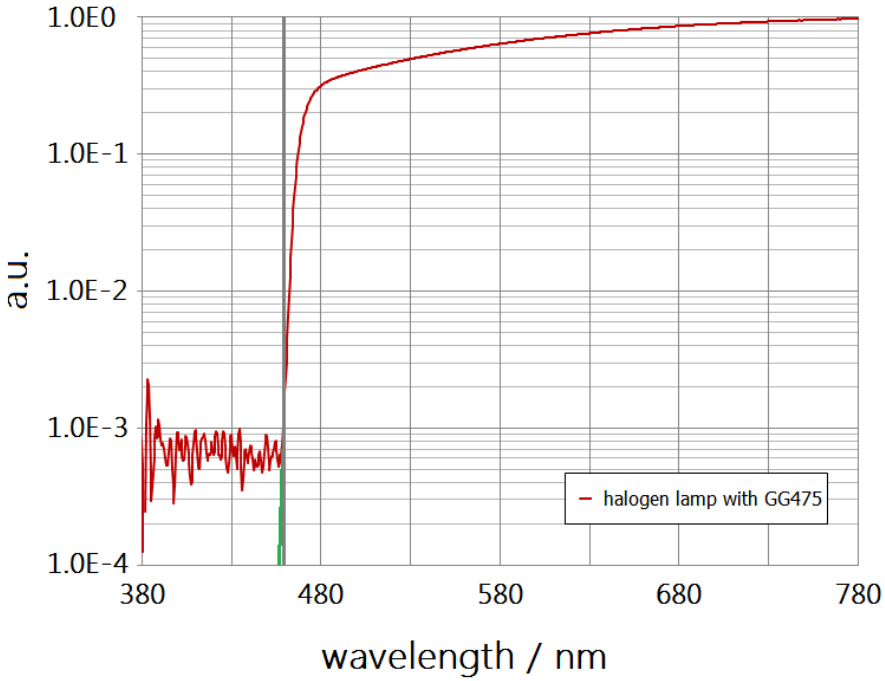

Figure 8 Transmission measurement of a GG475 filter with a halogen lamp as light source on an optical bench with BTS2048-VL-TEC spectroradiometer. The signal left of the grey marked border represents measurement noise superimposed with stray light (the real signal is extrapolated in green). This procedure gives an estimation for the stray light performance including out of range stray light of a spectroradiometer. However, a distinction between stray light and noise is difficult at low stray light levels.

In Section 2.3.1 state of the art correction methods for stray light are introduced.

4.1.4 Input optics and channel cross-talk

The input optics is part of the measurement system since its properties affect the radiometric calibration of the device or the optical bandpass since it determines how the entrance slit is illuminated (Nevas and Sperfeld, 2015). This is the reason why a spectroradiometer should always be characterized, if possible, with the same input optics that is used for the measurement (ISO/CIE, 1984; Nevas and Sperfeld, 2015).

The input optics itself must be characterized regarding the radiometric quantity that shall be measured. For spectral irradiance measurements a diffusor optics or integrating spheres with a low cosine error are used (ISO/CIE, 1984). The most common characterization is the angular response index $f_2(\lambda)$ which is described in ISO/CIE (2014). This characterization was applied in research article B.

For the measurement of spectral radiance usually imaging optics are used (ISO/CIE, 1984). A characterization is made by means of directional quality indexes, for instance the directional response index $f_{2,g}$ (ISO/CIE, 2014). However, this directional response index was designed for radiance devices with one measurement channel. Its applicability and its meaningfulness for a spectral snapshot imaging device is limited. A more meaningful characterization is for instance the determination of the angular response function of all measurement channels (E. Greivenkamp, 2004). This characterization was used in research article A and C.

Channel-to-channel crosstalk (often called channel crosstalk) degrades the measurement quality/increases the measurement uncertainty (Hagen and Kudenov, 2013; Feinholz *et al.*,

2012). The characterization of channel crosstalk can be very challenging and a great effort since in principle every single measurement channel has to be illuminated individually and the effect of this measurement to all other channels has to be evaluated (Neumann, 2014; Feinholz *et al.*, 2012). Furthermore, this evaluation has to be performed for many wavelength bands separately. However, by using the data of this characterization a mathematical correction can be performed following the concept of Feinholz *et al.* (2012).

A channel crosstalk characterization without correction was performed for the developed spectral snapshot imaging device in research article C.

4.1.5 Ambient conditions

Spectroradiometers which are used for field measurements are exposed to temperature and/or humidity differences. A temperature change can introduce a change in the mechanical setup which leads to a wavelength shift (Neumann, 2014; Bernhard and Seckmeyer, 1999), hence is a contribution to the measurement uncertainty. To reduce this uncertainty usually the spectroradiometer is incorporated in a temperature-controlled watertight box for field measurements (Bernhard and Seckmeyer, 1999).

The spectroradiometers developed/applied in research articles A and B exhibit a temperature controlled weatherproof housing.

4.2 Calibration of array spectroradiometer

4.2.1 Wavelength calibration

Common procedures for wavelength calibration (pixel to wavelength scale determination) of an array spectroradiometer are based on the measurement of e.g. atomic emission sources (Hg, Kr, Ne, Ar, etc.), or achieved on a set of lasers, or on etalons (interference patterns), or on absorption filters (CIE, 2019). For a definition of the wavelength scale with low uncertainty as many data points (detector pixel position with corresponding wavelength reference) as possible should be measured, ideally equally spaced over the whole wavelength range of the device (CIE, 2019). Different procedures can be combined to achieve this, e.g. the measurement of emission sources like Hg lamps with some additional laser lines. In the following literature more information can be found (Gaigalas *et al.*, 2009; Hopkinson *et al.*, 2004; Young and Häring, 2011; Martinsen *et al.*, 2008; CIE, 2019). For the interpolation between the measurement points, usually lower order polynomials are used (CIE, 2019). An extrapolation should be avoided if possible to introduce no additional uncertainty (Nevas and Sperfeld, 2015; CIE, 2019).

To validate the wavelength calibration and to check it, regular measurements of a reference light source may be of advantage (Nevas and Sperfeld, 2015). This could be performed for instance with a low pressure mercury (Hg) emission lamp which might be as well used in measurement campaigns for weekly checks (Bernhard and Seckmeyer, 1999). In addition Fraunhofer lines of solar radiation can be used for a wavelength check or correction (Egli, 2014).

Bernhard and Seckmeyer (1999) stated that already small wavelength alignment errors at solar measurements lead to a significant measurement uncertainty for spectral irradiance, due the strong decline in the UVB with decreasing wavelengths. Furthermore Bernhard and

Seckmeyer (1999) showed that for their used spectroradiometer a wavelength uncertainty of 0.04 nm causes an uncertainty of 0.7% for erythema weighted irradiance.

For the research article A and B the calibration was performed with atomic emission sources and a tunable laser. Furthermore a wavelength correction was done by the help of Fraunhofer lines according to Egli (2014). For research article C atomic emission sources where used.

4.2.2 Radiometric calibration and measurement uncertainty

The spectral responsivity of an array spectrometer system is mainly determined by the spectral responsivity of the detector, the spectral transfer function of the spectrometer unit (optical grating, optical mirrors, optical filters, etc.) and the spectral properties of the input optics (Neumann, 2014; Nevas and Sperfeld, 2015; CIE, 2019). For an absolute radiometric measurement, the measured raw signal must be related with the so-called radiometric calibration to a radiometric quantity (Germer *et al.*, 2014; Neumann, 2014; ISO/CIE, 1984; CIE, 2019).

A measurement of a calibration source, according to the calibration certificate description, is the basis for the radiometric calibration (Nevas and Sperfeld, 2015). The calibration source, also called calibration standard, should be traceable to a National Metrology Institute (NMI) like the Physikalisch-Technische Bundesanstalt (PTB) in Germany (ISO/CIE, 1984; Germer *et al.*, 2014). The spectral responsivity can be determined as:

$$r(\lambda) = \frac{S(\lambda)}{Cal(\lambda)} \tag{7}$$

where $S(\lambda)$ is the signal measured of the detector (e.g. count rate), $r(\lambda)$ the spectral responsivity and $Cal(\lambda)$ is the known spectral radiometric quantity of the calibration source as stated in the calibration certificate of the NMI.

The calibration setup for a specific radiometric quantity depends on the quantity itself. For this thesis, two setups are relevant. A spectral irradiance calibration setup which is described in ASTM (2012) for research article A and B and a setup for spectral radiance calibration (Pissulla *et al.*, 2009) for research article C.

For the quality assessment of a radiometric calibration according to CIE (2011a) a detailed measurement uncertainty budget of the whole calibration process is required. Contributions of the specific setup and measurement device (e.g. homogeneity within the FOV, lamp current, alignment of FOV, shielding of spatial stray light) and the calibration standard (obtained uncertainty of the NMI) have to be considered for this evaluation (Nevas and Sperfeld, 2015; CIE, 2011a, 2018).

The resulting so-called calibration uncertainty is the basis for the measurement uncertainty, which has to be determined for each specific measurement scenario separately. Beside the calibration uncertainty contributions as non-linearity, internal stray light, temperature dependency, etc. have to be considered (CIE, 2018). Bernhard and Seckmeyer (1999) and Cordero *et al.* (2013) published a detailed analysis for spectral solar UV irradiance measurements, Vaskuri et al. (2018) for total ozone derived from direct solar irradiance measurements.

4.3 Interpolation

Measurement data of spectroradiometers is commonly recorded in certain wavelength steps, for instance in the pixel/wavelength assignment of an array spectroradiometer. Since this assignment is usually nonlinear (see section 4.2.1) and different for each measurement device an interpolation of the data to equidistant wavelength steps might be needed in order to compare measurement results of different devices (Egli, 2014). Different interpolation methods (linear, cubic spline, polynomial, etc.) and fitting based interpolation methods exist (least square fit, polynomial fit, etc.) (Gardner, 2003; CIE, 2019). Depending on the sampling, the spectral shape of the measurement and the interpolation method an additional uncertainty might be introduced (Gardner, 2003).

Beside the interpolation of measurement results, the interpolation of the calibration standard used for the calibration of the device contributes to the overall uncertainty (CIE, 2019). Bernhard and Seckmeyer (1999) analyzed the introduced uncertainty within the scope of solar UV measurements. The results showed an uncertainty of $\pm 0.1\%$ for a quartz halogen lamp as long as no absorption and emission lines are present.

In this work, polynomial fits are used for wavelength calibration and cubic spline and linear methods for the interpolation of spectral distributions.

4.4 Peculiarity of spectral snapshot imaging technologies

The peculiarities are given by the multiple measurement channels compared to single channel devices. This advantage goes hand in hand with more complexity in many aspects.

The whole characterization and calibration process (wavelength calibration, radiometric calibration, FOV characterization, etc.) has to be performed for each measurement channel. Consequently, this process is more sophisticated and time consuming since the number of measurement channels is easily in the hundreds like for MUDIS of Riechelmann *et al.* (2013). Some of the characterizations might be done simultaneously, like the wavelength calibration of all measurement channels. However other characterizations like the FOV determination or correction methods like the mathematical stray light correction according to Zong *et al.* (2006) need to be performed for each measurement channel separately (Feinholz *et al.*, 2012).

Furthermore, an additional characterization step might be needed to establish a correlation between the measurement channels on the detector and the FOV. One possible method has been descripted in research article C on page 50, where the measurement data of a unique test pattern is used for the correlation.

In addition to this sophisticated characterization and calibration process, further challenges must be solved during data analysis. The usually large amount of spectral snapshot imaging measurement data results in 3D plot representations, which need to be analyzed. One possible solution is illustrated in Figure 9, where the focus of data presentation is the RGB image. As a result, it can be difficult to visualize the spectral distribution for every measurement channel. Since many different presentations are possible, in many cases the way of visualization is chosen to satisfy the requirement of the particular application. In Riechelmann *et al.* (2013)) for instance a RGB image is shown for different wavelengths of interest. In some cases interactive figures are needed (e.g. mouse over the measurement channels shows the spectral distribution next to it), for this purpose whole software packages have been developed (Kruse *et al.*, 1993; Mazer *et al.*, 1988).

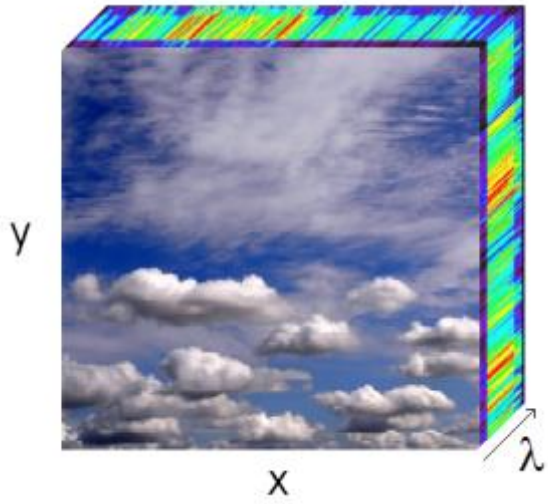

Figure 9 Schematical illustration of a spectral snapshot imaging measurement. The 2D picture requires a third dimension for spectral data.

5. Research articles of this cumulative thesis

In this Chapter the peer-reviewed publications of this cumulative thesis, which have been written during this PhD work, are presented. The declaration of the contribution of the author is given at the beginning of each Research article.

Research article A (section 0): A compact array spectroradiometer that enables measurements of solar UV spectral direct irradiance is presented. The internal stray light, which is often the limiting factor for array spectroradiometer measurements in the UV spectral range, is physically reduced with an optical filter approach so that no other stray light correction methods, such as mathematical corrections, are necessary. The instrument has been extensively characterized by Peter Sperfeld and Saulius Nevas at the Physikalisch-Technische Bundesanstalt (PTB). During an international total ozone measurement intercomparison at the Izaña Atmospheric Observatory in Tenerife, the applicability of the instrument was verified with measurements of the direct solar irradiance and subsequent TOC evaluations based on the spectral data measured between 12 and 30 September 2016. A TOC retrieval algorithm developed by Stefan Riechelmann (PTB) and Gunther Seckmeyer (IMuK) was used. The results showed deviations of the TOC of less than 1.5 % from most other instruments in most situations and not exceeding 3 % from established TOC measurement systems such as Dobson, Brewer or the QASUME traveling reference meter. The manuscript has been published in Atmospheric Measurement Techniques (AMT).

Research article B (section 0): Content of this publication is an intercomparison of two compact array spectroradiometers with a NDACC (Network for the Detection of Atmospheric Composition Change) device in a measurement campaign between 15 and 18 May 2017 at the Institute of Meteorology and Climatology of the University of Hannover (IMuK). The solar global spectral irradiance from 280 nm to 430 nm was measured by an array spectroradiometer similar to the one from Research article A. The other device is designed for the VIS to NIR spectral region (280 nm to 1050 nm). For the intercomparison both devices have been characterized and calibrated. Beside the solar global spectral irradiance, as well integrated quantities (UV-Index and Blue Light Hazard, both introduced in the article) have been compared during the day. The deviation for UV index measured by the UV device is within ±1% for solar zenith angles (SZA) below 70° and increased to a maximum of ±3% for SZA between 70° and 85° when synchronization in time between measurements was possible. The deviation of global spectral irradiance is smaller ± 2.5% in the spectral range from 300 nm to 420 nm (evaluated for SZA below 70°). The VIS device achieved the same deviation for Blue Light Hazard as the UV device for the UV index. The evaluations of global spectral irradiance data of the VIS device show a deviation smaller than ±2% in the spectral range from 365 nm to 900 nm (evaluated for SZA below 70°). Below 365 nm, the deviation rises up to +7% at 305 nm due to remaining stray light. The agreement within the limited time of the intercomparison is considered to be satisfactory for a number of applications and provides a good basis for further investigations. The manuscript has been published in IOP Measurement Science and Technology.

Research article C (section 5.3): This article introduces a novel approach for detecting spectral radiance by a spectral snapshot imaging spectroradiometer. The technology is based on a facet mirror optics, which duplicates the field of view at the position of the entrance slit

of the spectroradiometer. The different measurement channels are then selected from these duplicated images by a customized aperture, which acts additionally as an entrance slit of the spectrometer. A prototype with 196 measurement channels (14 x 14) was developed and characterized. This prototype has been designed for two different measurement tasks. A proof of concept measurement of a 10 mm x 10 mm test pattern in the spectral range of 380 nm to 800 nm with 10 nm optical bandwidth (FHWM) and a measurement of the sky zenith radiance with a FOV of 0.5° in the spectral range of 280 nm to 470 nm with 3 nm optical bandwidth (FWHM). Furthermore, the potential of the measurement system by adapting an entrance optics for hemispherical measurement with a FOV of 17° to 74°, developed by Ansgar Stührmann (IMuK), are pointed out. The manuscript has been published in IOP Measurement Science and Technology.

List of additional publications/conference contributions:

The following publications or conference papers refer to this thesis and are therefore listed here:

- Ralf Zuber.: Effective stray light suppression with the BTS2048-UV series array Spectroradiometer, UV News 12, 2017
- Ralf Zuber, Peter Sperfeld, Stefan Riechelmann, Saulius Nevas, Meelis Sildoja.: A stray light corrected array spectroradiometer for complex high dynamic range measurements in the UV spectral range,13th International Conference on New Developments & Applications in Optical Radiometry (NEWRAD 2017), SSR-PB-3, Tokyo, 2017
- Ralf Zuber, Mike Clark, Peter Sperfeld.: A stray light corrected array spectroradiometer for complex high dynamic range measurements in the UV spectral range, International Conference 'UV LED Technologies & Applications' (ICULTA-2018), Berlin, 2018
- Ralf Zuber, Peter Sperfeld, Stefan Riechelmann, Saulius Nevas, Meelis Sildoja.: Ein streulichtkorrigiertes Array-Spektroradiometer für komplexe hochdynamische Messungen im UV-Spektralbereich, DACH-Meteorologentagung, Garmisch-Partenkirchen, 2019
- Ralf Zuber, Mario Ribnitzky.: Combined Out-of-Range and In-Band Stray Light correction for array spectroradiometers, 29th Session of the CIE, Washington DC, 2019

5.1 Article A: Adaption of an array spectroradiometer for total ozone column retrieval using direct solar irradiance measurements in the UV spectral range

5.1.1 Declaration of my contribution

The author of this thesis adapted the BTS2048-UV-S-WP, which was developed by the author of this thesis (declaration of contribution of this device, see Section 5.2.1), together with Peter Sperfeld for direct solar irradiance measurements. The author of this thesis characterized and prepared the measurement system together with colleagues of Gigahertz-Optik GmbH. Peter Sperfeld and Saulius Nevas performed the characterizations at the Physikalisch-Technische Bundesanstalt (PTB). Peter Sperfeld and the author of this thesis prepared the international measurement campaign in Izaña, Tenerife. Peter Sperfeld carried out most of the measurements in Izaña; the author of this thesis supported the measurements in Izaña on several days. Stefan Riechelmann and Gunther Seckmeyer developed the TOC algorithm and Stefan Riechelmann carried out the TOC determination.

5.1.2 Published article

This article has been published with open access in Atmospheric Measurement Techniques.

Submitted: 14 July 2017
Accepted: 06 September 2017
Published: 27 April 2018

Zuber, R., Sperfeld, P., Riechelmann, S., Nevas, S., Sildoja, M., and Seckmeyer, G.: Adaption of an array spectroradiometer for total ozone column retrieval using direct solar irradiance measurements in the UV spectral range, Atmos. Meas. Tech., 11, 2477-2484, https://doi.org/10.5194/amt-11-2477-2018, 2018.

DOI: https://doi.org/10.5194/amt-2017-240l

Atmos. Meas. Tech., 11, 2477–2484, 2018
https://doi.org/10.5194/amt-11-2477-2018

Atmospheric Measurement Techniques
Open Access
EGU

Adaption of an array spectroradiometer for total ozone column retrieval using direct solar irradiance measurements in the UV spectral range

Ralf Zuber[1], Peter Sperfeld[2], Stefan Riechelmann[3], Saulius Nevas[2], Meelis Sildoja[2], and Gunther Seckmeyer[3]

[1] Gigahertz-Optik GmbH, 82299 Türkenfeld/Munich, Germany
[2] Physikalisch-Technische Bundesanstalt (PTB), Bundesallee 100, 38116 Braunschweig, Germany
[3] Leibniz Universität Hannover, Institute of Meteorology and Climatology, Hannover, Germany

Correspondence: Ralf Zuber (r.zuber@gigahertz-optik.de) and Peter Sperfeld (peter.sperfeld@ptb.de)

Received: 14 July 2017 – Discussion started: 28 September 2017
Revised: 28 February 2018 – Accepted: 5 April 2018 – Published: 27 April 2018

Abstract. A compact array spectroradiometer that enables precise and robust measurements of solar UV spectral direct irradiance is presented. We show that this instrument can retrieve total ozone column (TOC) accurately. The internal stray light, which is often the limiting factor for measurements in the UV spectral range and increases the uncertainty for TOC analysis, is physically reduced so that no other stray light reduction methods, such as mathematical corrections, are necessary. The instrument has been extensively characterised at the Physikalisch-Technische Bundesanstalt (PTB) in Germany. During an international total ozone measurement intercomparison at the Izaña Atmospheric Observatory in Tenerife, the high-quality applicability of the instrument was verified with measurements of the direct solar irradiance and subsequent TOC evaluations based on the spectral data measured between 12 and 30 September 2016. The results showed deviations of the TOC of less than 1.5 % from most other instruments in most situations and not exceeding 3 % from established TOC measurement systems such as Dobson or Brewer.

1 Introduction

Many applications in the ultraviolet spectral range cannot be addressed with array spectroradiometers since they are often limited by internal stray light effects (Egli et al., 2016). An example is an accurate measurement of solar irradiance in the UV-B spectral range. The intense radiation of the sun in the visible (VIS) and infrared (IR) generates stray light within the spectrometer, which often dominates over the less intense solar UV-B radiation. However, an accurate measurement of solar spectrum (Seckmeyer et al., 2001, 2010) is the basis for an accurate evaluation of many derived quantities such as total ozone column (TOC; Dobson, 1931; Mayer and Seckmeyer, 1998). Hence, these measurements are often performed with double-monochromator-based systems (Hülsen et al., 2016), offering high stray light reduction capabilities. Operating such instruments is often time- and cost-intensive and requires controlled ambient conditions and highly experienced personnel.

To overcome such limitations, Gigahertz-Optik GmbH developed the BTS2048-UV-S series array spectroradiometer. The system conjoins compact instrument design, a physical-filter-based stray light correction and versatile radiomet-ric applicability. One of the newly developed devices has been adapted specifically for direct solar irradiance measurements and was extensively characterised at the Physikalisch-Technische Bundesanstalt (PTB) in Germany. It then took part in the ATMOZ intercomparison campaign in Izaña, Tenerife, in 2016 in the framework of the European Metrology Research Programme (EMRP) project ENV59 ATMOZ – a total ozone measurement intercomparison organised by the Izaña Atmospheric Research Center of the Spanish Meteorological Agency (AEMET) and the World Radiation Center (PMOD-WRC), where new instruments and techniques developed within the project were compared to well-established Dobson and Brewer methods.

Published by Copernicus Publications on behalf of the European Geosciences Union.

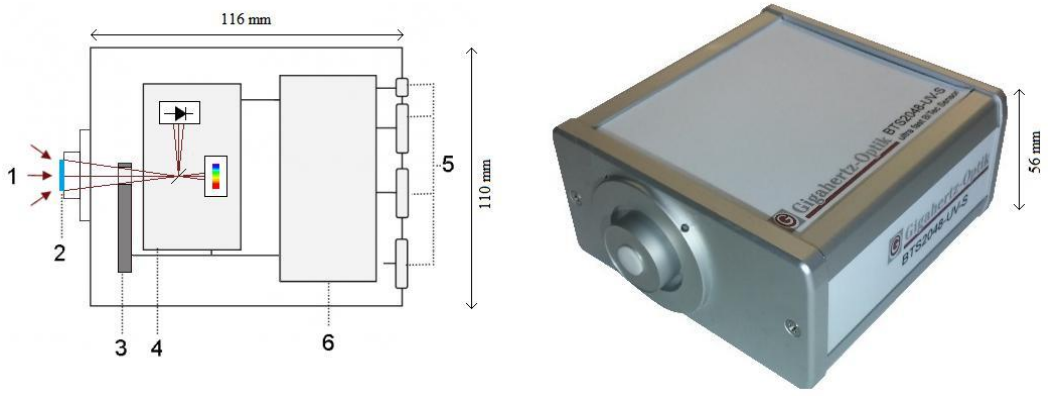

Figure 1. Schematical setup of the BTS2048-UV-S and photo of the instrument. (1) Incoming optical radiation, (2) direct entrance port with cosine diffuser, (3) filter wheel, (4) sensor system, (5) electrical connectors, (6) microprocessor for data processing and communication.

2 Instrument design

The BTS2048-UV-S series array spectroradiometers developed and manufactured by Gigahertz-Optik GmbH are based on the well-known Czerny–Turner (Shafer et al., 1964) spectrometer design. The spectrometer uses a temperature-controlled (8 C) back-thinned Hamamatsu CCD detector with 2048 pixels and an electronic shutter integrated in a compact optical bench with 16 bit analogue–digital converter (ADC) resolution. Integration times from 2 µs up to 60 s provide a high dynamic range of the instrument in the spectral range from 200 to 430 nm. The detector unit is complemented with a silicon carbide (SiC) photodiode to enable fast time-resolved radiometric measurements.

To enable stray light corrected measurements, a miniaturised filter wheel with up to six different optical filters is integrated into the optical path between the entrance optic and spectrometer unit (Fig. 1). A set of selected optical filters, such as bandpass- and edge-type filters, can be used to pre-select the radiation entering the sensor system. In the device one long-pass filter, a bandpass filter (298 to 390 nm) and four interference filters (centre wavelength: 254, 285, 300 and 400 nm) are integrated, which sufficiently block in the whole remaining spectral responsivity range of the detector. Hence, several sub-measurements with different filters in the optical path can be performed. The combination of these sub-measurements allows for optimised stray light reduced spectra. In addition, multiple different combinations of filters, integration times and sub-measurements optimise the measurement scenario to any kind of specific radiometric application. For instance, a so-called out-of-range (OoR) stray light correction method has been implemented, where an additional measurement with a long-pass filter is performed to quantify contribution of the out-of-range stray light to the measured signal, which can then be subtracted. In order to perform reliable solar UV measurements, a specific measurement scenario, the so-called solar bandpass correction method, was used. This measurement scenario is based on a series of measurements with several narrow-bandpass filters which complement each other (Shaw and Goodman, 2008). Hence, the overall measurement time to get a full spectral measurement is the sum of all integration times of the sub-measurements. Typically, this measurement time is in the range of a few seconds, depending on the light source to measure. This active stray light correction process is a straightforward alternative to mathematical stray light correction methods that have been established for array spectroradiometers (Zong et al., 2006; Nevas et al., 2012). In some cases, e.g. when silicon (Si) detectors are used solely in the UV spectral range, the introduced technology can reduce the stray light more efficiently. The mathematical stray light correction methods are based on a precise characterisation of the optical imaging performance with so-called line spread functions (LSFs). These functions should be determined at each detection wavelength of the spectroradiometer. This so-called in-range stray light can be corrected to improve the measurement threshold by about 2 orders of magnitude (Zong et al., 2006). However, this correction method is not able to correct for so-called out-of-range stray light that is generated in spectral intervals outside the spectroradiometer range where the detector used is still sensitive. If, for instance, a Si-detector-based spectroradiometer is designed for the spectral range from 200 to 400 nm, the in-range stray light can only be corrected for this spectral range. However, the Si detector itself is radiation-sensitive up to 1100 nm, and stray light originating from this out-of-range spectral region cannot be characterised with LSFs. This limitation might be resolved by measuring the responsivity of the spectroradiometer to the radiation at OoR wavelength using a calibrated detector or an additional spectroradiometer with extended wavelength range, for Si ideally up to 1100 nm (Nevas et al., 2014). However, such a correction method requires knowledge about the OoR spectrum not only during instrument calibration, which generally is readily available from the standard lamp calibration data, but also for the radiant sources under investigation, e.g. the direct solar irradiance, which may not

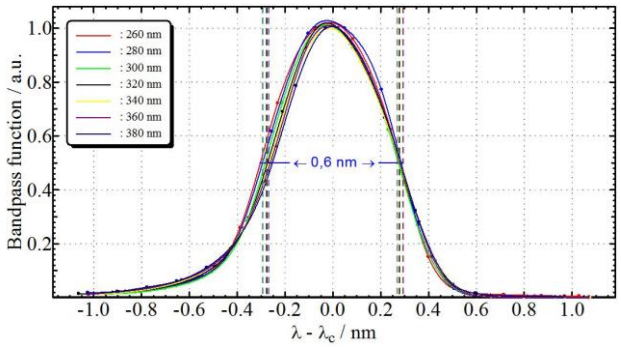

Figure 2. Bandpass function around centroid λ_c for different wave-lengths with bandwidth (FWHM, dashed lines) indicated.

be available for practical reasons. Hence, the presented optical-filter-based stray light correction technology of the BTS2048-UV-S series offers an attractive alternative, especially in the UV range.

3 Characterisation

At PTB, several instrument parameters have been characterised to verify the quality and measurement capability of the BTS2048-UV-S. The wavelength calibration was performed with the help of wavelength-tuneable laser systems and checked using mercury pen lamps. The uncertainty for the wavelength calibration was found to be better than 0.1 nm. For measurements of solar irradiance however, the wavelength scale was additionally adapted with standard deviations (SDs) better than 0.02 nm to the solar Fraunhofer lines using the MatShic algorithm (Egli et al., 2014). The spectral bandpass was determined using LSFs measured with tuneable laser systems (Nevas et al., 2014). The bandpass function appears to be nearly symmetrical below 360 nm with an average bandwidth of 0.6 nm, full width at half-maximum (FWHM) (see Fig. 2).

The linearity of the BTS2048-UV-S was tested using both the integration time and the irradiance variation methods (Pulli et al. 2017). For the integration time method, the spectral irradiance of the incident radiation is kept constant while the instrument's integration time is varied over a wide range. Although the measurement signal in raw counts then varies with the integration time, the normalised count rates per second should remain constant for all measurements. The irradiance variation is performed at constant integration times of the instrument, while the irradiance is linearly reduced between each measurement. Here the ratio of measurement signal (count rate) and spectral irradiance should remain constant for all measurements. By applying a mathematical correction for non-linearity, the spectrometer showed linearity with a deviation smaller than 1 % over the full dynamic range for the characterised measurement mode. For spectral measurements the instrument saturation level is kept below 80 % to operate the instrument in an optimum between saturation and linearity. By using the solar bandpass-filter method, with adapted spectral integration times for each submeasurement, the dynamic range of the instrument could be extended. Whenever the non-linearity exceeds 1 % (at very low signals), a non-linearity correction is automatically applied.

Table 1. Measurement uncertainties for the spectral irradiance measurement.

Uncertainty component	Standard uncertainty/%
Radiometric calibration	0.8
Lamp stability	0.2
Non-linearity and stray light	0.4
Stability	0.8
Temperature dependence	0.1
Measurement noise	0.2
Wavelength shift	0.1
Combined uncertainty (k = 1)	1.24
Expanded measurement uncertainty (k = 2)	2.5

The instrument has been radiometrically calibrated using 250 W halogen lamps and 30 W deuterium lamps as transfer standards to perform spectral irradiance measurements traceable to the PTB (Sperfeld et al., 2010). In the overlapping spectral region of the two different lamp types between 280 and 360 nm the calibration matches well within the achieved measurement uncertainties. This demonstrates the good linearity and stray light suppression capability of the instrument. Although these standard lamps required a comparably long integration time, due to a high dynamic range of the instrument (typically 5×10^{-5} to 5×10^{4} W $(m^2$ $nm)^{-1}$ at 300 nm) it was possible to perform reliable measurements with very short integration times on high-power UV sources, such as medium-pressure mercury lamps, without the need for an additional attenuation.

The standard lamps used allow recalibration of the instrument in the laboratory and in the field. The resulting expanded measurement uncertainty (k D 2) was estimated as 2.5 % in the short wavelength range. The uncertainty contributions are listed in Table 1 (see also Vaskuri et al., 2018).

During the measurement campaign, described below, the radiometric calibration of the BTS2048-UV-S could be verified with a SD of less than 1 % compared to the calibrations in the laboratory before and after the campaign. During the campaign, the instrument was removed from the tracker at night to perform calibration measurements on a portable optical bench.

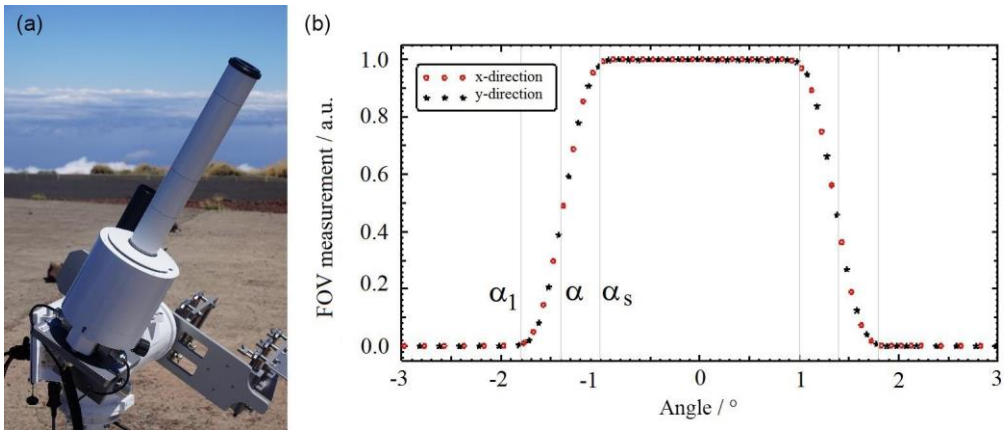

Figure 3. (a) The BTS2048-UV-S-WP modified for direct solar measurements mounted on a solar tracker at the Izaña Atmospheric Observatory in Tenerife. (b) Field-of-view (FOV) measurement in x and y direction for the entrance optics tube according to Blanc et al. (2014). $\alpha_s = 1°$ represents the slope angle, $\alpha_1 = 1.8°$ the limiting angle and $\alpha = 1.4°$ the half opening angle. The full opening angle results in $2 \times \alpha = 2.8°$.

4 Performance evaluation

4.1 Intercomparison of spectroradiometric measurements

For outdoor measurements of direct solar irradiance, a weatherproof (BTS2048-UV-S-WP) version of the BTS2048-UV-S was constructed. The instrument was integrated in a weatherproof housing which is temperature-controlled (ambient temperature range from - 25 to + 50 °C) and waterproof. During the 3-week measurement campaign in September 2016 at the Izaña Atmospheric Observatory (altitude: 2.373 m; coordinates: 28°18´32 N, 16°30´58 W), the typical temperature variation within the housing was below 0.1 °C (measured close to the spectrometer unit, with temperature set to 38 °C). There was cloudless sky during the measurements from which data have been used for this intercomparison. The housing was equipped with an entrance optic tube to limit the field of view to 2.8 (full opening angle; see Fig. 3). This tube is based on a baffle design to prevent stray light hitting the diffusor. Mounted on a solar tracker (EKO STR-32G) with a pointing accuracy of < 0.01°, the instrument measured direct solar irradiance. Solar measurements were performed using the solar bandpass correction method. Here, several narrow-bandpass filters are used in the spectral range between 280 and 420 nm. The single sub-measurements for every filter at varying integration times are subtracted by their assigned dark measurements with closed shutter and combined in their overlap region to one measurement of the full spectral range. This allows the steep slope of the solar spectrum to be measured below 300 nm with a high dynamic range (see Fig. 4). A full spectrum was recorded every 8 s. The duration of this measurement interval is mainly given by filter movement and dark-signal measurements, whereas the integration time for the measurements with different bandpass filters was optimised and varied with different solar zenith angles (SZAs). These settings allowed measurements with noise-equivalent irradiance in the range of 10^{-4} W (m^2 nm)$^{-1}$ (see Fig. 4).

The measurements were compared to the results of the double-monochromator-based Quality Assurance of Solar Spectral Ultraviolet Irradiance Measurements carried out in Europe (QASUME) instrument, which is extensively characterised for global irradiance (Gröbner and Sperfeld, 2005, Gröbner et al., 2005; Hülsen et al., 2016). For this intercomparison the QASUME instrument was equipped with a collimator-based entrance optic for direct solar irradiance measurements with a maximum field of view of 2.5° (full opening angle; Gröbner et al., 2017). To be able to compare two sets of data, the measured spectra of both instruments had to be synchronised in time and adapted in bandwidth. The QASUME system operates in sequential mode, measuring step by step from lower to higher wavelength. The recording of a full spectrum from 290 to 500 nm in steps of 0.25 nm takes about 16 min. Every measurement at a single wavelength is marked with a time stamp so that the corresponding measurement and the wavelength of the BTS2048-UV-S-WP (from now on called BTS) could be synchronised. As both spectroradiometer systems possess different bandwidth, the resulting spectra were convolved with a standard 1 nm triangular bandpass function. This data evaluation results in deviations between BTS and QASUME lower than ±2.5 % averaged from 300 to 420 nm (see Fig. 4).

The diurnal variation between QASUME and BTS of different waveband ratios shows deviations of less than ±2 %. The ratios rise for SZAs larger than 74 or an air mass larger than 3.6 (Fig. 5). At higher SZAs or air mass the signal-to-noise ratio decreases, especially at low wavelengths, due to

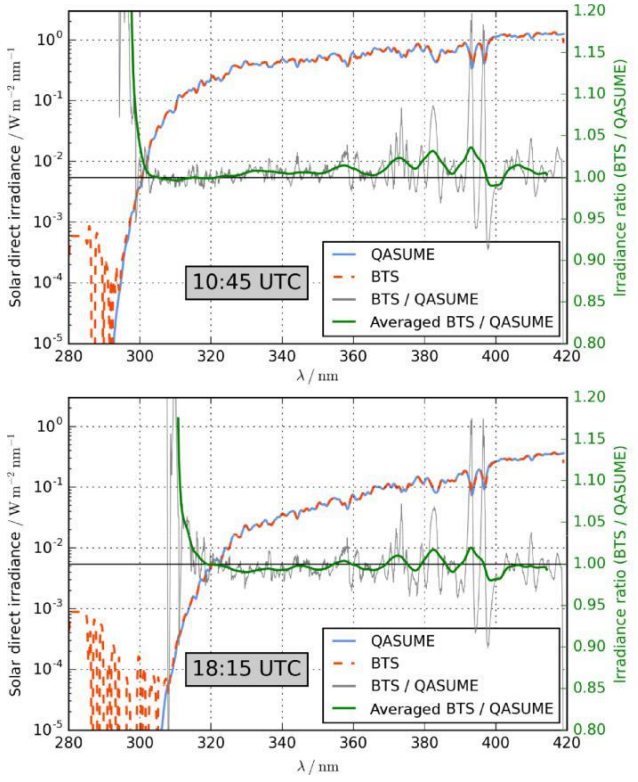

Figure 4. Direct spectral irradiance (blue and red line) measured by the BTS and the double-monochromator-based QASUME instrument in Izaña on 20 September, at 10:45 UTC and 18:15 UTC. The ratio (grey line for single data and green line for moving average) of measurements (right axis) shows satisfactory agreement with average deviations of less than 2.5 % between 300 and 420 nm for low solar zenith angles at around noontime. The unaveraged ratio (grey line) can be explained by remaining small differences in the optical bandwidth in combination with small wavelength shifts. Due to non-averaging of the BTS data and limited integration time (measurement every 8 s), noise of the 16 bit ADC in the spectral region below the UV-B solar edge can be observed.

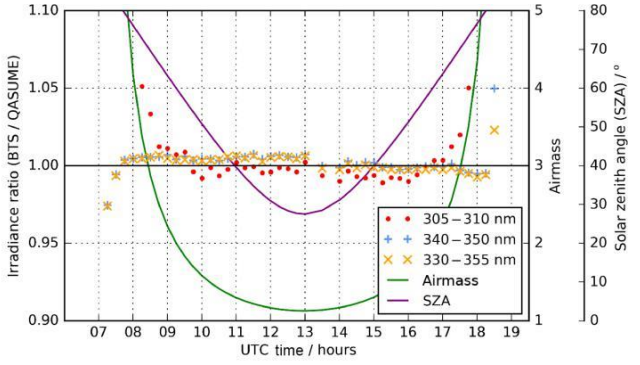

Figure 5. BTS=QASUME ratio of the wavebands used for the calculation of TOC values. The measurements were performed on 20 September 2016. The corresponding air mass of the direct irradiance and the solar zenith angle on the corresponding day are also shown (right axis). For solar zenith angles of more than 74° or an air mass above 3.6, deviations rise to 5 %.

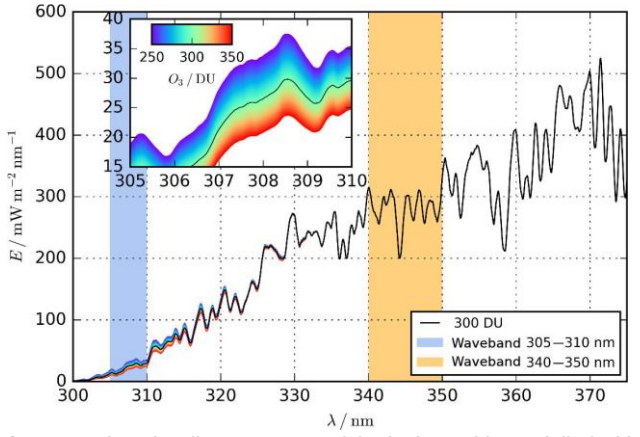

Figure 6. Direct irradiance spectra of the lookup table modelled with libRadtran. Shown are all spectra for an SZA of 48°, ranging from 250 (purple) to 320 DU (red) TOC. The wavebands used for the TOC retrieval are marked blue and orange.

the increasing atmospheric absorption path of the incident irradiance.

4.2 Intercomparison of TOC values

The spectral data have also been used to calculate the total ozone column based on a retrieval algorithm proposed by Masserot et al. (2002). For this purpose, the ratios of two wavelength bands, ranging from 305 to 310 nm and from 340 to 350 nm, have been calculated. The ratio is directly related to the TOC since the first band lies inside and the second one outside the ozone absorption range. By comparing these ratios to a set of pre-calculated model values stored in a lookup table, the most probable TOC value present during the measurement can be determined. The model values have been calculated with the libRadtran software package for radiative transfer calculations (Emde et al., 2016). The lookup table is a data cube with three dimensions and consists of roughly 6500 direct irradiance spectra with a wavelength range of 280 to 420 nm for SZAs between 24 and 90 and for TOC values between 250 and 350 DU (one Dobson unit (DU) is equivalent to 0.4462 mmol m^{-2}; Basher, 1982). For the calculation of the ozone value of a specific measurement, all modelled spectra at the SZA apparent during the time of the measurement are first selected from the lookup table (see Fig. 6), and the ratios between the BTS measurement and all selected spectra are calculated. For the calculation of the lookup table, the following values for the input parameters have been chosen: an albedo of 0.2, a pressure of 773 hPa, an altitude of 2.36 km, an atmospheric profile typical for mid-latitude summer (Anderson et al., 1986) and the ozone cross section of Bass and Paur (1984). The temperature and ozone profile of the chosen atmospheric profile lead to an effec-

Table 2. Comparison of the BTS-retrieved TOC values to other instrument values measured during the ATMOZ campaign. The data have been calculated based on measurements performed on 20 September 2016 between 09:00 and 11:00 UTC, shown in Fig. 8. For the comparison to the OMI data the average of the BTS TOC values measured between 12:30 and 13:00 UTC has been calculated. The SD of the averaged TOC values shows the dispersion of TOC values during that time period.

Instrument	TOC/DU	Time interval/UTC	Difference to BTS/%	SD of values used/DU
BTS	267.5	09:00–11:00	–	1.0
QASUME	271.7	09:00–11:00	+1:6	0.5
IZO Brewer	269.7	09:00–11:00	+0:8	0.4
NOAA Dobson	265.5	09:00–11:00	-0.8	0.6
BTS	270	12:30–13:00	–	0.7
Aura OMI	275	12:30–13:00	+1:8	–

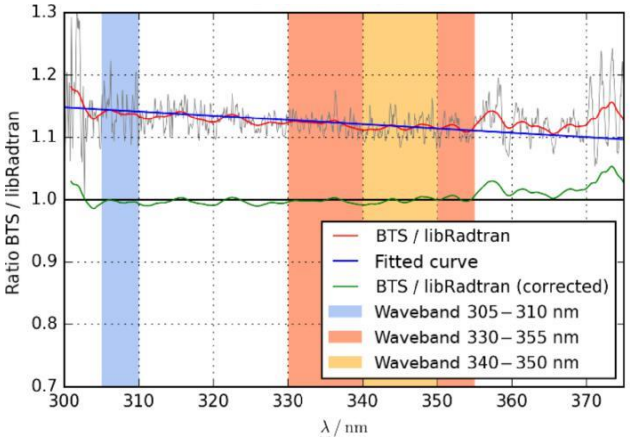

Figure 7. Example of the atmospheric correction applied to a TOC calculation of BTS data on 20 September 2016, 10:06 UTC. The waveband ranging from 330 to 355 nm was used to derive the slope of the blue fitting line. The green line is the ratio of a BTS measurement and a libRadtran calculation after subtracting the blue fitting line.

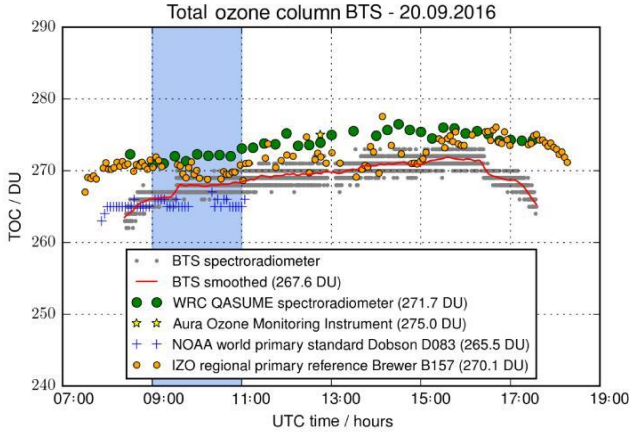

Figure 8. Total ozone column (TOC) derived by the direct solar measurements of the BTS in comparison to other instruments. The measurements have been conducted during the ATMOZ intercomparison campaign on 20 September 2016. The TOC values stated in the legend for each ground-based instrument have been derived by averaging the values between 09:00 and 11:00 UTC (blue area). Grey dots symbolise the BTS TOC measurements captured every 8 s; only integer values are apparent due to the 1 DU resolution of the lookup table.

tive ozone temperature of 232.3 K. In contrast to Masserot et al., direct irradiance instead of global irradiance has been modelled as input for the lookup table to adapt the algorithm to the measurements performed with the BTS. Despite the low aerosol content in Izaña the aerosol default values of libRadtran have been used. This crude modelling of aerosol parameters is intentional in order to reflect the usually limited knowledge of the atmospheric aerosol parameters. The chosen aerosol parameters will lead to deviations between measured and modelled spectra over the whole wavelength range due to differences between the actual atmospheric condition and the assumptions made for the modelled spectra. This is addressed by performing a linear fit to the ratio between 330 and 355 nm (see Fig. 7), where ozone absorption is negligible and no “local” spectral features due to, e.g., strong absorption lines in the solar spectrum are apparent. The derived linear fit is applied to each ratio afterwards, effectively adjusting the ratios for atmospheric scattering processes with low wavelength dependencies (e.g. Mie scattering by aerosols or cloud droplets). The ratios are then averaged in the two wavelength bands from 305 to 310 nm and 340 to 350 nm. The resulting numbers are divided by each other for each ratio. The ratio closest to 1 corresponds to the modelled spectrum with the most likely ozone value apparent during the BTS measurement.

In Fig. 8, the results of the TOC calculations based on spectra of the direct solar irradiance measured on 20 September 2016 are shown. In addition, measurements performed on the same day with other instruments are displayed, namely with the WRC QASUME spectroradiometer, the world primary standard Dobson ozone spectrophotometer D083 from the World Dobson Calibration Center (WDCC) at NOAA, the regional primary reference Brewer spectrophotometer B157 of the Izaña Atmospheric Observatory and satellite measurements from the Aura Ozone Monitoring Instrument

(OMI). Additionally, to directly compare the BTS-retrieved TOC to the other instrument data, the mean TOC values have been calculated during the time between 09:00 and 11:00 UTC. For the comparison with the Aura OMI data, the BTS data have been averaged 15 min around the flyover time of the Aura satellite, resulting in a BTS TOC of 270 DU. The results are illustrated in Table 2.

The systematic differences between BTS and QASUME TOC values, even if the spectra of both instruments agree well as shown in Fig. 4, arise from different model approaches which are used for the TOC determination. In addition, the modelled TOC values of BTS and QASUME are based on slightly different input parameters for the atmospheric conditions. This is the case since we have chosen our parameters without knowledge of the QASUME parameters to ensure an unbiased comparison.

During the other measurement days of the campaign, where direct irradiance measurements were performed with the BTS spectroradiometer, the deviation to the other instruments did not exceed 3 % between 09:00 and 17:00 UTC. At air masses larger than 4 during sunrise and sunset, the signal-to-noise ratio decreases in the shortwave region of the spectrum and, therefore, the TOC estimations becomes noisier. In addition, at lower irradiance levels the detection threshold of the instrument increasingly affects the wavelength band from 305 to 310 nm, which leads to higher systematic uncertainties for the calculation. An initial analysis of the TOC determination uncertainty of the BTS device, which is in the range of 5 DU, was carried out by Vaskuri et al. (2017) based on a Monte Carlo method.

5 Discussion and conclusion

The BTS2048-UV-S series spectroradiometer is a versatile measurement system for spectroradiometric measurements in the UV spectral range. Its compact design, the fast sensor system and the hardware-based stray light correction achieved with several optical filters may enable a wide range of radiometric applications.

After adapting the BTS2048-UV-S with a weatherproof housing for direct solar irradiance measurements (BTS2048-UV-S-WP) and an extensive device characterisation, the array spectroradiometer proved its capability in the challenging measurements of solar irradiance for atmospheric research.

Absolute direct solar irradiance measurements by the BTS2048-UV-S-WP showed deviations from the double-monochromator-based QASUME lower than 2.5 % averaged over the spectral range from 300 to 420 nm. In the spectral range below the UV-B solar edge the deviation rises mostly due to slight differences in the wavelength calibration and insufficient signal-to-noise ratio since no averaging of the BTS data or longer integration time was possible for the 8 s measurement interval. TOC values derived from BTS2048-UV-S-WP data show agreement comparable to those obtained by Dobson and Brewer reference instruments. Based on the results and the experience gained during the measurement campaign, the design and the radiometric sensitivity of the BTS measurement system could be further improved by a factor of 4. This will very likely improve the performance of the system especially at higher SZAs and shall be tested in future measurement campaigns.

Data availability. The data sets of the direct spectral irradi-ance measurements of the BTS2048-UV-S-WP at the Izaña Atmospheric Observatory on 20–22 September 2016 during the ATMOZ intercomparison campaign can be obtained at https://doi.org/10.6084/m9.figshare.6170345.v1 (Sperfeld et al., 2018).

Competing interests. The authors declare that they have no conflict of interest.

Acknowledgements. This work was supported by the European Metrology Research Programme (EMRP) within the joint research project EMRP ENV59 ATMOZ “Traceability for atmospheric total column ozone”. The EMRP is jointly funded by the EMRP participating countries within EURAMET and the European Union. The authors thank Julian Gröbner from PMOD for providing the QASUME data sets.

Edited by: Pawan K. Bhartia
Reviewed by: two anonymous referees

References

Anderson, G. P., Chetwynd, J. H., Clough, S. A., Shettle, E. P., and Kneizys, F. X.: AFGL atmospheric constituent profiles (0– 120km), Hanscom AFB, MA: Optical Physics Division, U.S. Air Force Geophysics Laboratory, 1986.

Basher, R. E.: Ozone absorption coefficients’ Role in Dobson in-strument ozone measurement accuracy, Geophys. Res. Lett., 9, 11, 1982.

Blanc, P., Espinar, B., Geuder, N., Gueymard, C., Meyer, R., Pitz-Paal, R., Reinhardt, B., Renné, D., Sengupta, M., Wald, L., and Wilbert, S.: Direct normal irradiance related definitions and ap-plications: The circumsolar issue, Sol. Energy, 110, 561–577, https://doi.org/10.1016/j.solener.2014.10.001, 2014.

Dobson, G. M. B.: A photoelectric spectrophotometer for measur-ing the amount of atmospheric ozone, P. Phys. Soc., 43, 324–339, 1931.

Egli, L.: Post processing of data from array spectroradiome-ter, UVnet workshop 2014, Davos, Switzerland, 15–16 July 2014, available at: https://projects.pmodwrc.ch/env03/images/documents_workshop/Egli_et_al.pdf (last access: 25 April 2018), 2014.

Egli, L., Gröbner, J., Hülsen, G., Bachmann, L., Blumthaler, M., Dubard, J., Khazova, M., Kift, R., Hoogendijk, K., Serrano, A., Smedley, A., and Vilaplana, J.-M.: Quality assessment of solar

UV irradiance measured with array spectroradiometers, Atmos. Meas. Tech., 9, 1553–1567, https://doi.org/10.5194/amt-9-1553-2016, 2016.

Emde, C., Buras-Schnell, R., Kylling, A., Mayer, B., Gasteiger, J., Hamann, U., Kylling, J., Richter, B., Pause, C., Dowling, T., and Bugliaro, L.: The libRadtran software package for radia-tive transfer calculations (version 2.0.1), Geosci. Model Dev., 9, 1647–1672, https://doi.org/10.5194/gmd-9-1647-2016, 2016.

Gröbner, J. and Sperfeld, P.: Direct traceability of the portable QA-SUME irradiance scale to the primary irradiance standard of the PTB, Metrologia, 42, 13, 2005.

Gröbner, J., Schreder, J., Kazadzis, S., Bais, A. F., Blumthaler, M., Görts, P., Tax, R., Koskela, T., Seckmeyer, G., Webb, A. R. and Rembges, D.: Traveling reference spectroradiometer for routine quality assurance of spectral solar ultraviolet irradiance measure-ments, Appl. Optics, 44, 5321–5331, 2005.

Gröbner, J., Kröger, I., Egli, L., Hülsen, G., Riechelmann, S., and Sperfeld, P.: The high-resolution extraterrestrial solar spectrum (QASUMEFTS) determined from ground-based solar irradiance measurements, Atmos. Meas. Tech., 10, 3375–3383, https://doi.org/10.5194/amt-10-3375-2017, 2017.

Hülsen, G., Gröbner, J., Nevas, S., Sperfeld, S., Egli, L., Porrove-chio. G., and Smid. M.: Traceability of solar UV measurements using the QASUME reference spectroradiometer, Appl. Optics, 55, 7265–7275, 2016.

Masserot, D., Lenoble, J., Brogniez, C., Houet, M., Krotkov, N., and McPeters, R.: Retrieval of ozone column from global irradiance measurements and comparison with TOMS data. A year of data in the Alps, Geophys. Res. Lett., 29, 1309, https://doi.org/10.1029/2002GL014823, 2002.

Mayer, B. and Seckmeyer, G.: Retrieving Ozone Columns from Spectral Direct and Global UV Irradiance Measurements, peer reviewed proceedings of the Quadrennial Ozone Symposium L'Aquila, edited by: Bojkov, R. D. and Visconti, G., Int. Assoc. for Meteorol. and Atmos. Sci., L'Aquila, Italy, 935–938, 1998.

Nevas, S., Wübbeler, G., Sperling, A., Elster, C., and Teuber, A.: Simultaneous correction of bandpass and stray-light effects in array spectroradiometer data, Metrologia, 49, S43–S47, 2012.

Nevas, S., Gröbner, J., Egli, L., and Blumthaler, M.: Stray light cor-rection of array spectroradiometer data for solar UV measure-ments, Appl. Optics, 53, 4313–43193, 2014.

Paur, R. J. and Bass, A. M.: The ultraviolet cross-sections of ozone: II Results and temperature dependence, in: Proc. Quadrennial Ozone Symposium, Halkidiki, 3–7 September 1984, Greece, 611–616, 1984.

Pulli, T., Nevas, S., El Gawhary, O., Van den Berg, S., Askola, J., Kärhä, P., Manoocheri, F., and Ikonen, E.: Nonlinearity charac-terization of array spectroradiometers for the solar UV measure-ments, Appl. Optics, 56, 3077–3086, 2017.

Seckmeyer, G., Bais, A., Bernhard, G., Blumthaler, M., Booth, C., Disterhoft, P., Eriksen, P., McKenzie, R., Miyauchi, M., and Roy, C.: Instruments to Measure Solar Ultraviolet Radiation, Part 1: Spectral Instruments, Global Atmosphere Watch Report No. 125, World Meteorological Organization (WMO), 2001.

Seckmeyer, S., Bais, A., Bernhard, G., Blumthaler, M., Johnsen, B., Lantz, K., and McKenzie, R.: Instruments to Measure Solar Ul-traviolet Radiation, Part 4: Array spectroradiometers, Global At-mosphere Watch Report No. 191, World Meteorological Organi-zation (WMO), 2010.

Shafer, A. B., Megill, L. R., and Droppleman, L.: Optimization of the Czerny–Turner Spectrometer, J. Opt. Soc. Am., 54, 879–87, 1964.

Shaw, M. and Goodman, T.: Array-based goniospectroradiometer for measurement of spectral radiant intensity and spectral total flux of light sources, Appl. Optics, 47, 1–11, 2008.

Sperfeld, P., Pape, S., and Barton, B.: From Primary Standard to mobile measurements – Overview of the spectral irradiance cal-ibration equipment at PTB, MAPAN-J. Metrol. Soc. I, 25, 11, https://doi.org/10.1007/s12647-010-0004-z, 2010.

Sperfeld, P., Riechelmann, S., and Zuber, R.: BTS direkt irradiance measurements Izana intercomparison 2016, https://doi.org/10.6084/m9.figshare.6170345.v1, 2018.

Vaskuri, A., Kärhä, P., Egli, L., Gröbner, J., and Ikonen, E.: Monte Carlo-Based Method for Determining Total Ozone Column Uncertainty: Izaña campaign, UV NEWS, 12, 13–15, 2017.

Vaskuri, A., Kärhä, P., Egli, L., Gröbner, J., and Ikonen, E.: Monte Carlo method for determining uncertainty of total ozone derived from direct solar irradiance spectra: Application to Izaña results, Atmos. Meas. Tech. Discuss., https://doi.org/10.5194/amt-2017-403, in review, 2018.

Zong, Y., Brown, S. W., Johnson, B. C., Lykke, K. R., and Ohno, Y.: Simple spectral stray light correction method for array spectro-radiometers, Appl. Optics, 45, 1111–1119, 2006.

5.2 Article B: Global spectral irradiance array spectroradiometer validation according to WMO

5.2.1 Declaration of my contribution

The author of this thesis had the idea about this specific designed filter approach and how to integrate it in a measurement device. The development of this specific designed spectroradiometer (optical design, ray tracing, etc.) was done by the author of this thesis. The electronics were developed by a Gigahertz-Optik supplier according to the specifications of the author of the thesis. Mario Ribnitzky supported the author of this thesis during the implementation, characterization of the approach and calibration procedure at Gigahertz-Optik GmbH. The measurement campaign was prepared by Mario Tobar (setup of the NDACC device) and the author of this thesis (setup of BTS devices and NDACC device). The author of this thesis carried out the measurements, analyzed the data and evaluated the results. During the campaign, the author of this thesis was supported by all other co-authors.

5.2.2 Published article

This article has been published with open access in IOP Measurement Science and Technology.

Submitted: 20 April 2018
Accepted: 14 August 2018
Published: 22 November 2017

Zuber, R., Ribnitzky, M., Tobar, M., Lange, K., Kutscher, D., Schrempf, M., Niedzwiedz, A. and Seckmeyer, G.: Global spectral irradiance array spectroradiometer validation according to WMO, *2018 Meas. Sci. Technol.* **29** 105801

DOI: https://doi.org/10.1088/1361-6501/aada34

OPEN ACCESS
IOP Publishing
Measurement Science and Technology
Meas. Sci. Technol. **29** (2018) 105801 (14pp)
https://doi.org/10.1088/1361-6501/aada34

Global spectral irradiance array spectroradiometer validation according to WMO

Ralf Zuber[1], Mario Ribnitzky[1], Mario Tobar[2], Kezia Lange[2], Dimitrij Kutscher[2], Michael Schrempf[2], Angelika Niedzwiedz[2] and Gunther Seckmeyer[2]

[1] Gigahertz-Optik GmbH, 82299 Türkenfeld/Munich, Germany

[2] Leibniz University Hanover, Institute of Meteorology and Climatology, Hanover, Germany

E-mail: r.zuber@gigahertz-optik.de

Received 20 April 2018, revised 10 August 2018
Accepted for publication 14 August 2018
Published 10 September 2018

Abstract

Solar spectral irradiance measured by two recently developed array spectroradiometers (called UV-BTS and VIS-BTS) are compared to the results of a scanning double monochromator system which is certified as a travelling reference instrument by the Network for the detection of atmospheric composition change (NDACC) and fulfils the specifications of S-2 UV instruments of the world meteorological organization (WMO). The comparison took place between 15 and 18 May 2017 at the Institute of Meteorology and Climatology of the University of Hanover (IMuK) between 4:00 and 17:00UTC. The UV-BTS array spectroradiometer is equipped with special hardware to significantly reduce internal stray light which has been the limiting factor of many array spectroradiometers in the past. It covers a wavelength range of 200 nm–430 nm. The VIS-BTS covers a wider spectral range from 280 nm up to 1050 nm, and stray light reduction is achieved by mathematical methods. For the evaluation, wavelength integrated quantities and spectral global irradiance are compared. The deviation for UV index measured by the UV-BTS, is within ±1% for solar zenith angles (SZA) below 70° and increased to a maximum of ±3% for SZA between 70° and 85° when synchronisation between measurements was possible. The deviation of global spectral irradiance is smaller ±2.5% in the spectral range from 300 nm to 420 nm (evaluated for SZA < 70°). The VIS-BTS achieved the same deviation for blue light hazard as the UV-BTS for the UV index. The evaluations of global spectral irradiance data of the VIS-BTS show a deviation smaller than ±2% in the spectral range from 365 nm to 900 nm (evaluated for SZA < 70°). Below 365 nm, the deviation rises up to ±7% at 305 nm due to remaining stray light. The agreement within the limited time of the intercomparison is considered to be satisfactory for a number of applications and provides a good basis for further investigations.

Keywords: UV index, stray light, spectroradiometer, NDACC intercomparison, blue light hazard, WMO S-2 UV instrument

(Some figures may appear in colour only in the online journal)

1. Introduction

Measurements of spectral irradiance from the ultraviolet (UV) to the infrared (IR) with low uncertainty are necessary for a variety of research, e.g. amongst others they are a fundamental quantity in remote sensing (Seckmeyer *et al* 1996, Kylling *et al* 2000, Thuillier *et al* 2003, Gröbner and Sperfeld 2005, Gröbner *et al* 2005). A typical example in the UV is the measurement of the erythema weighted irradiance or the UV index. The UV radiation is considered in research topics for instance as a contribution for melanoma skin cancer or eye and immune system disease (Armstrong and Kricker 2001, WHO 2002, Godar 2005, Seckmeyer *et al* 2010). The dimensionless quantity UV index is harmonized between the World Organisations for Metrology and Health (WMO and WHO) and the International Commission for protection against Non-Ionizing Radiation (ICNIRP) (WMO 1998, ICNIRP 1995, WHO 2002). In addition, the UV index is displayed in the daily weather forecast in some countries to inform the population about the maximum expected daily UV exposure and corresponding erythema risk (WHO 2002). Other investigations of the UV community are for example the deeper understanding of positive UV effects like vitamin D generation or a deeper understanding of changing atmospheric composition (e.g. ozone, aerosols, clouds), geographic differences and monitoring long term changes in solar UV radiation (Engelsen *et al* 2005, Webb and Engelsen 2006, McKenzie *et al* 2009, Seckmeyer *et al* 2013). According to the American Society of Agricultural and Biological Engineers (ASABE) standard, the UV to NIR region is of great interest for biological investigations in terms of plant growth or plant damage (ASABE 2017). The UV to NIR spectral region is of interest as well for albedo evaluations (Blumthaler and Ambach 1988). Albedo is becoming important these days since it seems to be a significant parameter in climate models (Brovkin *et al* 2013, He *et al* 2014). Photovoltaic simulations, which have become important due to the efficiency optimization of solar cells, are also based on irradiance data with high temporal resolution (Hofmann and Seckmeyer 2017).

In order to perform these measurements, different measurement devices are available. The scientifically accepted and most accurate measurement technology in terms of stray light reduction and linearity are double monochromator-based measurement systems (Seckmeyer *et al* 2001). Bernhard and Seckmeyer (1999) as well as Cordero *et al* (2013) analysed the uncertainty of spectral solar UV irradiance measurements of such devices in detail. However, double monochromators are usually in the higher price range. The spectral scanning leads to long measurement times, therefore the possibilities of time-resolved investigations are limited. In addition, the devices are difficult to transport due to their size. For this reason array spectroradiometers look like an attractive alternative. However, their drawback is usually an insufficient stray light reduction in the UV. Egli *et al* (2016) showed in an intercomparison of 14 array spectroradiometers that even thoroughly characterised devices with additional mathematical stray light reduction (Nevas *et al* 2014) are not able to detect solar UV radiation below 310 nm comparable to double monochromator systems. Furthermore, only some of the thoroughly characterised and stray light reduced devices are able to measure the UV index within 5% uncertainty compared to a double monochromator reference QASUME (Hülsen *et al* 2016) for a solar zenith angle (SZA) smaller than 50°. For a larger SZA, the uncertainty significantly rises for all tested devices.

To overcome this limitation, Gigahertz-Optik GmbH developed the BTS2048-UV-S series array spectroradiometers which allow very short measurement times by sufficient linearity and stray light reduction. The meter and its technology has been described and was validated for direct solar irradiance UV measurements in Zuber *et al* (2018).

A measurement system consisting of two array spectroradiometers, a BTS2048-UV-S-WP (UV) and a BTS2048-VL-TEC-WP (UV to NIR) was set up, to achieve a wavelength range from 200 nm to 1050 nm. The BTS2048-UV-S-WP is now on called UV-BTS and the BTS2048-VL-TEC-WP is called VIS-BTS in this paper. This system has been compared with a double monochromator-based device, which complies to the NDACC specifications (De Mazière *et al* 2018), at a measurement campaign for spectral global irradiance at the Institute of Meteorology and Climatology in Hanover (IMuK) with the aim to validate an array spectroradiometer as well with the stated NDACC specifications[1]. These specifications are identical to those of S2 instruments stated by the WMO recommendations (Seckmeyer *et al* 2001). The chosen double monochromator based device (now on called the NDACC device) participated in international intercomparisons where it proved its quality (Wuttke *et al* 2006, Lantz *et al* 2008) and it is similar to earlier instrument setups (Seckmeyer 1989, Seckmeyer *et al* 1997, Bais 1998, Webb *et al* 1998).

Note: In this paper, as in other publications, the difference between two measurement instruments is called deviation (Bernhard and Seckmeyer 1999, Cordero et al 2013, Egli et al 2016). % deviation = (1 − instrument1/instrument2)·100. This should not be confused with standard deviation, also called standard measurement uncertainty (JCGM 2012).

2. Instrument design

The UV-BTS is described in detail by Zuber *et al* (2018). To summarise the important information briefly, it is an array spectroradiometer based on a crossed Czerny–Turner design (Shafer *et al* 1964) with an active stray light reduction which is achieved with the help of several optical bandpass and edge filters. Thus, several sub-measurements can be performed with the different filters and combined in a smart way to achieve the best overall measurement result. It exhibits a spectral range of 200 nm to 430 nm at an optical bandwidth of 0.8 nm. A typical measurement time is in the range of a few seconds for global solar irradiance (see table 1). As a detector, a thermostatic (8 °C) back-thinned CCD with 2048 pixels and an electronic shutter is used. The entrance optic is a cosine corrected quartz diffuser for achieving a low cosine error (see

[1] (http://www.ndsc.ncep.noaa.gov/organize/protocols/appendix6/).

Table 1. Overview of some important optical parameters of the three used measurement devices.

Quantity	UV-BTS	VIS-BTS	NDACC device
Spectral range	200 nm to 430 nm	280 nm to 1050 nm	290 nm to 1050 nm
Bandwidth (FWHM)	0.8 nm	2 nm	0.5 nm
Scanning interval	~0.13 nm/pixel (by 2048 pixel)	~0.4 nm/pixel (by 2048 pixel)	0.5 nm
Entrance optics	diffuser	diffuser	diffuser
Temperature-controlled	yes	yes	yes
Typical measurement time	~1 s at 40 W m^{-2} (280 nm to 430 nm)	~25 ms at 500 W m^{-2} (280 nm to 1050 nm)	~35 min (290 nm to 1050 nm)

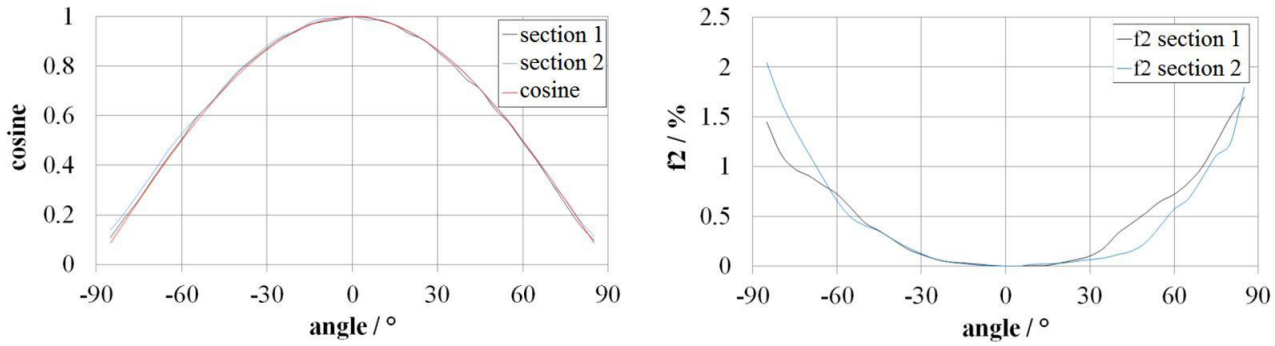

Figure 1. Left: Angular response of the UV-BTS. Right: Cosine error f_2 of the UV-BTS with a f_2 better than 2.5% for angles less than 80°. Sections 1 and 2 are measurements of two perpendicular sections of the diffuser, measured by isotropic irradiance illuminated with a halogen lamp and averaged over the full spectral range.

section 3.1). The whole spectrometer unit is integrated in a weather-proof housing which is temperature controlled to 38 °C in the temperature range −25 °C to +50 °C.

The VIS-BTS is based on the same technology and components (entrance optic, optical design, detector, electronics, housing etc.) as the UV version. However, the wavelength region is adjusted to 280 nm to 1050 nm with 2 nm optical bandwidth (full width at half maximum—FWHM (Seckmeyer *et al* 2001)). In addition, instead of optical bandpass and edge filters, optical density filters are integrated to increase the dynamic range of the device. Thus, stray light reduction with the optical filters cannot be applied. However, in order to achieve improved stray light reduction, a mathematical correction method according to Zong *et al* (2006) is applied.

The NDACC device is based on a scanning DTMc300 double monochromator (Bentham Instruments Ltd., Reading, United Kingdom) which is equipped with a weather-proof entrance optic for global irradiance. The entrance optic is connected by an optical fibre to the double monochromator. This measurement system is introduced in detail by Wuttke *et al* (2006). Table 1 shows an overview of the relevant optical measurement parameters.

3. Measurement device characterisation

3.1. UV-BTS

The UV-BTS was extensively characterised at the Physikalische Technische Bundesanstalt (PTB) for a former measurement campaign for total ozone column (TOC) determination. There, a wavelength accuracy better than ±0.1 nm, a nearly symmetrical bandpass function and a linearity deviation smaller than 1% in the full dynamic range was found (Zuber *et al* 2018).

A radiometric calibration was performed using a 250 W halogen lamp and a 30 W deuterium lamp as transfer standards. The transfer standards are traceable to PTB and exhibit an absolute calibration uncertainty in the relevant spectral range for the intercomparison of ±4% within 280 nm to 399 nm and ±3% within 400 nm to 430 nm (expanded calibration uncertainty $k = 2$).

In addition, the cosine error of the directly mounted quartz diffuser based entrance optic (no optical fibre) was characterised according to DIN EN 13032-1:2012-06 (DIN-EN 2012) and an average (of different sections) better than 2.5% was found for the quality index f_2 (see figure 1).

3.2. VIS-BTS

The wavelength calibration was performed with the help of a wavelength tuneable laser and intrinsic atomic lines. A wavelength check was performed with a mercury pen lamp at which a wavelength accuracy better than ±0.2 nm was found. Several line spread functions (LSF) were investigated with a tuneable laser (Nevas *et al* 2014) and found to be nearly symmetrical (see figure 2). However, the optical bandwidth (FWHM) increases slightly with an increasing wavelength.

The nonlinearity of an array spectroradiometer depends for instance on the used detector chip, the readout electronics (analog-to-digital converter (ADC)) and the remaining deviation after applying a correction based on a characterisation of the detector system (Pulli *et al* 2017). Since the electronics, detector chip and characterisation procedure are identical to the UV-BTS,

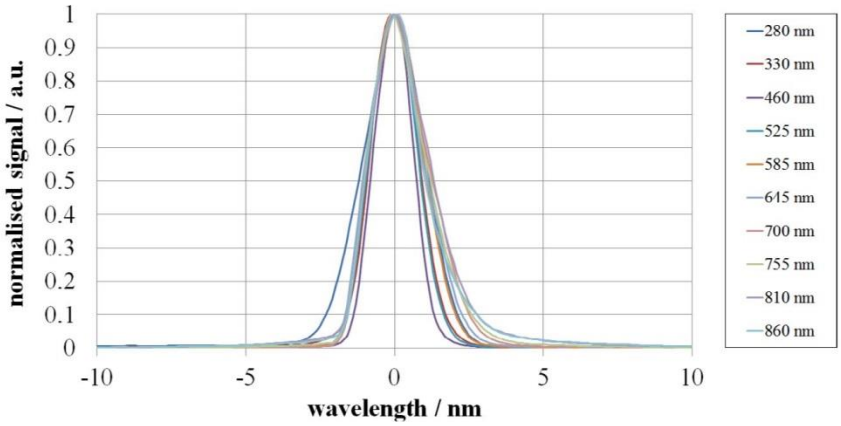

Figure 2. Slit functions captured with a tuneable laser dependent on wavelength. The line spread functions are nearly symmetrical.

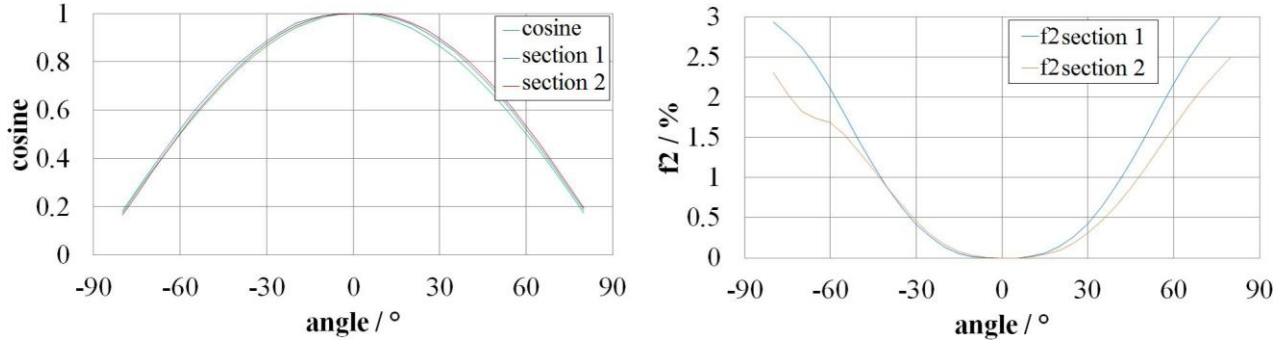

Figure 3. Left: Angular cosine error of the VIS-BTS. Right: The cosine error f_2 of the VIS-BTS is smaller than 3% for angles less than 80°. Sections 1 and 2 are measurements of two perpendicular sections of the diffuser, measured by isotropic irradiance illuminated with a halogen lamp and averaged over the spectral range of 380 nm to 780 nm.

the same linearity performance with a deviation smaller than 1% in the full dynamic range is likely (Zuber *et al* 2018).

The device was radiometrically calibrated by using the same traceable transfer standard which was used for the UV-BTS. The lamp standard exhibits an expanded calibration uncertainty (k = 2) in the relevant spectral range of the intercomparison of 4% within 280 nm to 399 nm, 3% within 400 nm to 799 nm and 4.5% within 800 nm to 1050 nm.

Analogous to the UV-BTS, the cosine error of the also directly mounted quartz diffuser based entrance optic was characterised according to DIN-EN (2012) and an average better than 3% was determined for f_2 (see figure 3). The f_2 was measured by isotropic irradiance illuminated with a halogen lamp and averaged over the spectral range of 380 nm to 780 nm. From 780 nm to 1050 nm the f_2 error raises to 4.5%, below 380 nm the f_2 error decreases to 2.5%.

3.3. NDACC device

Measurement devices which comply to the NDACC requirements, like the system of the Institute of Meteorology and Climatology in Hanover, have been widely used in many previous studies and have been a well-established measurement system since several decades (Seckmeyer *et al* 1997, Bais 1998, Webb *et al* 1998). Wuttke *et al* (2006) characterised the instrument used in this paper and the specifications are listed in their publication. These are briefly summarised in the following. It shows a wavelength accuracy better

Figure 4. Photo of the measurement devices mounted on the measurement platform. Left: UV-BTS, centre: entrance optic of the NDACC device, right: VIS-BTS.

than ±0.05 nm, a cosine error (averaged deviation over wavelength to ideal cosine error) of 3.1% (2.3% at 320 nm, 2.9% at 400 nm, and 4.0% at 500 nm) and a detection threshold of $9 \cdot 10^{-7}\,\mathrm{W\,m^{-2}\,nm^{-1}}$. As stray light, only noise below this detection threshold was found.

The radiometric responsivity calibration of the NDACC device was performed directly at the measurement location. Hence, no movement of the measurement device after the calibration was necessary which could introduce measurement uncertainties. The calibration was done by measuring a 100 W halogen lamp housed in a field calibrator (Seckmeyer 1989). This unit possesses a similar expanded calibration uncertainty (k = 2) of 4% within 280 nm to 399 nm, 3% within 400 nm to

Table 2. List of weather conditions during the measurement campaign and the activity during this day. Furthermore pictures taken with an all sky camera during the measurement activity are illustrated in the table.

Day	Weather conditions	Activity
15 May 2017	Partly cloudy (fast moving Cumulus) 	Calibration of the NDACC device and calibration check of the BTS
16 May 2017	Overcast sky (Altostratus) changed later to fast moving Stratocumulus 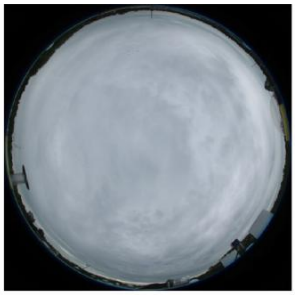	Measurements before noon, then calibration check NDACC device
17 May 2017	Partly cloudy (fast moving Cumulus) 	Calibration check NDACC device before noon, then measurements
18 May 2017	Clear sky before noon followed by a thunderstorm (Cumulonimbus) 	Measurements before noon, then calibration check NDACC device and both BTS devices

799 nm and 4.5% within 800 nm to 1050 nm. The wavelength calibration was as well performed in this housing by operating intrinsic atomic line lamps.

4. Measurement campaign and data processing

In order to validate the measurement system, a measurement campaign of global spectral irradiance from the 15 May 2017 to the 18 May 2017 was performed at the measurement platform of the Institute of Meteorology and Climatology in Hanover (IMuK; latitude 52° 23′ 29.4″ north, longitude 9° 42′ 16.9″ east). Figure 4 shows the measurement setup at the place of installation. All three measurement devices were equipped with an entrance optic for global spectral irradiance and adjusted separately. The weather conditions during the campaign can be described as dry but variable cloudiness, see table 2.

Table 3. Determined detection threshold in the UV by measuring global solar irradiance.

	UV-BTS	VIS-BTS
Detection threshold given by stray light and noise level	$5 \cdot 10^{-5}$ Wm^{-2} nm^{-1}	$2 \cdot 10^{-3}$ Wm^{-2} nm^{-1}
Corresponding wavelength	294.1 nm	298.3 nm

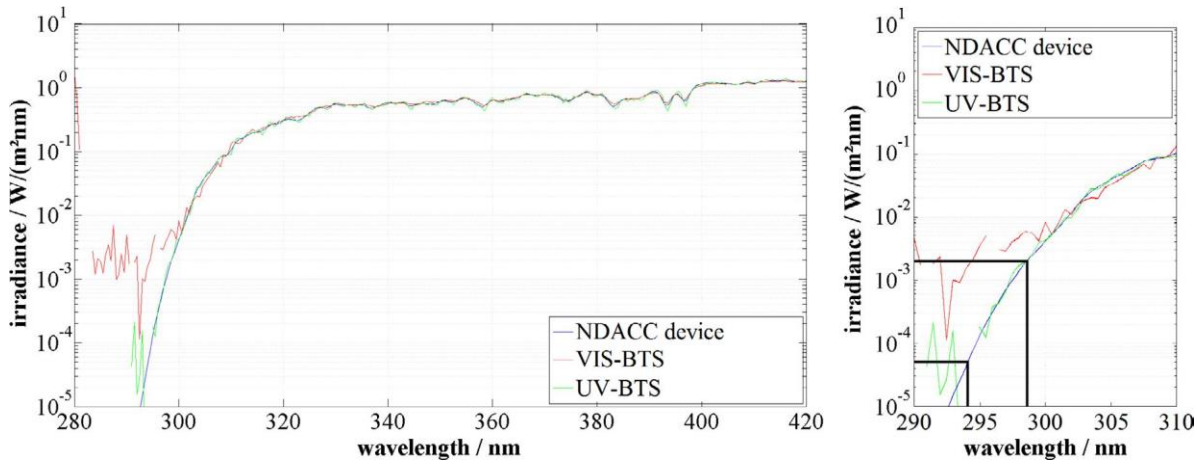

Figure 5. Logarithmic representation of the UV spectral region of a solar global irradiance measurement of all three measurement devices on 18 May 2017 in the synchronised time window from 10:45:59 UTC to 11:15:59 UTC. Left: 280 nm to 420 nm. Right: UV-B edge 290 nm to 310 nm.

A precise synchronisation in time is necessary to synchronise the fast-acquired data of the array spectroradiometers (full spectral scan within seconds, one timestamp for one full spectral distribution) with the data of the NDACC device (about 35 min for one full spectral scan, a timestamp for each wavelength). Based on the timestamp of each wavelength step of the NDACC device a corresponding measurement of the array spectroradiometers can be selected. Hence a synchronisation between the different measurement devices can be applied. To limit the amount of data during the measurement campaign, the array spectroradiometers single measurements were averaged in order to record one measurement every minute.

The typical temperature variation within the housing of the measurement device during the measurement campaign was better than ±0.2 °C for the NDACC device and better than ±0.1 °C for the UV-BTS and VIS-BTS. The ambient temperature ranged from 10 °C to 28 °C in this period in maximum. The relative humidity varied from 56% to 88% reaching its peak during stormy weather on 18 May 2017.

In order to compare the resulting spectral data of the three devices that all pose a different optical bandwidth (FWHM), a convolution to the same optical bandwidth (FWHM) was applied. The UV-BTS and NDACC device data were convolved with a 1 nm triangular bandpass for their intercomparison, the VIS-BTS and NDACC device data to 2.2 nm.

For global solar irradiance measurements, the spectral data of all devices were corrected using the MatShic algorithm in terms of wavelength accuracy (Egli 2014).

A check of the NDACC device, UV-BTS and VIS-BTS calibration was performed at the measurement platform with the help of the field calibrator (Seckmeyer 1989). This check was performed before and after the measurement campaign for both BTS and daily for the NDAAC device. In addition, after the measurement campaign, a stability test of the calibration was performed with the VIS-BTS for about one month.

The absolute measurement uncertainty of the UV-BTS for spectral irradiance was determined with a Monte Carlo based uncertainty evaluation (Vaskuri *et al* 2018). The resulting expanded measurement uncertainty ($k = 2$) was estimated as 2.5%. In this study the different contributions to the overall measurement uncertainty are also discussed.

5. Results of the measurement campaign

5.1. Spectroradiometric evaluation

In figure 5, the global spectral irradiance in the UV under clear sky conditions on 18 May 2017 of all three devices is presented for the synchronised time window from 10:45:59 UTC to 11:15:59 UTC. Based on this representative data, the stray light detection threshold and its corresponding wavelength by typical solar measurements are determined and stated in table 3. For the evaluation averaging was applied for both BTS measurements and the data has been compared to the NDAAC device which shows a stray light level and detection threshold of $9 \cdot 10^{-7}$ Wm^{-2} nm^{-1}(see section 3.3). Since noise and stray light could not be further separated for the BTS devices this level has been stated. The wavelength correction according the MatShic algorithm which was applied was during the measurement campaign in maximum for the

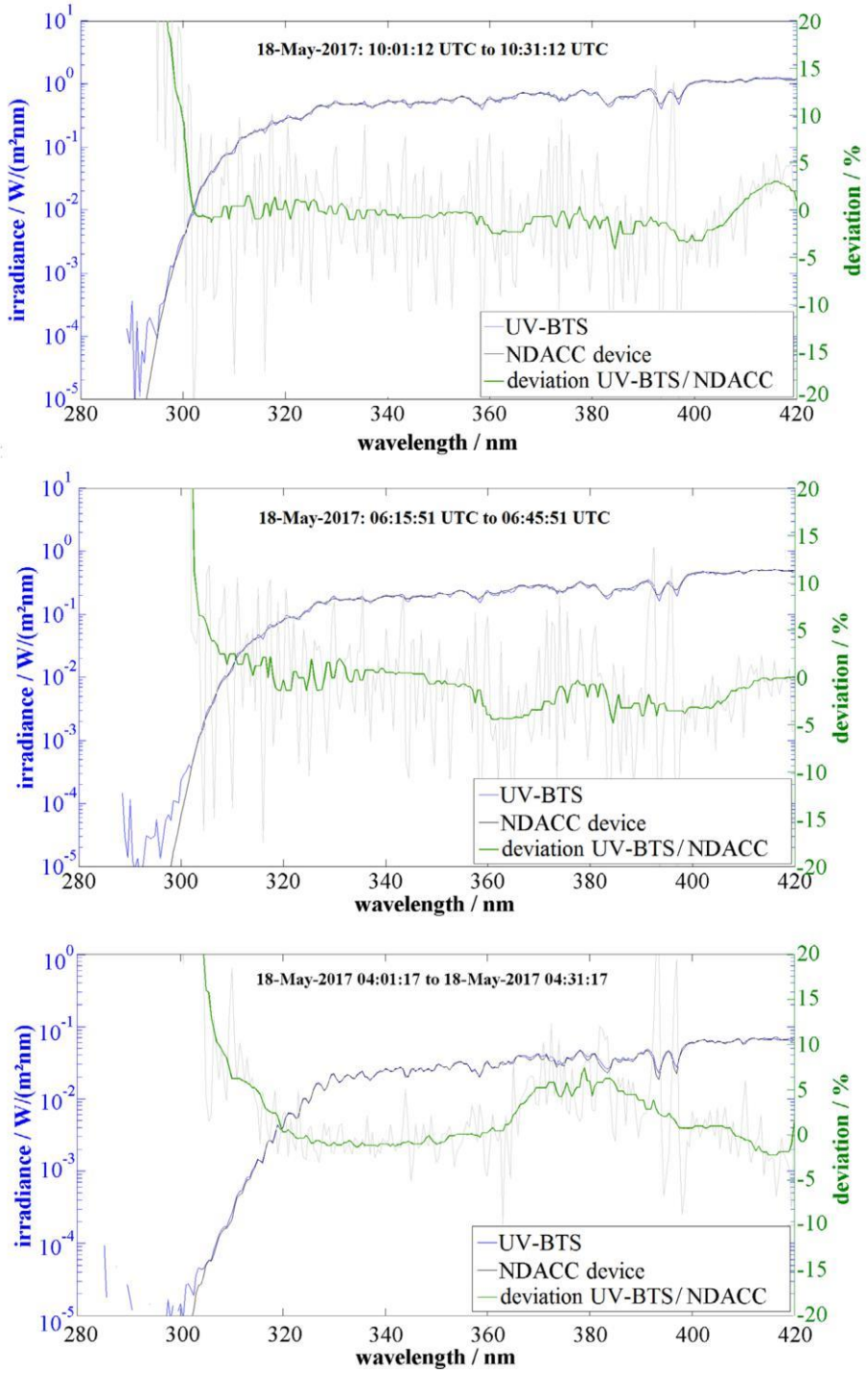

Figure 6. Logarithmic representation of the UV-BTS (blue) and the NDACC device (black) data in the spectral range 280 nm to 420 nm of the solar global irradiance measurement (left *y*-axis) on 18 May 2017 in the synchronised time window from 10:01:12 UTC to 10:31:12 UTC (SZA = 35.7°) in the upper part, from 06:15:51 UTC to 06:45:51 UTC (SZA = 66.2°) in the middle part and from 04:01:17 UTC to 04:31:17 UTC (SZA = 85.41°) in the lower part. The deviation in grey and the smoothed deviation (median filter—20 data points) in green are plotted (right *y*-axis).

UV-BTS −0.028 nm, for the VIS-BTS −0.23 nm and for the NDACC device −0.19 nm.

In figure 6, the global spectral irradiance data of the UV-BTS and the NDACC device and its deviation from each other are shown. A deviation (smoothed curve) lower than ±2.5% in the spectral range from 300 nm to 420 nm is achieved for the SZA below 70°. The non-smoothed curve shows larger deviations which can be explained by the remaining differences of the respective slit functions and optical bandwidths of the devices. In addition these data reflect the stated detection threshold of figure 5.

Figure 7 shows the global spectral irradiance data from the VIS-BTS and the NDACC device. Here, a deviation (smoothed curve) smaller than ±2% in the spectral range

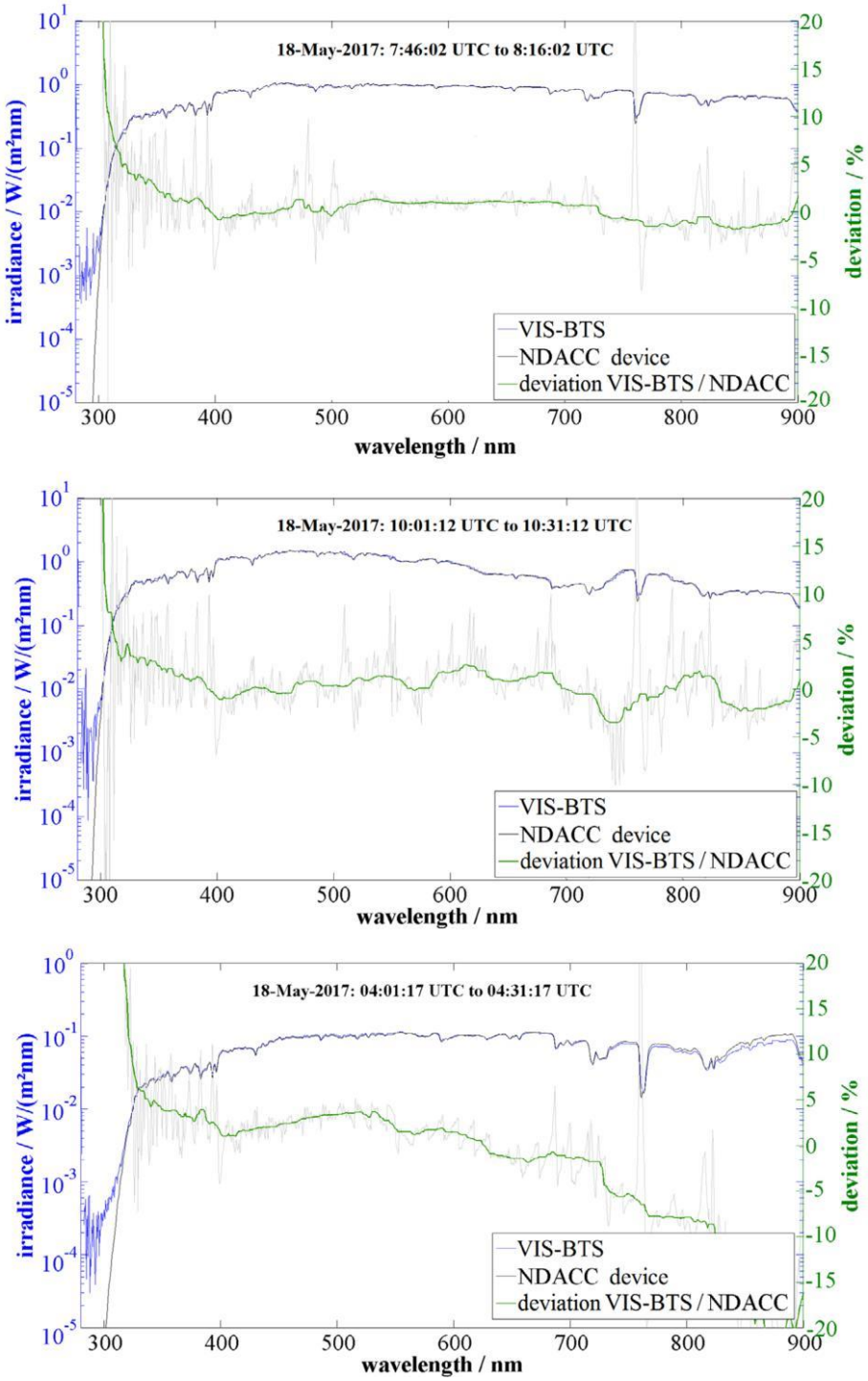

Figure 7. Logarithmic representation of the VIS-BTS (blue) and the NDACC device (black) data in the spectral region 280 nm to 900 nm of a solar global irradiance measurement (left *y*-axis) at 18 May 2017 in the synchronised time window from 7:46:02 UTC to 8:16:02 UTC (SZA = 52.2°) in the upper part and from 10:01:12 UTC to 10:31:12 UTC (SZA = 36.0°) in the middle part and from 04:01:17 UTC to 04:31:17 UTC (SZA = 85.41°) in the lower part. The deviation in grey and the smoothed deviation (median filter—20 data points) in green are plotted (right *y*-axis).

from 365 nm to 900 nm is achieved for SZA below 70°. Below 365 nm, the deviation rises to +7% at 305 nm. The non-smoothed curve shows larger deviations which can be again explained by the remaining differences in optical bandwidth between the devices. These data reflect as well the detection threshold of figure 5. For higher SZA (85.41°) the wavelength dependent cosine error of both devices (see sections 3.2 and 3.3) increases the deviation in the longer wavelength range.

To illustrate the radiometric stability of the measurement system during the measurement campaign, histograms of the smoothed relative standard deviation between the UV-BTS and the NDACC device from 300 nm to 420 nm of all measurements of the measurement campaign are presented (see

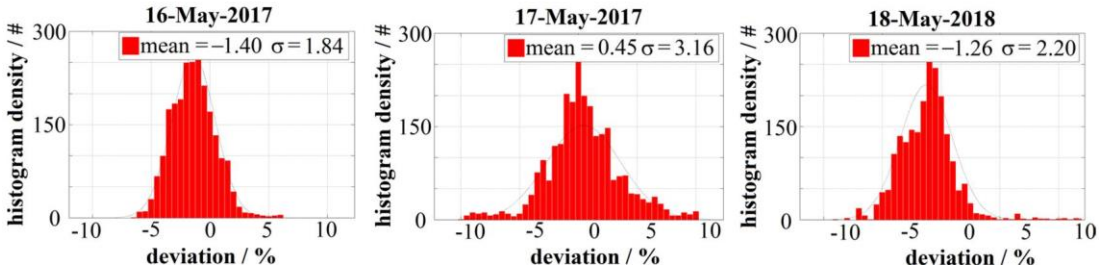

Figure 8. Histogram of the smoothed spectral relative standard deviation of the UV-BTS and the NDACC device between 300 nm to 420 nm.

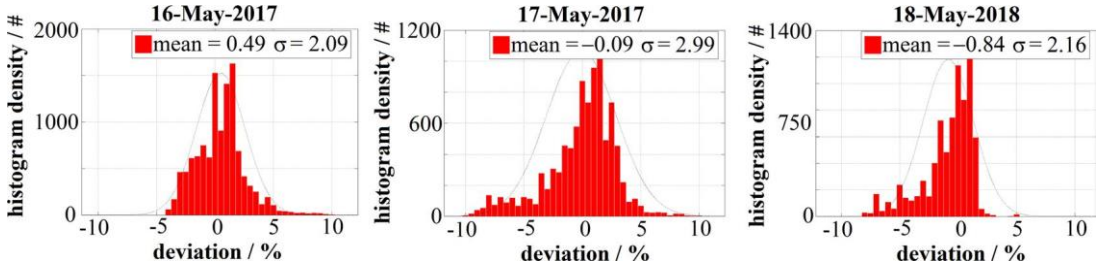

Figure 9. Histogram of the smoothed spectral relative standard deviation of the VIS-BTS and the NDACC between 400 nm to 900 nm.

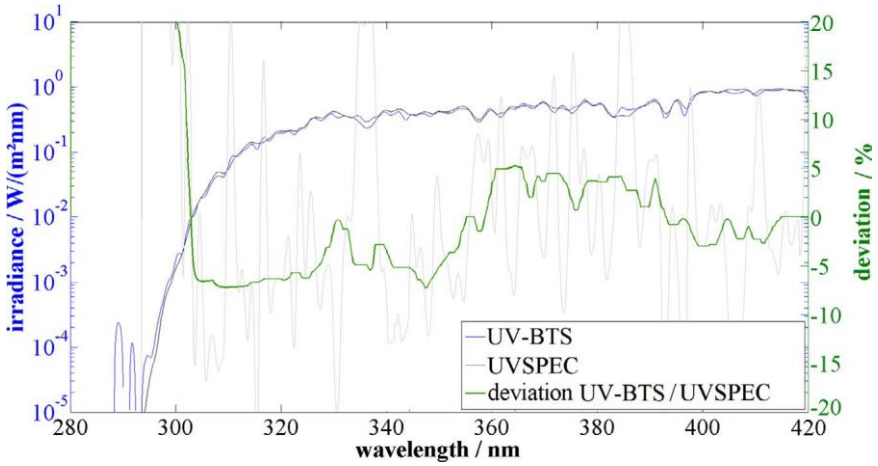

Figure 10. Intercomparison of UVSPEC (black) generated data with a UV-BTS (blue) measurement on 18 May 2017 8:13 UTC (left *y*-axis), SZA = 47°. The deviation in grey and the smoothed deviation (median filter) in green are plotted (right *y*-axis).

figure 8). Only measurements with insufficient synchronisation in time, which represent just 8% of all measurements, are not considered. On 17 May 2017, the relative standard deviation increases by about 1%, which is caused by an insufficient synchronisation in time as a result of the high cloud variability on this day (see table 2) The spectral dependency of these data do not change significantly compared to figure 6.

An analogue histogram visualization for the VIS-BTS and the NDACC device between 400 nm to 900 nm is presented in figure 9. The relative standard deviation between VIS-BTS and NDACC also shows a slightly higher relative standard deviation on the 17 May 2017 for the same reason: a higher cloud variability leading to a worse temporal synchronization. The spectral dependency of these data does not change significantly compared to figure 7.

The UV-BTS agrees within ±1.5% (average from 300 nm to 420 nm), the VIS-BTS within ±1% (average from 400 nm to 900 nm) with the NDACC device during the intercomparison. Additionally, an intercomparison of a UV-BTS global spectral irradiance measurement with UVSPEC/libradtran (Mayer and Kylling 2005, Emde *et al* 2016) generated data, within the clear sky period on 18 May 2017, has been evaluated. The UVSPEC/libradtran data (typical input parameters for Hanover with default values for aerosol by a visibility of 50 km and an albedo of 0.02 is used, which is typical for many surfaces in the UV wavelength region (Feister and Grewe 1995)): SZA 48.45°, SAA 294.70°, ozone 300 DU, albedo 0.02, altitude 52 m, libradtran version 1.7) was convolved to 0.8 nm FWHM in order to compare it with the UV-BTS measurement. A deviation of ±5% in the spectral range from 304 nm to 420 nm can be observed (see figure 10).

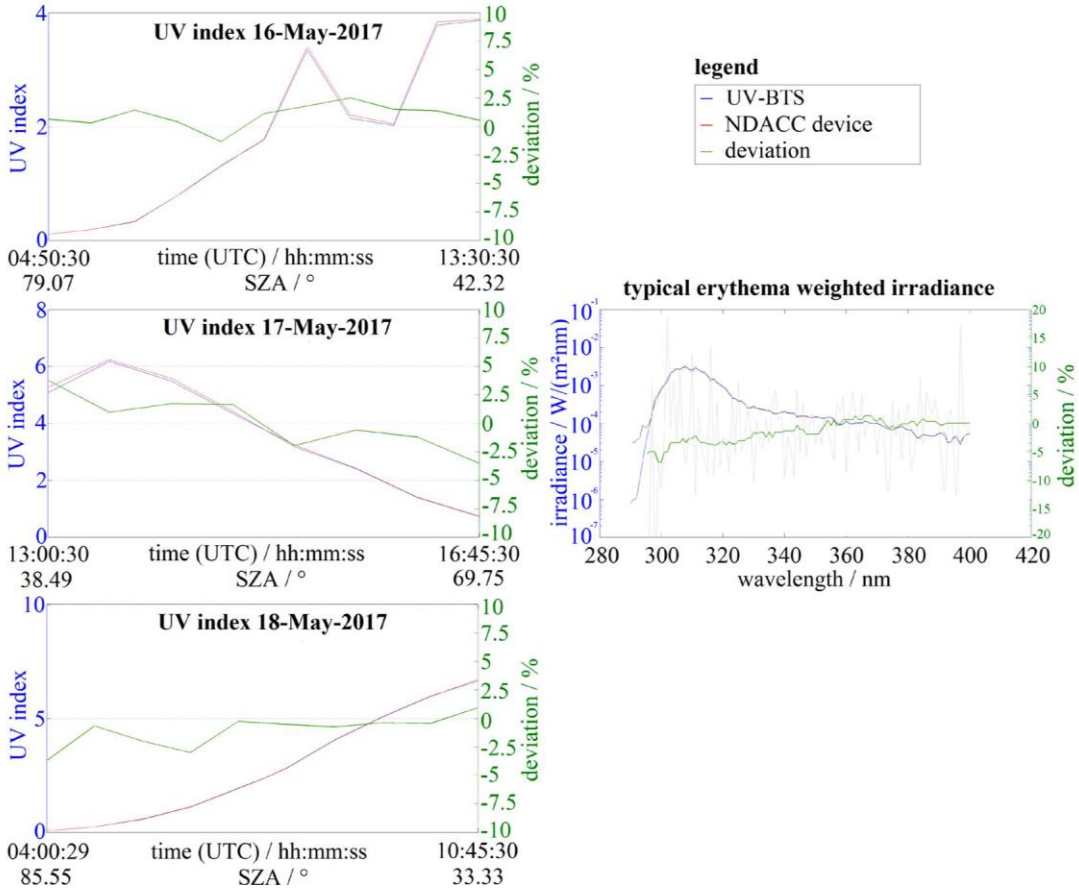

Figure 11. Diurnal variation of the integrated quantity UV index between the UV-BTS and the NDACC device from 16 to 18 May 2017. A deviation of less than ±1% is achieved on 18 May 2018 for SZA less than 70°. Only at SZAs higher than 70°, it is exceeds about −3%. The deviation is below ±2.5% on 16 May and below ±3% on 17 May 2017. On the right side, the erythema weighted spectral irradiance is presented.

5.2. Evaluation of some diurnal quantities

5.2.1. UV index/erythema. For evaluating the stability of the UV-BTS in terms of dynamic range, an integrated quantity is analysed in a diurnal comparison to the NDACC device (see figure 11). In the UV region, the UV index (WHO 2002), or the erythema weighted irradiance (McKinlay 1987), seems to be an appropriate quantity. A deviation smaller than ±1% was found where synchronisation in time is sufficiently good (see 18 May 2017) for SZA less than 70°. At SZA larger than 70° where longer integration times are needed and with high cloud variability (see especially 17 May 2017), the deviation rises to a maximum of ±3% due to insufficient synchronisation in time.

The UV index was as well determined with the VIS-BTS. Due to the insufficient reduction of stray light in the UV wavelength range of the VIS-BTS (see figure 5 and table 3), despite the mathematical stray light reduction, the deviation of UV index increased from 4% between a SZA of 33° to 35% and a SZA of 70° (18 May 2017). At higher SZA it steadily increases further (see figure 12). Therefore another less stray light sensitive integrated quantity was chosen to compare the data from the VIS-BTS to the NDACC.

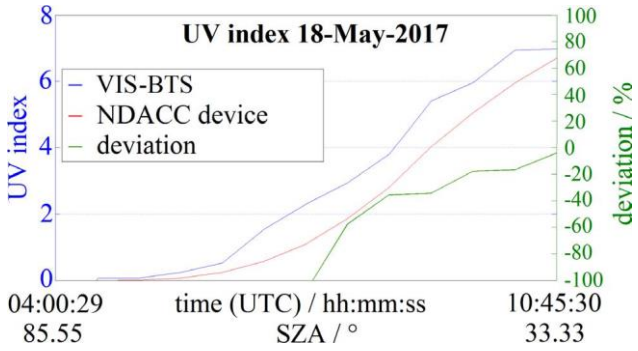

Figure 12. Diurnal variation of the integrated quantity UV index between the VIS-BTS and the NDACC device from 17 May 2017. The deviation increased from 4% between a SZA of 33° to 35% and a SZA of 70°. It steadily increases further for higher SZA.

5.2.2. Blue light hazard (BLH). For evaluating the stability and dynamic range of the VIS-BTS, an integrated quantity is analysed as well in diurnal variation. In the visible spectral region, the blue light hazard (BLH), also called photoretinitis, has been chosen (Pautler *et al* 1990). Its weighting function is defined between 300 nm to 700 nm with its maximum between

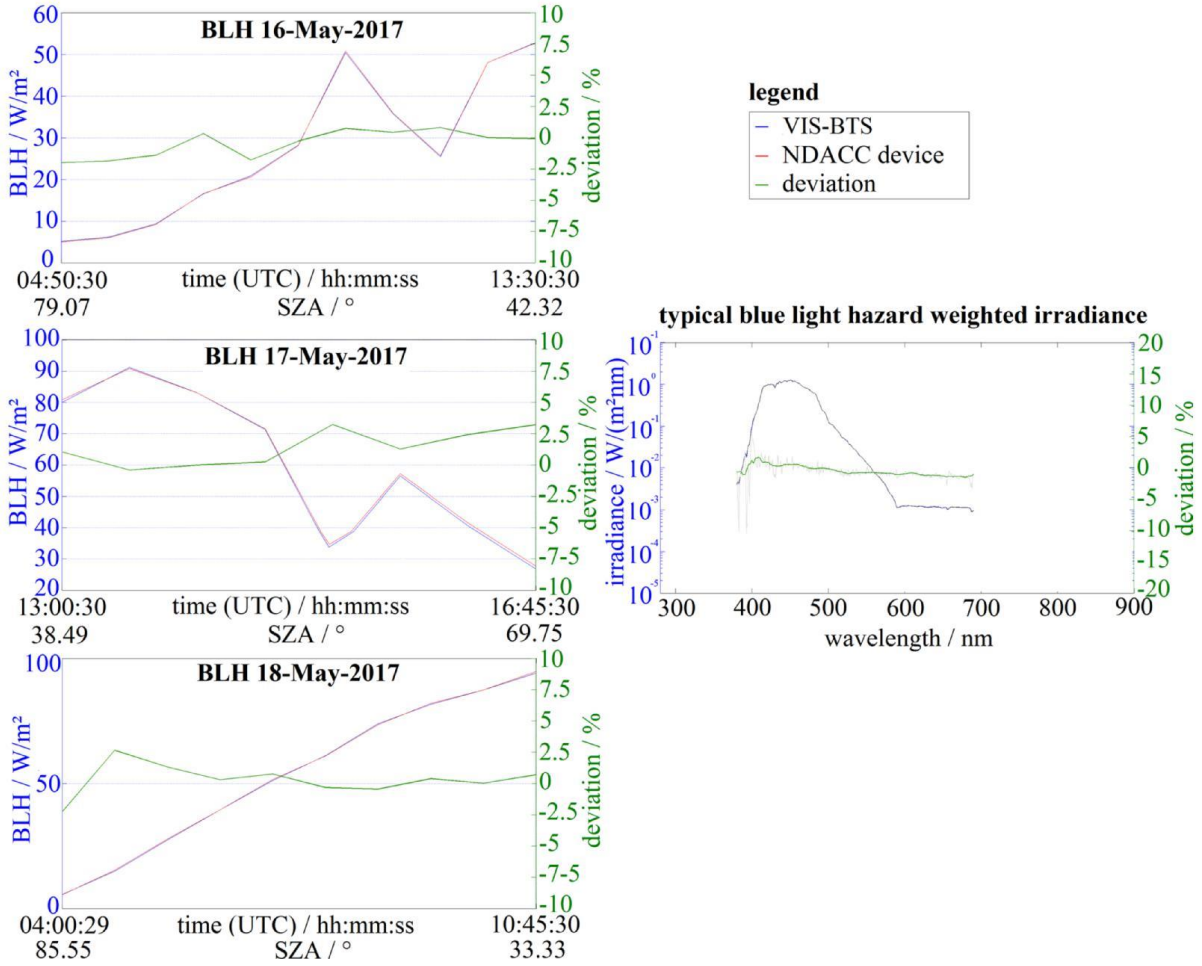

Figure 13. Diurnal variation of the integrated quantity BLH between the VIS-BTS and the NDACC device from 16–18 May 2017. A deviation of ±1% is only exceeded at low SZAs or by high cloud variability to ±3%, see especially 17 May 2017. On the right side, the blue light hazard weighted spectral irradiance is presented.

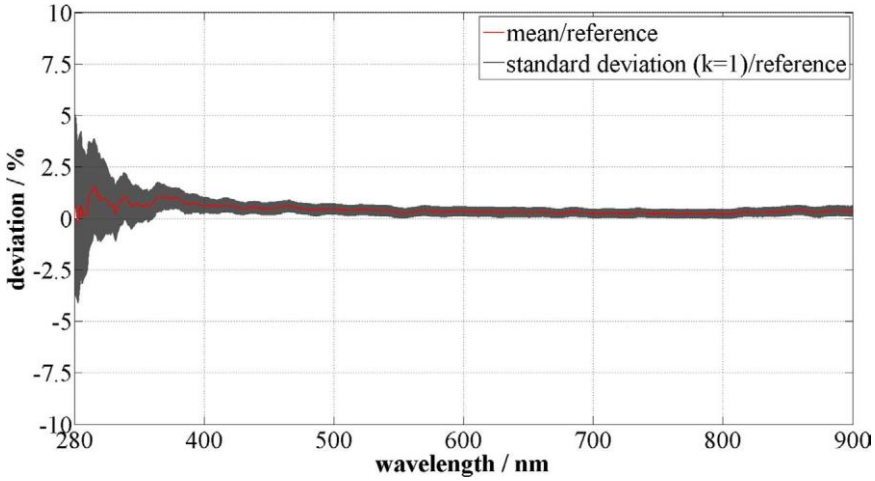

Figure 14. Spectroradiometric calibration stability of the VIS-BTS evaluated in the period 28 November 2017 to 17 January 2018 (weekly check). The deviation is below 1% between 350 nm to 900 nm. Below 350 nm, the deviation rises due to an insufficient signal to noise ratio by the measurement of the halogen calibration lamp.

400 nm to 500 nm. Figure 13 shows that a deviation smaller than ±1% was found. By high cloud variability and a SZA above 70°, the deviation rises to a maximum of ±3% due to insufficient synchronisation in time.

5.3. Stability test of the calibration

For evaluating the radiometric longer term calibration stability of the BTS2048 series, a test after this measurement campaign was performed. The VIS-BTS was first calibrated in the

Table 4. Comparison of the WMO specifications for double monochromators (Seckmeyer *et al* 2001) and array spectroradiometers (Seckmeyer *et al* 2010) with the UV-BTS. Green are marked quantities which meet the double monochromator specifications, orange are marked quantities which meet the array spectroradiometer specifications.

Quantity	WMO quality for double monochromators (S-2 instruments)	WMO quality for array spectroradiometers	UV-BTS
Cosine error	< ±5% for incidence angles <60°	< ±5% for incidence angles <60°	< ±3% for incidence angles <90°
Minimum spectral range	290 nm–400 nm	280 nm–400 nm	200 nm–400 nm
Bandwidth (FWHM)	<1 nm	<1 nm	0.8 nm
Wavelength precision	< ±0.03 nm	< ±0.05 nm	±0.05 nm
Wavelength accuracy	< ±0.05 nm	< ±0.1 nm	±0.05 nm
Slit function	$<10^{-3}$ of maximum at 2.5 FWHM away from centre $<10^{-5}$ of maximum at 6.0 FWHM away from centre	$<10^{-3}$ of maximum at 2.5 FWHM away from centre	10^{-3} of maximum at 2.5 FWHM away from centre
Sampling wavelength interval	<0.5 FWHM	<0.2 FWHM (>5 pixels/ FWHM)	0.16 FWHM (6 pixels/ FWHM)
Maximum irradiance	>2 $Wm^{-2}nm^{-1}$ (noon, maximum at 400 nm)	>2 Wm^{-2} nm^{-1} (noon, maximum at 400 nm)	100 000 Wm^{-2} nm^{-1} (noon, maximum at 400 nm)
Detection threshold	$<10^{-6}$ Wm^{-2} nm^{-1} (for SNR = 1 at 1 nm FWHM)	$<10^{-3}$ Wm^{-2} nm^{-1}	$5 \cdot 10^{-5}$ Wm^{-2} nm^{-1}
Stray light	$<10^{-6}$ Wm^{-2} nm^{-1} (for SNR = 1 at 1 nm FWHM) when the instrument is exposed to the sun at a minimum SZA	$< 10^{-3}$ Wm^{-2} nm^{-1}	$5 \cdot 10^{-5}$ Wm^{-2} nm^{-1}
Instrument temperature	Monitored; typical temperature stability < ±2 °C to achieve a sufficient overall instrument stability	Monitored and sufficiently stable to maintain overall instrument stability	Monitored and temperature stability better than ± 1 °C
Scan time	<10 min, e.g. for ease of comparison with models	>0.1 Hz	~100 Hz
Overall calibration uncertainty	< ±5% (unless limited by threshold)	< ±10% (unless limited by detection threshold)	< ±6%
Scan date and time	Recorded with each spectrum such that timing is known to within 10 s at each wavelength	Recorded with each spectrum such that timing is known to within 1 s	Recorded with each spectrum such that timing is known much better than 1 s
Nonlinearity	No statement	<2% for signals more than50 times above detection threshold	<1% for signals more than 50 times above detection threshold

laboratories of Gigahertz-Optik GmbH (reference measurement) and afterwards placed outside for measurements. During this period, its calibration was regularly checked by a halogen standard based irradiance calibration setup. During this time there was a temperature fluctuation of +14.2 °C to −6.5 °C and a relative humidity of 34% to 96%. In addition, the weather in this period was very unstable, so a variety of environmental influences could be tested (snow, strong wind, continuous rain and clear sky). The results are illustrated in figure 14. The deviation of the mean to the reference is below 1% in the whole spectral region. The standard deviation (k = 1) of the mean is as well below 1%, however it rises below 350 nm due to an insufficient signal to noise ratio of the halogen calibration lamp.

6. Discussion and conclusion

The measurement system consisting of a UV-BTS spectroradiometer and a VIS-BTS spectroradiometer is characterised and validated in a measurement campaign compared to a well-established double monochromator-based NDACC device.

The VIS-BTS, with mathematical stray light reduction, is able to measure solar global irradiance for wavelengths longer than 298.3 nm where it reaches its detection threshold for solar measurements of $2 \cdot 10^{-3}$ Wm^{-2} nm^{-1}. The UV-BTS is able to measure until 294.1 nm by a detection threshold of $5 \cdot 10^{-5}$ Wm^{-2} nm^{-1} which enables UV index measurements for many applications. These thresholds have been determined by a SZA of 33°. The campaign data suggests that the detection threshold does not change with the solar irradiance level for both devices. In addition, the cosine error with an f_2 below 2.5% for the UV-BTS and below 3% for the VIS-BTS is small compared to other similar instruments (Seckmeyer and Bernhard 1993).

Evaluations of the global spectral irradiance measurements show that a deviation lower than ±2.5% in the spectral range from 300 nm to 420 nm is achieved by the UV-BTS for SZA below 70°. The VIS-BTS shows a deviation smaller than ±2% in the spectral range from 365 nm to 900 nm and SZA below 70°. Below 365 nm, the deviation rises up to +7% at 305 nm due to remaining stray light. For SZA above 70° the

deviation increases for both BTS, especially for the VIS-BTS in the wavelength range above 730 nm, it rises to max. 20% at 900 nm and a SZA of 85°. This may be explained by the larger cosine error at higher wavelength of the VIS-BTS.

The histograms of the relative standard deviation of the global spectral irradiance data of both BTS to the NDACC device in figures 8 and 9 illustrate that the measurement systems were stable over the whole measurement campaign. The UV-BTS agrees within ±1.5% on average, the VIS-BTS within ±1% with the NDACC device in their corresponding overlapping wavelength range of this analysis (300 nm to 420 nm for the UV-BTS and 400 nm to 900 nm for the VIS-BTS) during the intercomparison. However, the data show that, especially on 17 May 2017, the relative standard deviation increases by about 1%. This may be explained by the high cloud variability on this day, hence the introduced additional deviation due to the measurement desynchronization. The double monochromator-based NDACC device scans one wavelength step in about 1 s, hence one total scan lasts about 35 min. The BTS2048 data was averaged in a way that about every minute a measurement was recorded at typical irradiance levels. These settings were chosen since we assumed that this is a good trade-off between amount of data to be stored and sufficient synchronisation for global irradiance measurements with low uncertainty. However, the results showed that within this minute, where about 60 nm are scanned by the NDACC device, significant changes of the spectral irradiance can occur under variable sky conditions. Therefore, the much shorter measurement intervals of the BTS devices are of interest.

During a clear sky period, an intercomparison of a UV-BTS measurement with UVSPEC generated data was performed. The results show a deviation better than ±5% in the range 304 nm to 420 nm. Cordero *et al* (2013) found an uncertainty for UVSPEC irradiance of about 3% for unpolluted and 5% for polluted atmospheres. Mayer *et al* (1997) found systematic differences of −11% to 2% between measurements and UVSPEC generated data within 295 nm to 400 nm. This suggests that the achieved agreement better than ±5% was well within the expected range. In addition, the curve shape of the ±5% deviation might follow an artefact of the UVSPEC algorithm which was suggested by Mayer *et al* (1997) who showed a similar deviation between NDACC measurement and model.

In order to investigate the dynamic range and stability of the system a diurnal comparison of the integrated quantities, UV index for both BTS and BLH for the VIS-BTS with the NDACC device, was compared. The deviation of the VIS-BTS for UV index is increasing from 4% between a SZA of 33° to 35% and a SZA of 70°. It steadily increases further for higher SZA. Since the device is not designed to determine the UV index (insufficient stray light reduction), this was to be expected. A deviation smaller than ±1% was found for the UV index determination of the UV-BTS and the BLH determination of the VIS-BTS provided sufficient synchronisation between measurements was possible and for SZAs below 70°. If synchronization could not be guaranteed the deviation rises to a maximum of ±3% for conditions with high cloud variability or a SZA larger than 70°. It is notable that, even at very high SZA values of about 85° during a period with sufficient synchronisation, only a deviation of −3% for UV index evaluations exists. This is a significant improvement to the 5% uncertainty by SZA values smaller than 50° determined by Egli *et al* (2016).

Further outdoor measurements showed that the change of the radiometric calibration of the VIS-BTS is below 1% in a period of about one month. This suggests that the measurement system should be suitable for long term outdoor measurements.

In table 4, the achieved quality of the UV-BTS is compared to the recommendations of the WMO (Seckmeyer *et al* 2001, 2010). The data shows that the array spectroradiometer UV-BTS meets almost all specifications for WMO S-2 instruments (typically double monochromator). Only the stray light level of $< 10^{-6}\,\mathrm{Wm^{-2}\,nm^{-1}}$ cannot be reached. However, the stray light level of $5 \cdot 10^{-5}\,\mathrm{Wm^{-2}\,nm^{-1}}$ is significantly better than the WMO array spectroradiometer specification of $< 10^{-3}\,\mathrm{Wm^{-2}\,nm^{-1}}$.

These evaluations showed that a sophisticated and for this application tuned array spectroradiometer system is able to measure solar global irradiance in the UV, VIS and NIR spectral region with comparable uncertainty than a double monochromator-based NDACC device.

ORCID iDs

Ralf Zuber https://orcid.org/0000-0001-7794-9730

References

Armstrong B K and Kricker A 2001 The epidemiology of UV induced skin cancer *J. Photochem. Photobiol.* B **63** 8–18

ASABE 2017 *Quantities and Units of Electromagnetic Radiation for Plants (Photosynthetic Organisms)* p 1

Bais A F 1998 Standardization of ultraviolet spectroradiometry in preparation of a European network (SUSPEN) *Final Report* European Commission, Dir. Gen. XII, Luxembourg

Bernhard G and Seckmeyer G 1999 Uncertainty of measurements of spectral solar UV irradiance *J. Geophys. Res. Atmos.* 104 14321–45

Blumthaler M and Ambach W 1988 Solar UVB-Albedo of various surfaces *Photochem. Photobiol.* **48** 85–8

Brovkin V, Boysen L, Raddatz T, Gayler V, Loew A and Claussen M 2013 Evaluation of vegetation cover and land-surface albedo in MPI-ESM CMIP5 simulations *J. Adv. Model. Earth Syst.* **5** 48–57

Cordero R R, Seckmeyer G, Alessandro D, Fernando L and David L 2013 Monte Carlo-based uncertainties of surface UV estimates from models and from spectroradiometers *Metrologia* **50** L1

De Mazière M *et al* 2018 The network for the detection of atmospheric composition change (NDACC): history, status and perspectives *Atmos. Chem. Phys.* **18** 4935–64

DIN-EN 2012 DIN EN 13032-1:2012-06

Egli L 2014 *Post Processing of Data From Array Spectroradiometer* (Davos: UVnet Workshop)

Egli L *et al* 2016 Quality assessment of solar UV irradiance measured with array spectroradiometers *Atmos. Meas. Tech.* 9 1553–67

Emde C *et al* 2016 The libRadtran software package for radiative transfer calculations (version 2.0.1) *Geosci. Model Dev.* 9 1647–72

Engelsen O, Brustad M, Aksnes L and Lund E 2005 Daily duration of Vitamin D synthesis in human skin with relation to latitude, total ozone, altitude, ground cover, aerosols and cloud thickness *Photochem. Photobiol.* **81** 1287–90

Feister U and Grewe R 1995 Spectral albedo measurements in the UV and visible region over different types of surfaces *Photochem. Photobiol.* **62** 736–44

Godar D E 2005 UV doses worldwide *Photochem. Photobiol.* 81 736–49

Gröbner J and Sperfeld P 2005 Direct traceability of the portable QASUME irradiance scale to the primary irradiance standard of the PTB *Metrologia* **42** 134

Gröbner J *et al* 2005 Traveling reference spectroradiometer for routine quality assurance of spectral solar ultraviolet irradiance measurements *Appl. Opt.* **44** 5321–31

He T, Liang S and Song D-X 2014 Analysis of global land surface albedo climatology and spatial-temporal variation during 1981–2010 from multiple satellite products *J. Geophys. Res. Atmos.* **119** 10.281–98

Hofmann M and Seckmeyer G 2017 Influence of various irradiance models and their combination on simulation results of photovoltaic systems *Energies* **10** 1495

Hülsen G, Gröbner J, Nevas S, Sperfeld P, Egli L, Porrovecchio G and Smid M 2016 Traceability of solar UV measurements using the Qasume reference spectroradiometer *Appl. Opt.* 55 7265–75

ICNIRP 1995 *Global Solar UV Index. A joint recommendation of the World Health Organization, the World Meteorological Organization, the United Nations Environment Programme, and the International Commission on Non-Ionizing Radiation Protection* (Oberschleißheim: International Commission on Non-Ionizing Radiation Protection)

JCGM 2012 *International Vocabulary of Metrology—Basic and General Concepts and Associated Terms (VIM)* 3rd edn (Sèvres: BIPM)

Kylling A, Persen T, Mayer B and Svenøe T 2000 Determination of an effective spectral surface albedo from ground-based global and direct UV irradiance measurements *J. Geophys. Res. Atmos.* **105** 4949–59

Lantz K O *et al* 2008 2003 North American interagency intercomparison of ultraviolet spectroradiometers: scanning and spectrograph instruments *SPIE* **33** 023547

Mayer B and Kylling A 2005 Technical note: the libRadtran software package for radiative transfer calculations—description and examples of use *Atmos. Chem. Phys.* **5** 1855–77

Mayer B, Seckmeyer G and Kylling A 1997 Systematic long-term comparison of spectral UV measurements and UVSPEC modeling results *J. Geophys. Res. Atmos.* **102** 8755–67

McKenzie R L, Liley J B and Björn L O 2009 UV radiation: balancing risks and benefits *Photochem. Photobiol.* **85** 88–98

McKinlay A F 1987 A Reference Action Spectrum for Ultraviolet Induced Erythema in Human Skin *CIE Research Note* vol 6

Nevas S, Gröbner J, Egli L and Blumthaler M 2014 Stray light correction of array spectroradiometers for solar UV measurements *Appl. Opt.* **53** 4313–9

Pautler E L, Morita M and Beezley D 1990 Hemoprotein(s) mediate blue light damage in the retinal pigment epithelium *Photochem. Photobiol.* **51** 599–605

Pulli T, Nevas S, El Gawhary O, van den Berg S, Askola J, Kärhä P, Manoocheri F and Ikonen E 2017 Nonlinearity characterization of array spectroradiometers for the solar UV measurements *Appl. Opt.* **56** 3077–86

Seckmeyer G 1989 Spektralradiometer für die ökologische Pflanzenforschung *Licht* **41** 501–6

Seckmeyer G and Bernhard G 1993 Cosine error correction of spectral UV-irradiances *Proc. SPIEE.* **2049**

Seckmeyer G, Bais A, Bernhard G, Blumthaler M, Booth C, Disterhoft P, Eriksen P, McKenzie R, Miyauchi M and Roy C 2001 *Instruments to Measure Solar Ultraviolet Irradiance. Part 1: Spectral Instruments Global Atmosphere* (*Watch Report No. 125*) (World Meteorological Organization) (https://library.wmo.int/pmb_ged/wmo-td_1066_en.pdf)

Seckmeyer G, Bais A, Bernhard G, Blumthaler M, Drueke S, Kiedron P, Lantz K, McKenzie R and Riechelmann S 2010 Instruments to Measure Solar Ultraviolet Radiation Part 4: Array Spectroradiometers *WMO TD No. 1538* (https://library.wmo.int/pmb_ged/wmo-td_1538.pdf)

Seckmeyer G, Erb R and Albold A 1996 Transmittance of a cloud is wavelength-dependent in the UV-range *Geophys. Res. Lett.* 23 2753–5

Seckmeyer G, Mayer B and Bernhard G 1997 *The 1997 Status of Solar UV Spectroradiometer in Germany: Results from the National Intercomparison of Spectroradiometers* (Aachen: Shaker)

Seckmeyer G, Schrempf M, Wieczorek A, Riechelmann S, Graw K, Seckmeyer S and Zankl M 2013 A novel method to calculate solar UV exposure relevant to Vitamin D production in humans *Photochem. Photobiol.* **89** 974–83

Shafer A B, Megill L R and Droppleman L 1964 Optimization of the Czerny–Turner spectrometer *J. Opt. Soc. Am.* **54** 879–87

Thuillier G, Hersé M, Labs D, Foujols T, Peetermans W, Gillotay D, Simon P C and Mandel H 2003 The solar spectral irradiance from 200 to 2400 nm as measured by the Solspec spectrometer from the Atlas and Eureca missions *Sol. Phys.* **214** 1–22

Vaskuri A, Kärhä P, Egli L, Gröbner J and Ikonen E 2018 Uncertainty analysis of total ozone derived from direct solar irradiance spectra in the presence of unknown spectral deviations *Atmos. Meas. Tech.* **11** 3595–610

Webb A R and Engelsen O 2006 Calculated ultraviolet exposure levels for a healthy Vitamin D status *Photochem. Photobiol.* 82 1697–703

Webb A R, Gardiner B G, Martin T J, Leszczynski K, Metzdoff J, Mohnen V A and Forgan B 1998 Guidelines for Site Quality Control of UV Monitoring *Rep. Ser. 126, Environ. Pollution Monitoring and Res. Programme* (Geneva: WMO)

WHO 2002 *Global Solar UV Index: A Practical Guide* (World Health Organization)

WMO 1998 Report of the WMO-WHO Meeting of Experts on Standardization of UV Indices and their Dissemination to the Public (Les Diablerets, Switzerland, 21–24 July 1997) *World Meteorological Organization Gobal Atmospheric Watch No. 127, WMO/TD-No. 921* (World Meteorological Organization)

Wuttke S, Seckmeyer G, Bernhard G, Ehramjian J, McKenzie R, Johnston P and O'Neill M 2006 New spectroradiometers complying with the NDSC standards *J. Atmos. Ocean. Technol.* 23 241–51

Zong Y, Brown S W, Johnson B C, Lykke K R and Ohno Y 2006 Simple spectral stray light correction method for array spectroradiometers *Appl. Opt.* **45** 1111–9

Zuber R, Sperfeld P, Riechelmann S, Nevas S, Sildoja M and Seckmeyer G 2018 Adaption of an array spectroradiometer for total ozone column retrieval using direct solar irradiance measurements in the UV spectral range *Atmos. Meas. Tech.* **11** 2477–84 (2018 1–12)

5.3 Article C: Technology for detecting spectral radiance by a snapshot multi-imaging spectroradiometer

5.3.1 Declaration of my contribution

The idea to this measurement system and its technology/procedure has been developed by the author of this thesis. In addition the author of this thesis made the design, construction, characterization and software programming of the measurement system. Furthermore, the author of this thesis performed the data evaluation of the measurements. Anton Gugg-Helminger supported the author of this thesis by the laboratory setup. Ansgar Stührmann developed the entrance optics for the hemispherical measurements. In addition, Ansgar Stührmann and Gunther Seckmeyer supported the measurement campaign.

5.3.2 Published article

This article has been published with open access in IOP Measurement Science and Technology.

Submitted: 11 August 2017
Accepted: 17 October 2017
Published: 22 November 2017

Zuber, R., Stührmann, A., Gugg-Helminger, A., and Seckmeyer, G.: Technology for detecting spectral radiance by a snapshot multi-imaging spectroradiometer, *2017 Meas. Sci. Technol. 28 125903*

DOI: https://doi.org/10.1088/1361-6501/aa9409

OPEN ACCESS
IOP Publishing

Measurement Science and Technology

Meas. Sci. Technol. **28** (2017) 125903 (9pp) https://doi.org/10.1088/1361-6501/aa9409

Technology for detecting spectral radiance by a snapshot multi-imaging spectroradiometer

Ralf Zuber[1,3], **Ansgar Stührmann**[2], **Anton Gugg-Helminger**[1] **and Gunther Seckmeyer**[2]

[1] Gigahertz-Optik GmbH, An der Kälberweide 12, 82299 Türkenfeld/Munich, Germany

[2] Institut für Meteorologie und Klimatologie, Leibniz Universität Hannover, Herrenhäuser Str. 2, 30419 Hannover, Germany

E-mail: r.zuber@gigahertz-optik.de

Received 11 August 2017, revised 13 October 2017
Accepted for publication 17 October 2017
Published 22 November 2017

Abstract

Technologies to determine spectral sky radiance distributions have evolved in recent years and have enabled new applications in remote sensing, for sky radiance measurements, in biological/diagnostic applications and luminance measurements. Most classical spectral imaging radiance technologies are based on mechanical and/or spectral scans. However, these methods require scanning time in which the spectral radiance distribution might change. To overcome this limitation, different so-called snapshot spectral imaging technologies have been developed that enable spectral and spatial non-scanning measurements. We present a new setup based on a facet mirror that is already used in imaging slicing spectrometers. By duplicating the input image instead of slicing it and using a specially designed entrance slit, we are able to select nearly 200 (14 × 14) channels within the field of view (FOV) for detecting spectral radiance in different directions. In addition, a megapixel image of the FOV is captured by an additional RGB camera. This image can be mapped onto the snapshot spectral image. In this paper, the mechanical setup, technical design considerations and first measurement results of a prototype are presented. For a proof of concept, the device is radiometrically calibrated and a 10 mm × 10 mm test pattern measured within a spectral range of 380 nm–800 nm with an optical bandwidth of 10 nm (full width at half maximum or FWHM). To show its potential in the UV spectral region, zenith sky radiance measurements in the UV of a clear sky were performed. Hence, the prototype was equipped with an entrance optic with a FOV of 0.5° and modified to obtain a radiometrically calibrated spectral range of 280 nm–470 nm with a FWHM of 3 nm. The measurement results have been compared to modeled data processed by UVSPEC, which showed deviations of less than 30%. This is far from being ideal, but an acceptable result with respect to available state-of-the-art intercomparisons.

Keywords: spectral snapshot imaging, sky radiance, snapshot multi-imaging spectroradiometer, spectroradiometer

(Some figures may appear in colour only in the online journal)

[3] Author to whom any correspondence should be addressed.

1. Introduction

Historically, technologies for assessing spectral imaging radiance data (also called hyperspectral imaging) are based on scanning in either the spectral (Hardeberg *et al* 2002, Gupta and Voloshinov 2004, Mathews 2008, Sigernes *et al* 2012) or spatial domain (Hu *et al* 2005). However, non-scanning, so-called snapshot spectral imaging technologies have become more popular in recent years (Content 1997, Matsuoka *et al* 2002, Henault *et al* 2004, Laurent *et al* 2006, Gehm *et al* 2007, Wagadarikar *et al* 2008, Gao *et al* 2010, Riechelmann *et al* 2013). These technologies allow time-resolved investigations of, e.g. cloud movements in atmospheric science, OLED (organic light emitting diode) panel investigations, chemical process analysis, mineralogy of planet surfaces (Brown *et al* 2010) and many more applications (Brown 2006). A detailed overview of the known spectral snapshot imaging technologies and applications is given in (Hagen and Kudenov 2013). In the following paragraph, a short appraisal is presented to explain the important differences between spectral-scanning, mechanical-scanning and spectral snapshot measurements (figure 1).

Spectral scans (figure 1, second from left) are achieved using, for example optical filter glasses, acoustooptical filters or interferometers. The spectral resolution and spectral domain of this approach is determined by the filtering technology and the measurement time. For higher resolution, a large number of measurements is needed. Furthermore, in some wavelength regions like the UV, only a few types of filters are available whereby the optical performance is limited. However, the advantage of these technologies is a very high spatial resolution since, in principle, high-resolution photographic cameras can be used (Bianco *et al* 2010). Mechanical scans (figure 1, point scanning on the left or line-scanning second from right) vary the field of view (FOV) by either moving the whole spectroradiometer (e.g. remote sensing with the help of satellites or aircraft) or by using mirror-based scanners. As a result, the spatial resolution of point-scanning devices (1D array detector) in both dimensions (x, y) depends on the number of scans. When using line-scanning devices (2D array detector), one spatial dimension (e.g. x) depends on the number of scans, the other (e.g. y) on the number of pixels that can be resolved by the device within the measurement line. This technology is also called push-broom scanning (Davis *et al* 2002, Brown *et al* 2008). Hence, the spatial resolution is limited by the measurement time. The advantage of this technology is based on the freedom in the choice of the spectrometer design and performance.

However, all scanning technologies have the common disadvantage that time-resolved effects can only be analyzed when they are significantly slower than the scanning itself. Spectral and point-scanning measurements take time and thus fast temporal effects like cloud movement cannot be resolved.

To analyze such kind of tasks, snapshot spectral imaging technologies are needed. One of many existent approaches is based on imaging a coded spatial and spectral information mixture on the detector and mathematically reconstructing the spectral snapshot image (Gehm *et al* 2007, Wagadarikar *et al* 2008). Another approach is the so-called integral field spectroscopy (IFS) snapshot technology, such as fiber bundle-based technologies (IFS-F), where single fibers capture the signal of one measurement channel (Hagen and Kudenov 2013). These fibers are lined up on the entrance slit of a line-scanning spectrometer. Subsequently, the maximum spatial resolution is limited by the number of fibers that can be mechanically lined up and optically imaged without channel crosstalk on the detector. A higher resolution system has been achieved by Riechelmann *et al* (2013) with a spatial resolution of 113 channels. Furthermore, a couple of image slicing spectrometer (ISS) technologies (one example being IFS-M) are known for applications in astronomy or for microscopy purposes (Content 1997, Henault *et al* 2004, Laurent *et al* 2006, Gao *et al* 2009). These approaches are based on a facet mirror optical design, which slices the image into single parts that are spectrally resolved.

In this paper, a new type of IFS approach is presented. A facet mirror is used to produce duplicated images instead of slicing the image as with known IFS-M technologies. For the spatial resolution, different parts of each duplicated image are selected by the entrance slit of a line-scanning spectrometer. These parts are spectrally resolved and can be rearranged by software to obtain the spectral snapshot image afterwards. In addition, a RGB camera can take a high resolution image of one duplicated image by the facet mirror. These data can be used as meta information to simplify further data analysis. For example, the image can be mapped to the lower resolution spectral snapshot imaging data.

The new design is based on very few optical parts and a well-known line-scanning spectrometer with freedom in design of spectral range, spectral resolution and optical bandwidth (full width at half maximum or FWHM Seckmeyer *et al* (2001)). The new system is called 4D Imager since measurements of an image (2D), spectral resolution (1D) and snap-shot in time (1D) with well-balanced performance in all four dimensions could be achieved.

1.1. *Fundamental concept of the 4D Imager*

The essential part of the 4D Imager is a facet mirror (figure 2(b)), which is reflecting the incoming image (figure 2(a)) in different directions. The reflection angle α depends on the specific facet angle β:

$$\alpha = 2 \cdot \beta. \quad (1)$$

As shown in figure 2 with one larger mirror (figure 2(c)), these signals can be imaged at the image plane d. Depending on their reflecting angle α, multiple images are generated since they are lined up as duplicated images in the imaging plane (figure 2(d)) in different heights h. The height h depends on the reflection angle α, focal length of the mirror, object and imaging distance. These quantities can be determined by the well-known imaging formulas. For gathering further information about the object, one part of the signal can imaged on an additional camera to obtain a higher spatial resolution image (figure 2(e)).

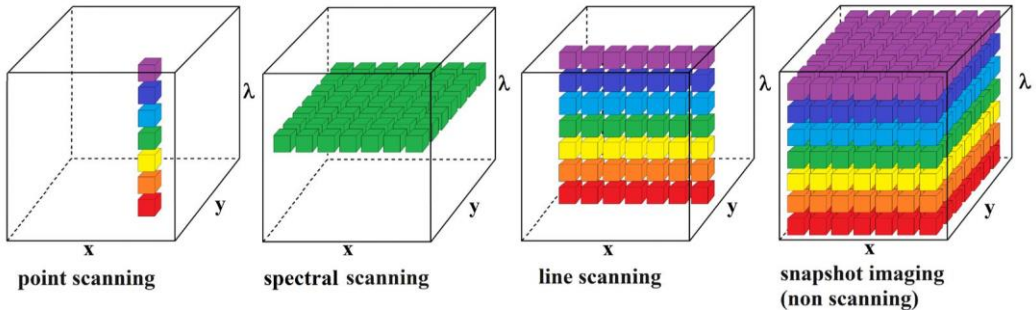

Figure 1. Schematical overview of different type of imaging spectrometer technologies.

The lined up images (figure 2(d)) are physically identical and contain the same information. The number of images is determined by the number of facets. In order to extract different information, or parts, out of each image, a customized aperture is used. After the aperture, the lined up image parts enter a well-known line-scanning spectrometer and can be spectrally resolved. Due to a fixed correlation between the slit position and image pixel, the measured data can be rearranged to get the spectral snapshot image voxels (x, y, λ). This imaging process is schematically shown in figure 3.
This technology has been successfully patented (Zuber 2015).

2. Design considerations

The size and angle of the mirror facets have to be chosen in such a way that they fit to the whole spectrometer design. The number of facets m of the facet mirror defines the spatial nominal resolution in one dimension (e.g. x). The spatial resolution in the other dimension (y) is given by the following formula:

$$y = \frac{n}{m} - u \tag{2}$$

where n represents the number of pixels, which can be resolved spectrally by the line-scanning spectrometer. u is a parameter depending on the system design and represents the amount of pixels that cannot be used per measurement (see figure 3(e)). The width of the single slits of the customized aperture (figure 3(c)) is not only determining the part of the image that is selected, it directly affects the optical bandwidth (FWHM) since it represents the entrance slit of the spectrometer. The spectral range and resolution of this technology only depends on the design of the line-scanning spectrometer (l/mm of the grating, etc.). Due to the image duplication and selection process, the entrance slit of the spectrometer is shaped like a saw tooth (figure 3(c)). This directly affects the spectral range, which is slightly shifted (o_n) at each set of channels (figure 3(e)). In terms of alignment, the key task of this technology is the mapping of the customized aperture (figure 3(c)) to the duplicated images (figure 3(b)). Tilts, rotation, and a shifting of the aperture would directly lead to an incorrect selection of spatial pixels of the duplicated images.

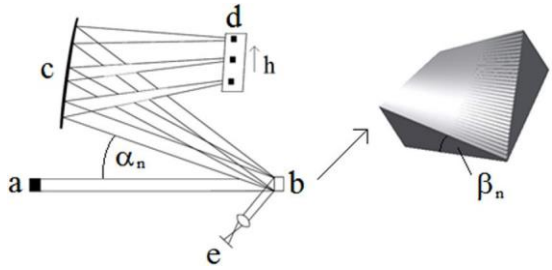

Figure 2. Left side: Principal path of the imaging rays. (a) The FOV, (b) the facet mirror, (c) the imaging mirror, (d) the imaging plane and (e) the additional high resolution camera. Right side: Facet mirror; each facet has a different angle β.

3. Characterization of the 4D Imager prototype

In order to perform proof of concept measurements, a 4D Imager prototype has been developed and configured for the visible spectral region with a spatial resolution of 14 × 14 channels. The measurement object is a 10 mm × 10 mm test pattern with a distance of 1 m. An additional facet is used to provide a spatially higher resolution image, captured with an RGB camera.
The prototype is based on UV enhanced mirrors (Edmund Optics) and optical gratings (Newport) from stock. As a detector a Princeton Instruments Pixis 400B has been chosen. As a RGB camera, for the additional image, a AVT MAKO G-125C POE was used. The facet mirror has been produced by Gigahertz-Optik GmbH.
In the following, the calibration steps of this setup and measurement results are presented.

3.1. Channel calibration (object position to detector position)

The incoming signal is spectrally analyzed by a line-scanning spectrometer. To assign each pixel on the chip with the dimensions (x, λ) to a measurement point (channel) in the 3D cube with the dimensions (x, y, λ), the measured data need to be rearranged to the original image. Therefore, the correlation between the pixels of the detector and the channels of the image has to be determined (figure 3, step (e)–(f)). This was achieved by observing an unambiguous test pattern and identifying the position of each channel of the test pattern on the detector.

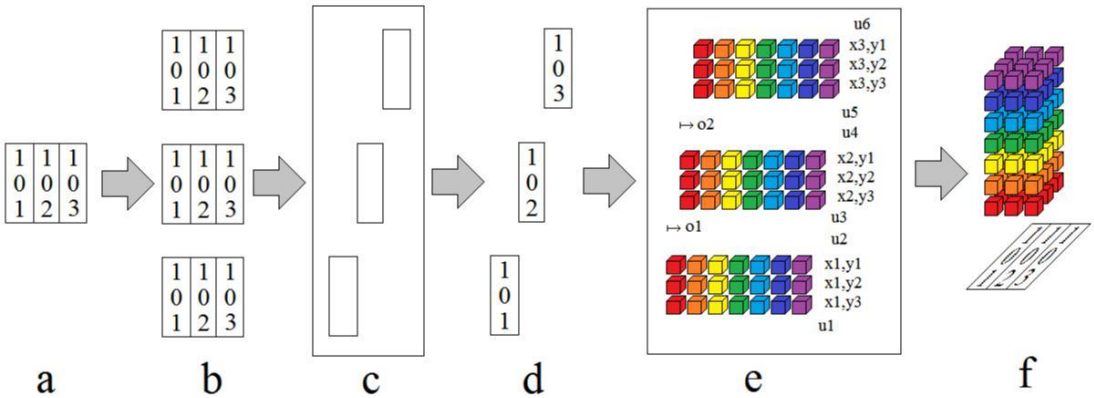

Figure 3. Schematic illustration of the imaging process of the 4D Imager where color indicates wavelength. The image (a) is multiple images with the help of the facet mirror (b). The different spatial information gets selected by a customized aperture (c). The selected data (d) are entering a line-scanning spectrometer where the single pixels are spectrally resolved (e). This data can be rearranged to get the spectral snapshot imaging voxels (f). Details of (e): between two sets of channels, such as (x_1, y_m) and (x_2, y_m), a few channels cannot be used (u_n). According to the saw tooth shape of the entrance slit (c), the wavelength range of each set is slightly shifted (o_n) to the next set. The measurement data can be remapped (f) into voxels (x, y, λ).

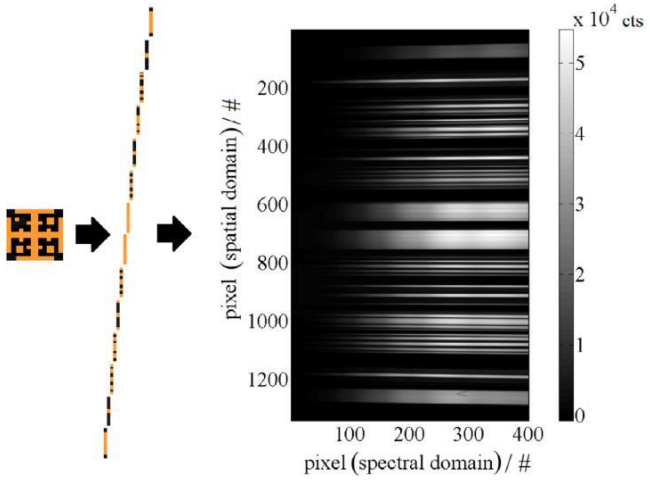

Figure 4. Measured raw data of the test pattern in counts (right side). For illustration purposes, the image and the selected parts after the aperture are shown on the left.

Due to image distortions within the spectrometer, the single channels are not imaged exactly along one pixel row in the spectral domain of the detector. An additional curve fitting individual for each channel on the detector along the signal in the spectral domain similar to Gao *et al* (2010) has been applied to correct these image distortions. In addition, the higher resolution data gained from the additional camera can be mapped to the spatial lower resolution spectral snapshot imaging measurement.

3.2. Wavelength calibration and optical bandwidth

The wavelength calibration of each channel has been achieved with the help of intrinsic lines of several pen ray lamps. The spectral range of a single channel enables a delta of 500 nm, e.g. 380 nm–880 nm in this configuration. However, as shown in figure 3(e), each set of channels is slightly shifted in the spectral domain. Thus, the common spectral range of all channels is 380 nm–800 nm with an optical bandwidth (FWHM) of 10 nm.

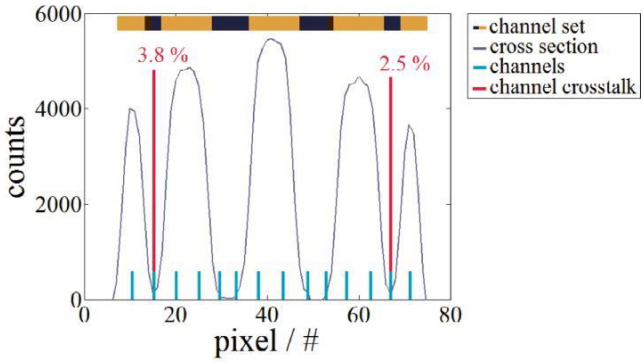

Figure 5. Shown is the measured cross-section of one set of channels in grey, the test pattern of this set of channels in yellow/black and the used channels in blue. The maximum channel crosstalk is highlighted in red.

3.3. Radiometric calibration

The radiometric calibration of the 4D Imager has been performed by using a 210 mm integrating sphere based uniform light source traceable to the Physikalische Technische Bundesanstalt (PTB). The calibration uncertainty of this standard is 2% (k = 2) in the spectral range above 450 nm and is linearly increasing below 450 nm to 3.2% at 380 nm. The radiance distribution of the 65 mm exit port of the integrating sphere has to be very homogeneous within the FOV of the 4D Imager to ensure low calibration uncertainties. The inhomogeneity of the calibration source used is better than ± 0.20%. The 4D Imager has been calibrated at the measurement location so that no movement of the instrument between calibration and measurement is needed.

3.4. Measurement results

A proof of concept measurement has been performed to analyze the spatial performance (channel separation) of the 4D Imager. As a measurement object, a 10 mm × 10 mm laser cut test pattern with 14 × 14 pixels has been backside illuminated with a tungsten lamp. To clarify the channel separation, the raw signal on the detector chip is presented in figure 4. The raw signal

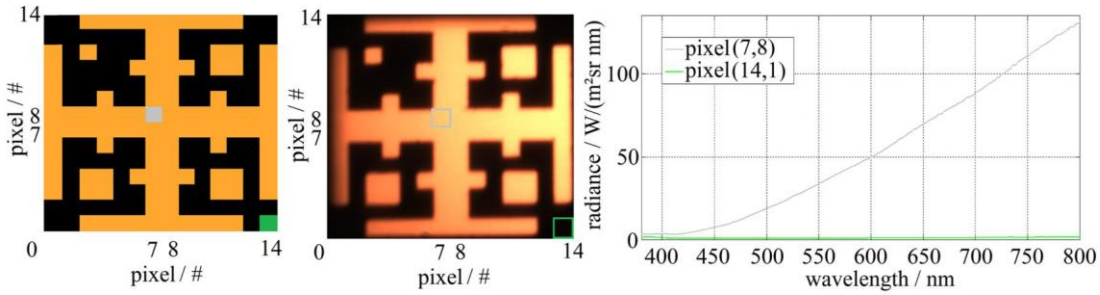

Figure 6. Results of the 14 × 14 pixel test pattern measurement. Left: Resolution of the spectral snapshot image. Center: Higher resolution image captured by the additional RGB camera. Right: Two representative measurement channels are illustrated in spectral radiance.

Figure 7. Left: Prototype of the 4D Imager equipped with an entrance optic for sky zenith measurements with a FOV of 0.5°. Right: Entrance optic for a wide angle FOV of 16.8°–73.5°. This optic can be mounted on the entrance optic for sky zenith measurements.

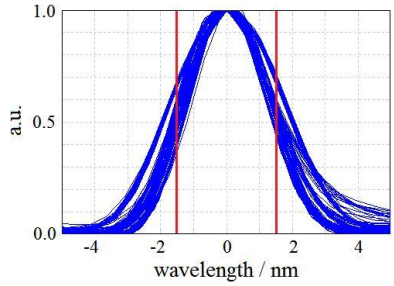

Figure 8. Optical bandpass of all 196 channels with the UV setup. A mean optical bandwidth (FWHM) of 3 nm has been achieved.

shows 14 imaged channel sets from which 14 channels can be used each. In principle, more detector pixels than could be used in each channel set. However, only 14 are clearly separated by a channel crosstalk of less than 4% (see figure 5). This investigation of the crosstalk is based on a perfectly aligned test pattern to the FOV of the 4D Imager. A slight offset, which might be present, leads to signals that appear like channel crosstalk.

The described calibration process has been applied to this raw data. Furthermore, the measured spectral snapshot imaging data have been mapped by the measurement software to the higher resolution image (0.58 megapixels) taken with the additional camera. In addition, the spectral data of two channels are illustrated in figure 6.

The measurement has been performed for all 196 channels simultaneously with an integration time of 3 s. No averaging or smoothing has been applied.

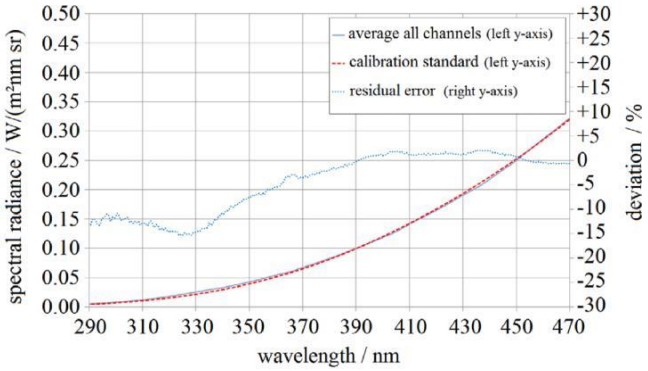

Figure 9. Radiance measurement of a uniform spectral radiance calibration standard. The data shows good agreement in the spectral range 370 nm–470 nm. Below 370 nm the residual deviation is rising mainly due to insufficient signal to noise ratio.

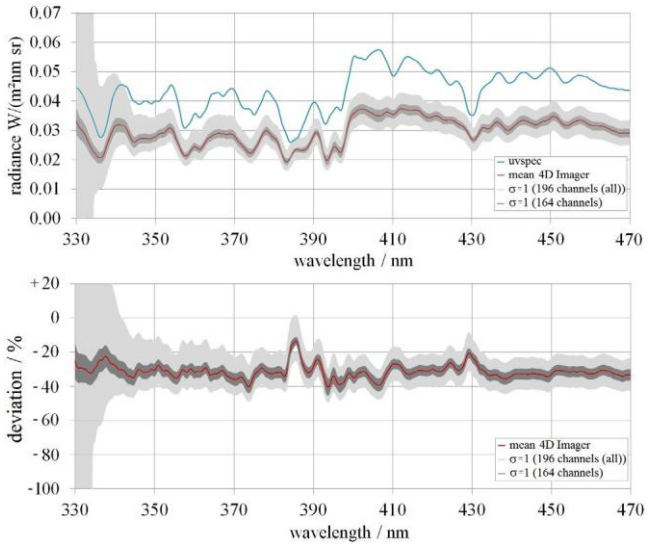

Figure 10. Solar zenith sky radiance measurements in the UV region from 330 nm–470 nm with 3 nm optical bandwidth (FWHM) of a clear sky (2017-02-15 14:15 UTC + 1 48°06′03.6″N 11°04′46.3″E) and ratio to UVSPEC generated data (convolved to 3 nm FWHM) are illustrated. In addition, the standard deviation of 196 channels (all) and 164 channels is shown. Some channels exhibit significant stray light, which can be recognized by the increase of the standard deviation, especially below 340 nm.

This measurement indicates a successful separation of the channels on the detector chip. However, to show the spectral radiometric capabilities of the new instrument, measurements

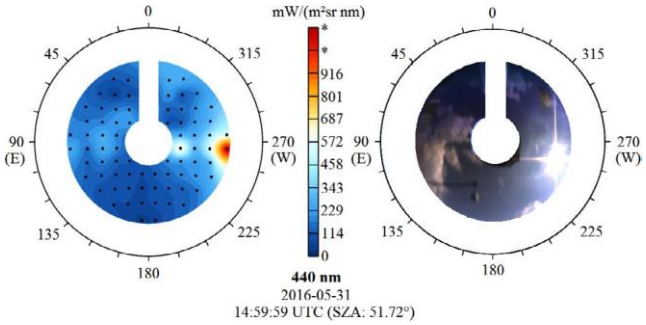

Figure 11. Left: Illustrated is a spectral sky radiance distribution at 400 nm (integration time of 1 s) in a color scale gradient representation. The black dots represent the central points of the single measurement channels. Right: Higher resolution RGB image captured by the additional camera.

of an object with a different spectral distribution compared to the calibration lamp have to be performed.

4. Application of the 4D Imager for spectral sky radiance measurements

For the analysis of the spectral radiometric performance of the 4D Imager and its capability in the UV, snapshot radiance measurements of the sky zenith were performed. Due to a large dynamic and high spectral stray light, solar radiation is difficult to measure, especially in the UV (Seckmeyer *et al* 2001). Hence, the optical design of the 4D Imager has been modified to access the UV spectral range and to achieve a smaller optical bandwidth (FWHM). Furthermore, the device has been equipped with an entrance optic to achieve a 0.5° FOV of zenith sky radiance, see figure 7, left.

4.1. Calibration

The calibration process was performed in the same manner as the VIS setup as described before. The calibration uncertainty of the standard increases linearly in the UV from 2% (k = 2) at 450 nm to 5% (k = 2) at 280 nm. A spectral range of 280 nm to 470 nm with a mean optical bandwidth of 3 nm (FWHM) was achieved (see figure 8). The measurements are corrected for stray light using a simple method similar to Riechelmann *et al* (2013), which is based on subtracting stray light signals from the measurement channel signals using detector channels that are not illuminated by the light source (see figure 3(e), channels *u*).

4.2. Measurement results

In figure 9 a measurement of a uniform spectral radiance calibration standard, which is as well traceable to PTB, has been performed to check the absolute radiometric capability of the measurement system. This standard is different to the used standard during calibration. The calibration uncertainty of this standard is 3.5% (k = 2) in the spectral range above 350 nm and is linearly increasing with decreasing wavelength below 350 nm to 6.5% at 280 nm. The measurement results show an agreement with a deviation of less than ±3% in the spectral range 370 nm–470 nm. Below 370 nm the residual deviation is rising to about −15% in maximum mainly due to an insufficient signal to noise ratio.

In figure 10, the results of a clear blue sky zenith radiance measurement (2017-02-15 14:15 UTC + 1 48°06′03.6″N 11°04′46.3″E) are compared in the spectral range of 330 nm–470 nm to data processed with UVSPEC (Emde *et al* 2016). For this measurement scenario with a FOV of 0.5°, a constant spectral radiance distribution within the FOV is assumed. The UVSPEC data shown (input parameters UVSPEC: SZA 65.03°, SAA 28.47°, ozone 300 DU, albedo 0.02, altitude 599 m) are convolved to a comparable optical bandwidth of 3 nm (FWHM).

The measurement results show that all channels of the 4D Imager possess an offset of about −30% compared to the UVSPEC simulation results within the wavelength range 330 nm–470 nm. In addition, this offset shows a spectral variation due to not perfectly matched optical bandwidths for all channels at the Fraunhofer lines since every channel has a different FWHM (see figure 8). Furthermore, the standard deviation for the mean of 164 channels compared the standard deviation of 196 channels (all) shows that 32 channels exhibit significant stray light, especially below 340 nm.

In figure 11, a first measurement of a spectral sky radiance distribution using a wide angle entrance optic (FOV: 16.8° to 73.5°) is shown. This entrance optic (see figure 6, right) is mirror based and its design is according to Chahl and Srinivasan (1997). The measurement was captured within an integration time of 1 s.

5. Discussion and conclusions

Spectral snapshot imaging measurements have been performed with the 4D Imager, which is a new type of IFS technology. This technology is based on only a few optical parts which key component is a facet mirror that duplicates the object image. For the spectral analysis, a line-scanning spectrometer can be used. Hence, the spectral range and resolution of this technology is defined by the design of the spectrometer (l/mm of the grating, etc.) whereby applications in the UV are also possible. These are the key advantages compared to other IFS approaches. The achievable spatial resolution can be as well designed with freedom since it depends on the number of facets, the detector resolution and the quality of the image selection process (customized aperture) connected with the imaging quality of the line-scanning spectrometer. The challenge of this technology is to image the duplicated images precisely on the entrance slit of the line-scanning spectrometer to support the selection process. An overview of the 4D Imager compared to different IFS technologies is presented in table 1.

Table 1. Overview of some IFS technologies with respect to its advantages and disadvantages.

	IFS-M	IFS-F	4D Imager
Advantage	- Since it is mirror based the spectral range is not limited	- Freedom in the FOV design since every fiber can be separately aligned - Freedom in the spectral design since standard line-scanning spectrometer can be used. In principle multiple line spectrometers can be combined	- Only a few optical parts are needed - Freedom in the spectral design since standard line-scanning spectrometer can be used - Since it is mirror based the spectral range is not limited
Disadvantage	- Many optical parts are needed since every sliced image needs a small mirror to be imaged at the pupil	- FOV is wavelength dependent due to wavelength dependent numerical aperture of the optical fibers	- Since the accessible wavelength range is shifted, for each set of channels which correspond to one facet, the useable common wavelength range is reduced compared to other techniques. It is reduced by the detector pixels which correspond to the width of a single entrance slit multiplied by the amount of facets
	- Hard to align since every mirror has to be aligned individually	- Movement of the measurement system can change the responsivity of the single measurement channels (fiber movement) - Different fibers are needed for the full spectral range from UV to IR - Amount of channels is limited mechanical by the number of fibers which means increase in measurement channels will be linear in increase of effort	- Due to the image multiplication and selection process only a part of the incoming available signal can be used (fraction is given by the number of facets)
Challenge	- Alignment of the system is non-trivial - Amount of measurement channels is difficult to increase since due to the many optical parts an optical imaging with many channels and acceptable image distortions is difficult to achieve	- Manufacturability of the fibers - Light coupling into the fiber	- A precise and unique entrance slit for the line spectrometer is needed
Resolution channel- crosstalk	100 × 100 × 25 (x, y, λ) Unknown (Gao *et al* 2009)	113 × 875 (x, λ) Unknown (Riechelmann *et al* 2013)	14 × 14 × 400 (x, y, λ) <4%

In this paper, proof of concept radiance measurements of a 10 mm × 10 mm test pattern with a distance of 1 m and a spatial resolution of 14 × 14 channels (196) are shown. A channel crosstalk of less than 4% was attained. The channel crosstalk could be even smaller since the investigated signal is a mixture of the real channel crosstalk (optical imaging performance) and the alignment of the test pattern to the FOV of the 4D Imager. The device has been radiometrically calibrated, traceable to PTB, in the spectral range of 380 nm–800 nm with an optical bandwidth of 10 nm (FWHM). Furthermore, the spectral snapshot imaging data (196 channels) have been mapped with a higher resolution RGB image that was captured by an additional facet and camera.

To demonstrate the spectral capabilities of this technology, spectral zenith sky radiance measurements in the UV region have been performed. Therefore, the prototype was adapted for a spectral range of 280 nm–470 nm with a mean optical bandwidth of 3 nm (FWHM), a FOV of 0.5° and 196 channels. To check the radiometric capabilities of the measurement system a radiance measurement of a calibration standard was carried out. The results show a good agreement with a residual deviation of less then ±3% in the spectral range 370 nm– 470 nm where sufficient signal to noise ratio is given by the used calibration standard. After this validation a spectral zenith sky radiance measurement was realized. The comparison of this measurement with UVSPEC generated data showed an

average offset of −30% in the range of 330 nm–470 nm. The reason for this deviation could not been determined exactly.
The uncertainty of any radiation measuring instrument is given by the combined calibration and measurement uncertainty. When comparing with modeled values, the uncertainty of the model and its input parameters must be considered as well. The UVSPEC model uncertainty is mainly dominated by the input parameters, e.g. aerosol characteristics of the atmosphere. This uncertainty has been investigated by Cordero *et al* (2013) for spectral UV irradiance. He found uncertainties for the UV–A range of about 3% for unpolluted atmospheres and about 5% for polluted atmospheres if realistic input uncertainties are assumed. The publication from van Weele *et al* (2000) showed that a difference of up to 20% at 305 nm between different UV models exists. Mayer *et al* (1997) found systematic differences between irradiance measurements and the UVSPEC model in the range between −11% to +2% for wavelengths between 295 nm and 400 nm and solar zenith sky angles up to 80°. The uncertainty of spectral UV irradiance measurements have been systematically assessed by Bernhard and Seckmeyer (1999) and found to be about 13% at 300 nm under ideal circumstances. Such uncertainties were later confirmed with a Monte-Carlo-approach by Cordero *et al* (2013). Pissulla *et al* (2009) showed that five independent calibrated systems exhibit a spectral radiance difference to UVSPEC between 3% and about 35%.

This suggests that an offset of −30% for spectral radiance is not very good, but still in the range of an acceptable agreement between the UVSPEC model and the 4D Imager. Furthermore, this comparison between UVSPEC and the 4D Imager measurement is based on the assumption of a clear sky, which might be not the case during the measurement (2017-02-15 14:15 UTC + 1 48°06′03.6″N 11°04′46.3″E).
It should be noted that the measurement showed that 36 channels exhibit significant stray light, especially below 340 nm. This is mainly caused by the prototype using an optical table setup at which the spectrometer housing was not yet completely light tight.
In this publication we do not want to show the possible endpoint of longer development, but just want to describe a proof of a new concept. The measurement results show the potential of the 4D Imager technology to measure spectral radiance using snapshot imaging. However, for high accuracy measurements, especially in the UV, a fixed setup with optimized light traps and a machine processed spectrometer housing would be needed. The optical table-based prototype used for these measurements clearly showed its limits when using it outdoors.

Acknowledgments

This work has been supported by the BMWi project KF 3091801DF2. Furthermore, the authors would like to thank Kezia Lange from the IMuK for providing the UVSPEC data.

ORCID iDs

Ralf Zuber https://orcid.org/0000-0001-7794-9730

References

Bernhard G and Seckmeyer G 1999 Uncertainty of measurements of spectral solar UV irradiance *J. Geophys. Res.* **104** 14321–45
Bianco P, Pisani M and Zucco M 2010 High throughput, compact imaging spectrometer *Int. Conf. on Space Optics ICSO 2010*
Brown A J 2006 Spectral curve fitting for automatic hyperspectral data analysis *IEEE Trans. Geosci. Remote Sens.* **44** 1601–8
Brown A J, Hook S J, Baldridge A M, Crowley J K, Bridges N T, Thomson B J, Marion G M, de Souza Filho C R and Bishop J L 2010 Hydrothermal formation of clay-carbonate alteration assemblages in the Nili Fossae region of Mars *Earth Planet. Sci. Lett.* **297** 174–82
Brown A J, Sutter B and Dunagan S 2008 The MARTE VNIR imaging spectrometer experiment: design and analysis *Astrobiology* **8** 1001–11
Chahl J S and Srinivasan M V 1997 Reflective surfaces for panoramic imaging *Appl. Opt.* **36** 8275–85
Content R 1997 New design for integral field spectroscopy with 8-m telescopes *Proc. SPIE.* **2871** 1295–305
Cordero R R, Seckmeyer G, Alessandro D, Fernando L and David L 2013 Monte Carlo-based uncertainties of surface UV estimates from models and from spectroradiometers *Metrologia* **50** L1
Davis C O *et al* 2002 Ocean PHILLS hyperspectral imager: design, characterization, and calibration *Opt. Express* **10** 210–21
Emde C *et al* 2016 The libRadtran software package for radiative transfer calculations (version 2.0.1) *Geosci. Model Dev.* 2 1647–72
Gao L, Kester R T, Hagen N and Tkaczyk T S 2010 Snapshot image mapping spectrometer (IMS) with high sampling density for hyperspectral microscopy *Opt. Express* **18** 14330–44
Gao L, Kester R T and Tkaczyk T S 2009 Compact image slicing spectrometer (ISS) for hyperspectral fluorescence microscopy *Opt. Express* **17** 12293–308
Gehm M E, John R, Brady D J, Willett R M and Schulz T J 2007 Single-shot compressive spectral imaging with a dual-disperser architecture *Opt. Express* **15** 14013–27
Gupta N and Voloshinov V 2004 Hyperspectral imager, from ultraviolet to visible, with a KDP acousto-optic tunable filter *Appl. Opt.* **43** 2752–9
Hagen N and Kudenov M W 2013 Review of snapshot spectral imaging technologies *Opt. Eng.* **52** 090901
Hardeberg J Y, Schmitt F and Brettel H 2002 Multispectral color image capture using a liquid crystal tunable filter *Opt. Eng.* **1** 2532–48
Henault F, Bacon R, Content R, Lantz B, Laurent F, Lemonnier J-P and Morris S L 2004 Slicing the universe at affordable cost: the quest for the MUSE image slicer *Proc. SPIE* **5249** 134–45
Hu P, Lu Q, Shu R and Wang J 2005 An airborne pushbroom hyperspectral imager with wide field of view *Chin. Opt. Lett.* **3** 689–91
Laurent F, Henault F, Renault E, Bacon R and Dubois J P 2006 Design of an integral field unit for MUSE, and results from prototyping *Publ. Astron. Soc. Pacific* **118** 1564–73
Mathews S A 2008 Design and fabrication of a low-cost, multispectral imaging system *Appl. Opt.* **47** F71–6
Matsuoka H, Kosai Y, Saito M, Takeyama N and Suto H 2002 Single-cell viability assessment with a novel spectro-imaging system *J. Biotechnol.* **94** 299–308

Mayer B, Seckmeyer G and Kylling A 1997 Systematic long-term comparison of spectral UV measurements and UVSPEC modeling results *J. Geophys. Res.* **102** 8755–67

Pissulla D *et al* 2009 Comparison of atmospheric spectral radiance measurements from five independently calibrated systems *Photochem. Photobiol. Sci.* **8** 516–27

Riechelmann S, Schrempf M and Seckmeyer G 2013 Simultaneous measurement of spectral sky radiance by a non-scanning multidirectional spectroradiometer (MUDIS) *Meas. Sci. Technol.* **24** 125501

Seckmeyer G, Bais A, Bernhard G, Blumthaler M, Booth C, Disterhoft P, Eriksen P, McKenzie R, Miyauchi M and Roy C 2001 Instruments to measure solar ultraviolet irradiance. Part **2** spectral instruments *Global Atmosphere Watch Report* No. 125 World Meteorological Organization (WMO)

Sigernes F *et al* 2012 Hyperspectral all-sky imaging of auroras *Opt. Express* **20** 27650–60

van Weele M *et al* 2000 From model intercomparison toward benchmark UV spectra for six real atmospheric cases *J. Geophys. Res.* **105** 4915–25

Wagadarikar A, John R, Willett R and Brady D 2008 Single disperser design for coded aperture snapshot spectral imaging *Appl. Opt.* **47** B44–51

Zuber R 2015 Spetroskopiesystem *Ger Patent* 102013112376

6. Discussion and conclusions

Within this thesis, an optical filter-based internal stray light correction procedure for UV array spectroradiometers has been developed. A measuring system called BTS2048-UV-S, which applies this approach, participated in two intercomparison campaigns. In Hannover (Germany), the global spectral irradiance and in Izaña (Tenerife, Spain) the direct spectral irradiance of the sun was measured.

During the campaign it could be shown that a stray light level of $5 \cdot 10^{-5}$ $Wm^{-2}nm^{-1}$ is achieved with the developed measurement system. This exceeds the WMO recommendation for array spectroradiometers regarding stray light which is $<1 \cdot 10^{-3}$ $Wm^{-2}nm^{-1}$ and comes close to the recommendation for double monochromators (S-2 instruments) $<1 \cdot 10^{-6}$ $Wm^{-2}nm^{-1}$.

The Hannover measurements showed a deviation of less than 1% for the UV index compared to a NDACC double monochromator reference for SZA below 70°. The deviation in global spectral irradiance was 1.5% compared to the NDACC device in the wavelength range of 300 nm to 420 nm evaluated for SZA below 70°. This is a significant improvement compared to all array spectrometers analyzed in Egli *et al.* (2016) where only the best and extensively characterized devices achieved an deviation of 5% for the UV index and the global spectral irradiance at 310 nm for SZA smaller 50° to the traveling reference spectroradiometer QASUME.

The direct solar spectral irradiance measurements in Izaña showed deviations smaller than 2.5% compared to the QASUME in a wavelength range from 300 nm to 420 nm (evaluated for low solar zenith angles at around noontime). Vaskuri *et al.* (2018) evaluated the data of all participating systems and showed that the expanded uncertainty (k=2) of the developed measurement system for the TOC evaluation is 1.3%, which is according to Vaskuri *et al.* (2018) identical to the QASUME double monochromator reference expanded uncertainty (k=2). Vaskuri *et al.* (2018) also demonstrated that an array spectrometer based system, called AVODOR, showed a significant larger expanded uncertainty of 3.3% (k=2) in the same measurement campaign. The used TOC retrieval algorithm for this measurement campaign has been developed by Stefan Riechelmann (PTB) and Gunther Seckmeyer (IMuK).

In conclusion it can be stated: That measurement devices based on the developed approach have the potential to replace the mostly cumbersome and scanning double monochromator (e.g. Bentham DMc 150) systems. In addition, compared to double monochromators e.g. temporally higher-resolution measurements of UV spectral irradiance are now possible. Due to the simple transport given by its compact design, low weight and already incorporated weather-proof housing measurements in challenging places like high mountains are now easier possible. Especially since the measurement campaign in Izaña showed that the calibration was maintained during transport from the calibration laboratory to the field. Ongoing and open tasks of the developed approach are discussed in Chapter 7.

The developed stray light correction procedure is based on a filtering approach with optical bandpass-, interference- and edge-filters. These filters are placed in front of the spectrometer entrance slit but after the entrance optics. With the help of these filters the signal, which is coupled in the spectrometer itself, can be spectrally tuned. Hence, the optical radiation, which can generate stray light in the device, is significantly reduced or serves to characterize the stray

light of the spectroradiometer. Resulting, different filter measurements can be combined for a stray light corrected measurement of the whole spectral range of the device. The advantage in significantly improved internal stray light correction is associated with a reduction of the temporal resolution compared to a single array spectroradiometer measurement, since multiple filter measurements are necessary for one measurement of the full spectral range. However, the total measurement time (e.g. 8 s for solar radiation) is still short compared to spectral scanning double monochromators (typical 16 min at a comparable spectral resolution). However, it has to be mentioned that changes of the spectral irradiance within the stated 8 seconds measurement time can lead to higher measurement uncertainties compared to uncertainties, which are demonstrated by intercomparison campaigns using double monochromators. Due to scanning double monochromators offers a time stamp for each wavelength step, which have uncertainties of fractions of a second.

A second major task of this work was the development of a new spectral snapshot imaging approach.

As a proof of concept a simultaneous spectral radiance measurement of 10 mm x 10 mm test pattern with 196 measurement channels in the spectral range of 380 nm to 800 nm with 10 nm of optical bandwidth (FHWM) was performed with a prototype based on the new approach. The measurement results showed a measurement channel crosstalk of less than 4%. Furthermore, by adapting the prototype, a zenith radiance field measurement with an average FOV of 0.5° (FOV with square shape) by 196 measurement channels in the spectral range of 280 nm to 470 nm with 3 nm optical bandwidth (FWHM) was realized. The achieved deviation of -30% to UVSPEC is not very good but an acceptable agreement. Especially for a prototype, which is improvable in terms of light tightness, mechanical implementation and whose housing is non-tempered. Pissulla *et al.* (2009) demonstrated for instance that five independent calibrated devices exhibit spectral radiance difference between 3% and about 35% to UVSPEC. It has to be mentioned, that an optical bandwidth of 3 nm (FWHM) increases the measurement uncertainty for especially UVB solar measurements significantly. According to Bernhard and Seckmeyer (1999) 2 nm optical bandwidth (FWHM) can increase the measurement uncertainty for DNA weighed irradiance up to 4% if no correction is applied. Parallel to the spectral snapshot imaging measurement an RGB camera took a picture with mega pixel resolution of the same FOV. This meta-information can enable a better data interpretation, especially for measurement objects with a lot of variation within the image, such as images with large spatial variations of clouds. Supplementary, an additional entrance optics with different FOV was adapted to the measurement system prototype in order to show the potential of the approach for different applications. This additional entrance optics, developed by Ansgar Stührmann (IMuK), allowed hemispherical measurements with a FOV of 17° to 74 °.

The goal of the prototype was mainly to analyze the potential of the new approach. In this respect, the achieved results are to be assessed as a feasibility and potential study of the new procedure. Since this newly developed approach is based on a input optics design consistent of only three optical components (facet mirror (14 single facets), imaging mirror and aperture), a significant reduction of optical components compared to hundreds of optical fibers (Riechelmann *et al.*, 2013; Seckmeyer *et al.*, 2018) was achieved. Furthermore, due to the small size of the input optics it can be directly mounted on the spectrometer unit. As a result, the

measurement system can be fully characterized and calibrated in the laboratory and moved to the place of measurement without disassembling, which could be an additional source of error.

In addition, an slight increase of measurement channels (196) compared to 113 of Riechelmann *et al.* (2013) and 150 of the device under test from Seckmeyer *et al.* (2018) was accomplished. However, Riechelmann *et al.* (2013) and Seckmeyer *et al.* (2018) performed hemispherical measurements in contrast to spatially resolved solar zenith radiance measurement (FOV of about 0.5°). Direct comparable measurements have been shown in the potential study by the use of the entrance optics of Ansgar Stührmann with 120 usable measurement channels, which is in-between the mentioned two systems. The total amount of 196 was reduced by incomplete use of the FOV (-42 channels) and due to mechanical shading (-34 channels) of the entrance optics itself. However, this study has successfully shown that it is possible to adapt the FOV using the same prototype.

As stated the mechanical implementation of the prototype, missing temperature control of the housing and insufficient light thingness needs to be improved for a fully applicable measurement system, which can compete in intercomparison campaigns. These and other future views on this technological approach are discussed in Chapter 7.

This spectral snapshot imaging approach is based on a newly developed input optics, which is directly mounted to a well-known push-broom spectrometer. The principle functionality of this input optics is a multiple duplication of the measurement object (radiance distribution to be measured) with the help of a facet and imaging mirror. The amount of duplicated images depends on the amount of facets. These resulting multiple images are lined-up in the imaging plane of the imaging mirror, thus a suitable opto-mechanical filtering (customized aperture) is able to select different parts of each image and thus different measurement channels. These selected measurement channels are spectrally resolved in the following push-broom (line scanning) spectrometer unit.

The major challenge of this approach is the channel selection by the opto-mechanical filtering (customized aperture) since the optical imaging of the introduced input optics underlies different imaging aberrations and production tolerances. Resulting the position of the duplicated images in the imaging plane is different to ray tracing models. In order to compensate, respectively consider these effects, the opto-mechanical filter needs to be customized according the real positions of the multiple images. However, the determination of these real slit positions is a challenging measurement due to its small dimensions in the µm range. Additionally, the manufacturing of such a customized slit in the µm range requires a carefully chosen manufacturing process.

7. Outlook

In order to evidence that the new procedure for stray light correction in the UV is fully applicable, stability studies over a longer period (years) have to be performed. Currently, such studies are for instance ongoing at the Bundesamt für Strahlenschutz (BfS) in Oberschleißheim/Neuherberg and on the mountain Zugspitze for global spectral irradiance (Lorenz *et al.*, 2018) and at PMOD/WRC in Davos for TOC (Egli and Gröbner, 2018). Furthermore, the retrieval algorithm could be extended with aerosol optical depth (AOD) and SO_2 determinations based on the direct solar UV spectral irradiance measurements (Huber *et al.*, 1995; Cachorro *et al.*, 1987; Kerr, 2002; Wuttke *et al.*, 2012).

As already stated in Chapter 6, the developed devices might allow novel investigations, e.g. investigations that are based on temporally higher-resolution measurement of UV spectral irradiance compared to double monochromators. In addition, measurements in challenging locations, such as high-mountain areas, are easier to carry out compared to double monochromator based systems. This is given due to easier transportation (compact size) and maintenance of the calibration during transport as long as suitable packaging is used.

In addition, a combination of the new procedure with already known mathematical stray light correction methods is promising. The potential has already been shown in Zuber and Ribnitzky (2019). However, an independent validation in e.g. global spectral solar irradiance measurement intercomparison campaign has to be performed.

The next step for the introduced spectral snapshot imaging procedure will certainly be the conversion of the prototype in a robust weatherproof version, which can be evaluated at measurement campaigns/intercomparisons.

This step is necessary to analyze e.g. the long-term stability of the instrument in terms of radiometric calibration stability, measurement channel separation, temperature stability and a complete characterization of the measurement uncertainty budget. An intercomparison with established systems like scanning double monochromator based systems (e.g., NDACC certified spectroradiometers) in certain measurement channels or with the mentioned measurement systems MUDIS or AMUDIS (section 2.3.2) would be an option. Furthermore, the system can be improved to achieve a higher number of measurement channels and/or smaller optical bandwidth, by improving the optical design with for instance suitable aspherical mirrors in order to reduce the imaging aberrations introduced by the used standard spherical mirrors of the prototype. The maximum number of measurement channels is limited not only by optical imaging aberrations but also by the size of the detectors that are available. Based on the experience with the prototype, ray-tracing simulations and the currently available detectors it is estimated that a doubling of the measurement channels is possible.

Finally, both technologies can be combined in one device, which in turn allows further investigations in the UV spectral range. However, with the improved stray light correction a kind of scanning due to the multiple filter measurements would be introduced for the presented spectral snapshot imaging approach.

Bibliography

Allinson S, Asmuss M, Baldermann C, Bentzen J, Buller D, Gerber N, Green A, Greinert R, Kimlin M, Kunrath J, Matthes R, Pölzl-Viol C, Rehfuess E, Rossmann C, Schüz N, Sinclair C, van Deventer E, Webb A, Weiss W and Ziegelberger G 2012 Validity and use of the UV index: report from the UVI working group, Schloss Hohenkammer, Germany, 5-7 December 2011 *Health physics* **103** 301-6

Armstrong B K and Kricker A 2001 The epidemiology of UV induced skin cancer *J Photochem Photobiol B* **63** 8-18

ASTM 2012 ASTM G138-12, Standard Test Method for Calibration of a Spectroradiometer Using a Standard Source of Irradiance

Baczynska K A and Khazova M 2015 Methods of dark signal determination for CCD array spectroradiometers used in solar UVR measurements *Radiation Protection Dosimetry* **163** 387-93

Baczynska K A, Price L L A and Khazova M 2016 DYNAMIC RESPONSE OF CCD ARRAY SPECTRORADIOMETERS *Radiation Protection Dosimetry* **171** 291-6

Bais A F 1998 Standardization of ultraviolet spectroradiometry in preparation of a European network (SUSPEN) *final report, Eur. Comm., Dir. Gen. XII, Luxembourg*

Bais A F, Bernhard G, McKenzie R L, Aucamp P J, Young P J, Ilyas M, Jöckel P and Deushi M 2019 Ozone–climate interactions and effects on solar ultraviolet radiation *Photochemical & Photobiological Sciences* **18** 602-40

Bais A F, Lucas R M, Bornman J F, Williamson C E, Sulzberger B, Austin A T, Wilson S R, Andrady A L, Bernhard G, McKenzie R L, Aucamp P J, Madronich S, Neale R E, Yazar S, Young A R, de Gruijl F R, Norval M, Takizawa Y, Barnes P W, Robson T M, Robinson S A, Ballare C L, Flint S D, Neale P J, Hylander S, Rose K C, Wangberg S A, Hader D P, Worrest R C, Zepp R G, Paul N D, Cory R M, Solomon K R, Longstreth J, Pandey K K, Redhwi H H, Torikai A and Heikkila A M 2018 Environmental effects of ozone depletion, UV radiation and interactions with climate change: UNEP Environmental Effects Assessment Panel, update 2017 *Photochemical & photobiological sciences : Official journal of the European Photochemistry Association and the European Society for Photobiology* **17** 127-79

Bais A F, McKenzie R L, Bernhard G, Aucamp P J, Ilyas M, Madronich S and Tourpali K 2015 Ozone depletion and climate change: impacts on UV radiation *Photochemical & Photobiological Sciences* **14** 19-52

Bernhard G and Seckmeyer G 1999 Uncertainty of measurements of spectral solar UV irradiance *Journal of Geophysical Research: Atmospheres* **104** 14321-45

Bianco P, Pisani M and Zucco M 2010 High throughput, compact imaging spectrometer *International Conference on Space Optics* **ICSO 2010**

Blumthaler M 2018 UV Monitoring for Public Health *International journal of environmental research and public health* **15** 1723

Bohn B and Lohse I 2017 Calibration and evaluation of CCD spectroradiometers for ground-based and airborne measurements of spectral actinic flux densities *Atmos. Meas. Tech.* **10** 3151-74

Brovkin V, Boysen L, Raddatz T, Gayler V, Loew A and Claussen M 2013 Evaluation of vegetation cover and land-surface albedo in MPI-ESM CMIP5 simulations *Journal of Advances in Modeling Earth Systems* **5** 48-57

Brown A J, Sutter B and Dunagan S 2008 The MARTE VNIR imaging spectrometer experiment: design and analysis *Astrobiology* **8 5** 1001-11

Byer R L 1976 Parametric Oscillators. In: *Tunable Lasers and Applications,* ed A Mooradian*, et al.* (Berlin, Heidelberg: Springer Berlin Heidelberg) pp 70-80

Cachorro V E, de Frutos A M and Casanova J L 1987 Determination of the Angstrom turbidity parameters *Appl. Opt.* **26** 3069-76

Chipperfield M P, Dhomse S S, Feng W, McKenzie R L, Velders G J M and Pyle J A 2015 Quantifying the ozone and ultraviolet benefits already achieved by the Montreal Protocol *Nature Communications* **6** 7233

CIE 1996 *The Photometry and Goniophotometry of Luminaires*: CIE Central Bureau)
CIE 2011a CIE 198: Determination of measurement uncertainties in photometry
CIE 2011b S 017, ILV: International Lighting Vocabulary
CIE 2014 CIE 214:2014 Effect of Instrumental Bandpass Function and Measurement Interval on Spectral Quantities. Vienna: PB - CIE Central Bureau , 2014 ISBN 978-3-902842-53-4, 84 pp. *Color Research & Application*
CIE 2018 CIE 198: Determination of Measurement Uncertainties in Photometry - Supplement 2: Spectral measurements and derivative quantities.
CIE 2019 CIE 233: Calibration, Characterization and Use of Array Spectroradiometers, ISBN 978-3-902842-75-6.
Content R 1997 New design for integral field spectroscopy with 8-m telescopes. pp 1295-305
Cordero R R, Seckmeyer G, Alessandro D, Fernando L and David L 2013 Monte Carlo-based uncertainties of surface UV estimates from models and from spectroradiometers *Metrologia* **50** L1
Cordero R R, Seckmeyer G, Pissulla D, DaSilva L and Labbe F 2008 Uncertainty evaluation of spectral UV irradiance measurements *Measurement Science and Technology* **19** 045104
Cordero R R, Seckmeyer G, Pissulla D and Labbe F 2007 Uncertainty of experimental integrals: application to the UV index calculation *Metrologia* **45** 1-10
Czerny M and Turner A F 1930 *Z. Phys. 61, 792*
Davis C O, Bowles J, Leathers R A, Korwan D, Valerie Downes T, Snyder W A, Rhea W J, Chen W, Fisher J, Bissett W P and Reisse R A 2002 Ocean PHILLS hyperspectral imager: design, characterization, and calibration *Optics Express* **10** 210-21
Demain C, Journée M and Bertrand C 2013 Evaluation of different models to estimate the global solar radiation on inclined surfaces *Renewable Energy* **50** 710-21
Dezhi Z, Jingjie G, Xinbo S and Ming G 2010 Low Noise CCD System Design and Implementation Based on Thermoelectric Refrigerating Unit. In: *2010 First International Conference on Pervasive Computing, Signal Processing and Applications*, pp 406-9
DIN 2019 DIN 5032-10:2019 Lichtmessung - Teil 10: Leuchtdichtemesskamera, Begriffe, Eigenschaften und deren Kennzeichnung
Dobson G M B 1931 A photoelectric spectrophotometer for measuring the amount of atmospheric ozone *Proceedings of the Physical Society* **43** 324
E. Greivenkamp J 2004 Field Guide to Geometrical Optics *DOI: 10.1117/3.547461 ISBN: 9780819478160*
Ebert H 1889 *Ann. Phys. 38, 489*
Egli L 2014 *Post processing of data from array spectroradiometer* (Davos: UVnet workshop)
Egli L and Gröbner J 2018 A Novel Array-Spectroradiometer System for Total Column Ozone Retrieval *Annual Report PMOD/WRC*
Egli L, Gröbner J, Hülsen G, Bachmann L, Blumthaler M, Dubard J, Khazova M, Kift R, Hoogendijk K, Serrano A, Smedley A and Vilaplana J M 2016 Quality assessment of solar UV irradiance measured with array spectroradiometers *Atmos. Meas. Tech.* **9** 1553-67
Eichstädt S, Schmähling F, Wübbeler G, Anhalt K, Bünger L, Krüger U and Elster C 2013 Comparison of the Richardson–Lucy method and a classical approach for spectrometer bandpass correction *Metrologia* **50** 107
Engelsen O, Brustad M, Aksnes L and Lund E 2005 Daily Duration of Vitamin D Synthesis in Human Skin with Relation to Latitude, Total Ozone, Altitude, Ground Cover, Aerosols and Cloud Thickness *Photochemistry and Photobiology* **81** 1287-90
Feinholz M E, Flora S J, Brown S W, Zong Y, Lykke K R, Yarbrough M A, Johnson B C and Clark D K 2012 Stray light correction algorithm for multichannel hyperspectral spectrographs *Appl. Opt.* **51** 3631-41
Fest E 2013 Stray Light Analysis and Control
Fu H, Liu Y, Chen T, Wang C and Chou P 2014 The Study of Spectral Correction Algorithm of Charge-Coupled Device Array Spectrometer *IEEE Transactions on Electron Devices* **61** 3796-802

Gaigalas A K, Wang L, He H-J and DeRose P 2009 Procedures for Wavelength Calibration and Spectral Response Correction of CCD Array Spectrometers *Journal of Research of the National Institute of Standards and Technology* **114** 215-28

Gao L, Kester R T, Hagen N and Tkaczyk T S 2010 Snapshot Image Mapping Spectrometer (IMS) with high sampling density for hyperspectral microscopy *Optics Express* **18** 14330-44

Gardner J L 2003 Uncertainties in Interpolated Spectral Data *Journal of Research of the National Institute of Standards and Technology* **108** 69-78

Gehm M E, John R, Brady D J, Willett R M and Schulz T J 2007 Single-shot compressive spectral imaging with a dual-disperser architecture *Optics Express* **15** 14013-27

Germer T A, Zwinkels Joanne C and Tsai Benjamin K 2014 Spectrophotometry: Accurate measurement of optical properties of materials *Academic Press Elsevier* **46**

Godar D E 2005 UV Doses Worldwide *Photochemistry and Photobiology* **81** 736-49

Gröbner J, Schreder J, Kazadzis S, Bais A F, Blumthaler M, Görts P, Tax R, Koskela T, Seckmeyer G, Webb A R and Rembges D 2005 Traveling reference spectroradiometer for routine quality assurance of spectral solar ultraviolet irradiance measurements *Appl. Opt.* **44** 5321-31

Gueymard C A 2008 REST2: High-performance solar radiation model for cloudless-sky irradiance, illuminance, and photosynthetically active radiation – Validation with a benchmark dataset *Solar Energy* **82** 272-85

Gupta N and Voloshinov V 2004 Hyperspectral imager, from ultraviolet to visible, with a KDP acousto-optic tunable filter *Appl. Opt.* **43** 2752-9

Hagen N and Kudenov M W 2013 Review of snapshot spectral imaging technologies *Optical Engineering* **52** 090901-

Hardeberg J Y, Schmitt F and Brettel H 2002 Multispectral color image capture using a liquid crystal tunable filter *Optical Engineering* **41** 2532-48

He T, Liang S and Song D-X 2014 Analysis of global land surface albedo climatology and spatial-temporal variation during 1981–2010 from multiple satellite products *Journal of Geophysical Research: Atmospheres* **119** 10,281-10,98

Henault F, Bacon R, Content R, Lantz B, Laurent F, Lemonnier J-P and Morris S L 2004 Slicing the universe at affordable cost: the quest for the MUSE image slicer. pp 134-45

Hofmann M, Riechelmann S, Crisosto C, Mubarak R and Seckmeyer G 2014 Improved Synthesis of Global Irradiance with One-Minute Resolution for PV System Simulations *International Journal of Photoenergy* **2014** 10

Hofmann M and Seckmeyer G 2017 Influence of Various Irradiance Models and Their Combination on Simulation Results of Photovoltaic Systems *Energies* **10**

Hopkinson G R, Goodman T M and Prince S R 2004 *A Guide to the Use and Calibration of Detector Array Equipment*: SPIE Press)

Huber M, Blumthaler M, Ambach W and Staehelin J 1995 Total atmospheric ozone determined from spectral measurements of direct solar UV irradiance **22** 53-6

Hülsen G, Gröbner J, Nevas S, Sperfeld P, Egli L, Porrovecchio G and Smid M 2016 Traceability of solar UV measurements using the Qasume reference spectroradiometer *Appl. Opt.* **55** 7265-75

Ineichen P 2011 Global irradiance on tilted and oriented planes: model validations. (Genève

ISO/CIE 1984 The spectroradiometric measurement of light sources *CIE 63*

ISO/CIE 2014 Characterization of the performance of illuminance meters and luminance meters *ISO/CIE S023, first edition 2014-06-01*

ISO/CIE 2017 High-Speed Testing Methods for LEDs *CIE 226*

Kerr J 2002 New methodology for deriving total ozone and other atmospheric variables from Brewer spectrophotometer direct sun spectra *Journal of Geophysical Research-Atmospheres* **107**

Kruse F A, Lefkoff A B, Boardman J W, Heidebrecht K B, Shapiro A T, Barloon P J and Goetz A F H 1993 The spectral image processing system (SIPS)—interactive visualization and analysis of imaging spectrometer data *Remote Sensing of Environment* **44** 145-63

Lantz K O, Disterhoft P, Slusser J R, Gao W, Berndt J L, Bernhard G, Bloms S, Booth C R, Ehramjian J C, Harrison L C, Janson G T, Johnston P, Kiedron P W, McKenzie R L, Kimlin M G, Neale P J, O'Neill M, Quang V V, Seckmeyer G J, Taylor T, Wuttke S and Michalsky J J 2008 2003 North American

interagency intercomparison of ultraviolet spectroradiometers: scanning and spectrograph instruments. SPIE) p 33
Läuchli A 1929 Zur Absorption der ultravioletten Strahlung in Ozon *Zeitschrift für Physik* **53** 92-4
Lorenz S, Sandmann H and Weiskopf D 2018 BTS array radiometer validation for solar UV radiation monitoring and integration of the aplin climate region into the nationwide measuring network *NIR Conference/Dresden*
Loutzenhiser P G, Manz H, Felsmann C, Strachan P A, Frank T and Maxwell G M 2007 Empirical validation of models to compute solar irradiance on inclined surfaces for building energy simulation *Solar Energy* **81** 254-67
Luke L A P, Rebecca J H and Marina K 2014 Effects of ambient temperature on the performance of CCD array spectroradiometers and practical implications for field measurements *Journal of Radiological Protection* **34** 655
Martinsen P, Jordan B, McGlone A, Gaastra P and Laurie T 2008 Accurate and Precise Wavelength Calibration for Wide Bandwidth Array Spectrometers *Applied Spectroscopy* **62** 1008-12
Mathews S A 2008 Design and fabrication of a low-cost, multispectral imaging system *Appl. Opt.* **47** F71-F6
Matsuoka H, Kosai Y, Saito M, Takeyama N and Suto H 2002 Single-cell viability assessment with a novel spectro-imaging system *Journal of Biotechnology* **94** 299-308
Mazer A S, Martin M, Lee M and Solomon J E 1988 Image processing software for imaging spectrometry data analysis *Remote Sensing of Environment* **24** 201-10
McKenzie R, Aucamp P, Bais A, Björn L, Ilyas M and Madronich S 2011 *Ozone depletion and climate change: Impacts on UV radiation* vol 10
McKenzie R L, Liley J B and Björn L O 2009 UV Radiation: Balancing Risks and Benefits *Photochemistry and Photobiology* **85** 88-98
Meek D W, Hatfield J L, Howell T A, Idso S B and Reginato R J 1984 A Generalized Relationship between Photosynthetically Active Radiation and Solar Radiation1 **76** 939-45
Meyer E 1903 Über die Absorption der ultravioletten Strahlung in Ozon **317** 849-59
Mithal A, Wahl D A, Bonjour J P, Burckhardt P, Dawson-Hughes B, Eisman J A, El-Hajj Fuleihan G, Josse R G, Lips P, Morales-Torres J and on behalf of the I O F C o S A N W G 2009 Global vitamin D status and determinants of hypovitaminosis D *Osteoporosis International* **20** 1807-20
Montzka S A, Dutton G S, Yu P, Ray E, Portmann R W, Daniel J S, Kuijpers L, Hall B D, Mondeel D, Siso C, Nance J D, Rigby M, Manning A J, Hu L, Moore F, Miller B R and Elkins J W 2018 An unexpected and persistent increase in global emissions of ozone-depleting CFC-11 *Nature* **557** 413-7
Neumann W 2014 Fundamentals of Dispersive Optical Spectroscopy Systems *SPIE*
Nevas S 2015 CIE Tutorial and Practical Workshop on CIE S 025 - Spectroradiometry
Nevas S, Gröbner J, Egli L and Blumthaler M 2014 Stray light correction of array spectroradiometers for solar UVmeasurements *Appl. Opt.* **53** 4313-9
Nevas S and Sperfeld P 2015 CIE Tutorial and Practical Workshop on CIE S 025 - Spectroradiometry
Nevas S, Teuber A, Sperling A and Lindemann M 2012a Stability of array spectroradiometers and their suitability for absolute calibrations *Metrologia* **49** S48
Nevas S, Wübbeler G, Sperling A, Elster C and Teuber A 2012b Simultaneous correction of bandpass and stray-light effects in array spectroradiometer data *Metrologia* **49** S43
Newman P A and McKenzie R 2011 UV impacts avoided by the Montreal Protocol *Photochemical & Photobiological Sciences* **10** 1152-60
Ohno Y 2005 A Flexible Bandpass Correction Method for Spectrometers *Proc. AIC Colour 05—10th Congress of the Int. Colour Association (Grenada, Spain) pp 697–700*
Pacheco-Labrador J, Ferrero A and Martín M P 2014 Characterizing integration time and gray-level-related nonlinearities in a NMOS sensor *Appl. Opt.* **53** 7778-86
Pissulla D, Seckmeyer G, Cordero R R, Blumthaler M, Schallhart B, Webb A, Kift R, Smedley A, Bais A F, Kouremeti N, Cede A, Herman J and Kowalewski M 2009 Comparison of atmospheric spectral radiance measurements from five independently calibrated systems *Photochemical & Photobiological Sciences* **8** 516-27

Pribram J K and Penchina C M 1968 Stray Light in Czerny-Turner and Ebert Spectrometers *Appl. Opt.* **7** 2005-14

Pulli T, Nevas S, El Gawhary O, van den Berg S, Askola J, Kärhä P, Manoocheri F and Ikonen E 2017 Nonlinearity characterization of array spectroradiometers for the solar UV measurements *Appl. Opt.* **56** 3077-86

Riechelmann S 2014 Simultaneous measurement of spectral sky radiance: Development, characterization and validation of a non-scanning multidirectional spectroradiometer *Hannover, Technische Informationsbibliothek u. Universitätsbibliothek*

Riechelmann S, Schrempf M and Seckmeyer G 2013 Simultaneous measurement of spectral sky radiance by a non-scanning multidirectional spectroradiometer (MUDIS) *Measurement Science and Technology* **24** 125501

Salim S G R, Fox N P, Theocharous E, Sun T and Grattan K T V 2011 Temperature and nonlinearity corrections for a photodiode array spectrometer used in the field *Appl. Opt.* **50** 866-75

Saptari V 2003 Fourier-Transform Spectroscopy Instrumentation Engineering **TT61** 136

Schubert F, Klameth K, Darou S and Spinner D 2015 Measurement Uncertainties of a Compact Array Spectrometer *Energy Procedia* **77** 179-86

Seckmeyer G 1989 *Spektralradiometer für die ökologische Pflanzenforschung* vol 41, 501–506: Licht)

Seckmeyer G, Bais A, Bernhard G, Blumthaler M, Booth C, Disterhoft P, Eriksen P, McKenzie R, Miyauchi M and Roy C 2001 *Instruments to measure solar ultraviolet irradiance. Part 1: Spectral instruments* vol Global Atmosphere Watch Report No. 125: World Meteorological Organization (WMO))

Seckmeyer G, Bais A, Bernhard G, Blumthaler M, Drueke S, Kiedron P, Lantz K, McKenzie R and Riechelmann S 2010 *Instruments to measure solar ultraviolet radiation Part 4: Array spectroradiometers (WMO TD No. 1538)*

Seckmeyer G, L. L R, C. G, W. H J and M. S 2018 Biologische und medizinische Wirkungen solarer Bestrahlung - Biological and medical effects of solar radiation *promet Meteorologische Fortbildung DWD*

Seckmeyer G, Mayer B and Bernhard G 1997 The 1997 Status of Solar UV Spectroradiometer in Germany: Results from the National Intercomparison of Spectroradiometers *Garmisch-Partenkirchen, August 1997, 169 pp., Shaker, Aachen, Germany, 1998.*

Seckmeyer G, Schrempf M, Wieczorek A, Riechelmann S, Graw K, Seckmeyer S and Zankl M 2013 A Novel Method to Calculate Solar UV Exposure Relevant to Vitamin D Production in Humans *Photochemistry and Photobiology* **89** 974-83

Seckmeyer G, Zittermann A, McKenzie R and Greinert R 2012 *Encyclopedia of Sustainability Science and Technology,* ed R A Meyers (New York, NY: Springer New York) pp 9649-72

Shafer A B, Megill L R and Droppleman L 1964 Optimization of the Czerny–Turner Spectrometer* *Journal of the Optical Society of America* **54** 879-87

Shaw M and Goodman T 2008 Array-based goniospectroradiometer for measurement of spectral radiant intensity and spectral total flux of light sources *Appl. Opt.* **47** 2637-47

Sigernes F, Ivanov Y, Chernouss S, Trondsen T, Roldugin A, Fedorenko Y, Kozelov B, Kirillov A, Kornilov I, Safargaleev V, Holmen S, Dyrland M, Lorentzen D and Baddeley L 2012 Hyperspectral all-sky imaging of auroras *Optics Express* **20** 27650-60

Starks P J, Walter-Shea E A, Schiebe F R and Markham B L 1995 Temperature sensitivity characterization of a silicon diode array spectrometer *Remote Sensing of Environment* **51** 385-9

Stearns E I and Stearns R E 1988 An example of a method for correcting radiance data for Bandpass error *Color Research & Application* **13** 257-9

UN e p 1987 Website of the ozone secretariat of the united nations http://ozone.unep.org (24.07.2017)

Vaskuri A, Kärhä P, Egli L, Gröbner J and Ikonen E 2018 Uncertainty analysis of total ozone derived from direct solar irradiance spectra in the presence of unknown spectral deviations *Atmos. Meas. Tech.* **11** 3595-610

Wagadarikar A, John R, Willett R and Brady D 2008 Single disperser design for coded aperture snapshot spectral imaging *Appl. Opt.* **47** B44-B51

Walsh A 1952 Multiple Monochromators. I. Design of Multiple Monochromators *Journal of the Optical Society of America* **42** 94-5
Webb A R 2006 Considerations for lighting in the built environment: Non-visual effects of light *Energy and Buildings* **38** 721-7
Webb A R and Engelsen O 2006 Calculated Ultraviolet Exposure Levels for a Healthy Vitamin D Status *Photochemistry and Photobiology* **82** 1697-703
Webb A R, Gardiner B G, Martin T J, Leszczynski K, Metzdoff J, Mohnen V A and Forgan B 1998 Guidelines for site quality control of UV monitoring *Rep. Ser. 126, Environ. Pollution Monitoring and Res. Programme, WMO, Geneva, 1998.*
Wendisch M and Yang P 2012 Theory of Atmospheric Radiative Transfer - A Comprehensive Introduction 321 pp
WHO 2002 *Global Solar UV Index: A Practical Guide*: World Health Organization)
William D V, Michael C C and John T R 2004 Nonlinearity Corrections and Statistical Uncertainties Associated with Near-Infrared Arrays *Publications of the Astronomical Society of the Pacific* **116** 352
WMO 2018 Scientific Assessment of Ozone Depletion: 2018 *Global Ozone Research and Monitoring Project — Report No. 58, 588 pp., Geneva, Switzerland*
Woolliams E R, Baribeau R, Bialek A and Cox M G 2011 Spectrometer bandwidth correction for generalized bandpass functions *Metrologia* **48** 164
Wuttke S, Kreuter A and Blumthaler M 2012 Aerosol climatology in an Alpine valley *Journal of Geophysical Research (Atmospheres)* **117** 20202
Wuttke S, Seckmeyer G, Bernhard G, Ehramjian J, McKenzie R, Johnston P and O'Neill M 2006 New Spectroradiometers Complying with the NDSC Standards *Journal of Atmospheric and Oceanic Technology* **23** 241-51
Young R and Häring R 2011 Wavelength calibration of array spectroradiometers *Proceedings of the 27th Session of the CIE 2011 Sun City, South Africa*
Zong Y, Brown S W, Johnson B C, Lykke K R and Ohno Y 2006 Simple spectral stray light correction method for array spectroradiometers *Appl. Opt.* **45** 1111-9
Zuber R and Ribnitzky M 2019 Combined Out of Range and In Band stray light correction for array spectroradiometers *CIE Session 2019 - OP76*

Acknowledgements

At this point, I would like to thank everybody who supported me during the time of my PhD work. It was on the one hand a very exciting time but the other hand as well a very exhausting time. Without the support of many people, especially those listed here, it would not have been possible for me to complete this work successfully.

- First, I have to thank my advisor Prof. Dr. Gunther Seckmeyer for supporting me from the first minute on. You gave me the opportunity to do this thesis despite the great distance to the IMuK. We had many great discussions, not only concentrated on science. In addition, I learned a lot from your experience in science and life.

- Prof. Dr. Manfred Wendisch and Prof. Dr. Detlev Ristau who acted as the co-reviewers of this PhD thesis.

- Dipl. Ing. Anton Gugg-Helminger and Wolfgang Dähn who made this thesis on the side of Gigahertz-Optik GmbH possible.

- The people who supported me at the IMuK, especially Ansgar Stührmann, Michael Schrempf, Angelika Niedzwiedz, Kezia Lange and Mario Tobar. As well Peter Sperfeld and Stefan Riechelmann from the PTB.

- My colleagues here at Gigahertz-Optik GmbH who helped me whenever needed. I would like to name to persons who supported me by doing measurements: Anton Gugg-Helminger, Roman Koch and Mario Ribnitzky.

- I would like to thank as well my proofreaders of this thesis: Wolfgang Weigand, Anton Gugg-Helminger, Angelika Niedzwiedz, Michael Schrempf and Stefan Riechelmann.

- I cannot imagine how my family and friends could have helped me better during this time. Thank you very much for this support.

- Finally, the biggest thanks to my great wife Marina. You have always given me support and strength. This work is our success.

This PhD project was partly funded by BMWi (Bundesministerium für Wirtschaft und Energie) project KF3091801DF2 and by Gigahertz-Optik GmbH.

Curriculum Vitae

Personal Details	Family Name	Zuber
	First Name	Ralf
	Middle Name	Georg
	Date of birth	03 September 1987
	Place of birth	Roth, Germany
	Nationality	German

University education	10/2006 – 08/2010	Bachelor in engineering physics. University of applied sciences Munich.
	10/2008 – 03/2009	Practical semester at Max Planck Institute for plasma physics (IPP), Garching.
	10/2009 – 04/2010	Bachelor Thesis: Development, Construction and Application of a photometric 3D Goniometer for far field measurements. Gigahertz-Optik GmbH, Puchheim.
	10/2010 – 10/2012	Master in advanced optical technologies. University Erlangen-Nürnberg.
	03/2010 – 10/2012	Master Thesis: Investigation and analysis of error sources regarding deflectometry measurements. Max Planck Institute for Light (MPI), Erlangen.
Career	11/2012 – 07/2015	Product manager at Gigahertz-Optik GmbH
	07/2015 – today	Development manager at Gigahertz-Optik GmbH
Measurement Campaigns	09/2016	Participation at an international intercomparison in the framework of "Traceability for atmospheric total column ozone (ATMOZ ENV59)" at Izaña, Tenerife.
	05/2017	Performing an NDACC intercomparison at the Institute of Meteorology and Climatology, Leibniz Universität Hannover, Germany.
	07/2019	Participation at an international intercomparison in the framework of "14th Intercomparison campaign of the regional brewer calibration center-Europe" for TOC measurements with BST2048-UV-S-WP at Arenosillo (Huelva), Spain

Publications

Zuber, R., Sperfeld, P., Riechelmann, S., Nevas, S., Sildoja, M., and Seckmeyer, G.: Adaption of an array spectroradiometer for total ozone column retrieval using direct solar irradiance measurements in the UV spectral range, Atmos. Meas. Tech., 11, 2477-2484, https://doi.org/10.5194/amt-11-2477-2018, 2018.

Zuber, R., Stührmann, A., Gugg-Helminger, A., and Seckmeyer, G.: Technology for detecting spectral radiance by a snapshot multi-imaging spectroradiometer, 2017 Meas. Sci. Technol. 28 125903, https://doi.org/10.1088/1361-6501/aa9409

Ralf Zuber, Mario Ribnitzky, Mario Tobar, Kezia Lange, Dimitrij Kutscher, Michael Schrempf, Angelika Niedzwiedz, Gunther Seckmeyer.: Global spectral irradiance array spectroradiometer validation according to WMO, 2018 Meas. Sci. Technol. 29 105801

Evelyn Olesch, Christian Faber, Roman Krobot, Ralf Zuber, Gerd Häusler.: Quantitative Deflectometry Challenges Interferometry, 2014 In: Osten W. (eds) Fringe 2013. Springer, Berlin, Heidelberg

Ralf Zuber.: Effective stray light suppression with the BTS2048-UV series array Spectroradiometer, UV News 12, 2017

Conference contributions

Ralf Zuber, Peter Sperfeld, Stefan Riechelmann, Saulius Nevas, Meelis Sildoja.: A stray light corrected array spectroradiometer for complex high dynamic range measurements in the UV spectral range,13th International Conference on New Developments & Applications in Optical Radiometry (NEWRAD 2017), SSR-PB-3, Tokyo, 2017

Ralf Zuber, Mike Clark, Peter Sperfeld.: A stray light corrected array spectroradiometer for complex high dynamic range measurements in the UV spectral range, International Conference 'UV LED Technologies & Applications' (ICULTA-2018), Berlin, 2018

Ralf Zuber, Peter Sperfeld, Stefan Riechelmann, Saulius Nevas, Meelis Sildoja.: Ein streulichtkorrigiertes Array-Spektroradiometer für komplexe hochdynamische Messungen im UV-Spektralbereich, DACH-Meteorologentagung, Garmisch-Partenkirchen, 2019

Ralf Zuber, Mario Ribnitzky.: Combined Out-of-Range and In-Band Stray Light correction for array spectroradiometers, 29th Session of the CIE, Washington DC, 2019

Patent

Ralf Zuber.: Spektrometersystem, Publication number: DE 102013112376,

Publication of the patent: 01.12.2016

CIE Work (Link)

Member and author of:

- CIE TC2-69: CIE Classification Systems of Illuminance and Luminance Meters (published as CIE 231)
- CIE TC2-78: The Goniophotometry of Lamps and Luminaires
- CIE TC2-79: Integrating sphere photometry and spectroradiometry
- CIE TC2-80: Spectroradiometric measurement of light sources
- CIE TC2-87: Broadband UV LED radiometric measurements between 320 nm and 420 nm
- CIE TC2-89: Measurement of Temporal Light Modulation of Light Sources and Lighting Systems
- CIE TC2-90: LED Reference Spectrum for Photometer Calibration
- CIE TC2-91: Optical Measurement Methods of LED Packages and LED Arrays

---